TESIS DE LA UNIVERSIDAD DE ZARAGOZA

2020

132

Adrián Gómez Pueyo

Computational and Theoretical Developements for (Time Dependent) Density Functional Theory

Departamento
Física Teórica

Director/es
Castro Barrigón, Alberto

ISSN 2254-7606

Prensas de la Universidad
Universidad Zaragoza

ISSN 2254-7606

Universidad Zaragoza
1542

Tesis Doctoral

COMPUTATIONAL AND THEORETICAL DEVELOPEMENTS FOR (TIME DEPENDENT) DENSITY FUNCTIONAL THEORY

Autor

Adrián Gómez Pueyo

Director/es

Castro Barrigón, Alberto

UNIVERSIDAD DE ZARAGOZA

Física Teórica

2020

Computational and Theoretical Developements for (Time Dependent) Density Functional Theory

Exchange and correlation functionals, numerical propagators, and combination with optimal control theory

Universidad Zaragoza

Adrián Gómez Pueyo

Advisor: Alberto Castro

Institute for Biocomputation and Physics of Complex Systems
University of Zaragoza

This dissertation is submitted for the degree of
Doctor in Physics

University of Zaragoza April 2020

To my parents.

Article List

1. Gómez Pueyo, A., Budagosky M., J. A., and Castro, A. (2016). Optimal control with nonadiabatic molecular dynamics: Application to the Coulomb explosion of sodium clusters. Physical Review A, 94:063421.

2. Gómez Pueyo, A., Marques, M. A. L., Rubio, A., and Castro, A. (2018). Propagators for the Time-Dependent Kohn–Sham Equations: Multistep, Runge–Kutta, Exponential Runge–Kutta, and Commutator Free Magnus Methods. Journal of Chemical Theory and Computation, 14(6):3040–3052.

3. Gómez Pueyo, A. and Castro, A. (2018). About the relation of electron–electron interaction potentials with exchange and correlation functionals. The European Physical Journal B, 91(6):1420.

4. Gómez Pueyo, A., Blanes, S., and Castro, A. (2020). Propagators for Quantum-Classical Models: Commutator-Free Magnus Methods. Journal of Chemical Theory and Computation, 16:1420-1430.

5. Tancogne-Dejean, N., *et al.* (2020). Octopus, a computational framework for exploring light-driven phenomena and quantum dynamics in extended and finite systems. Journal of Chemical Physics, 16:124119.

6. Gómez Pueyo, A., Blanes, S., and Castro, A. (2020). Performance of fourth and sixth-order commutator-free Magnus expansion integrators for Ehrenfest dynamics. Computational and Mathematical Methods, accepted.

Adrián Gómez Pueyo
April 2020

Acknowledgements

I would like to thank Dr. Jorge A. Budagosky for his help and support at the beginning of this thesis, specially for the discussions about optimal control and how to approach the simulations we were doing at the time.

I would also like to thank Dr. Miguel A. L. Marques and Dr. Ángel Rubio for their insightful comments about the symplecticity of the Kohn-Sham equations.

Finally, I acknowledge the superb theoretical support in the field of numerical propagators, more concretely those applied to classical-quantum hybrid systems, from Dr. Sergio Blanes.

Abstract

In this thesis we present computational and theoretical developments for density functional theory (DFT) and time dependent density functional theory (TDDFT). We have explored a new possible route to improve exchange and correlation functionals (XCF) in DFT, tested and developed numerical propagators for TDDFT, and applied a combination of optimal control theory with TDDFT.

In recent years, DFT has become the most used method in the electronic structure field thanks to its unparalleled precision/computational cost relationship. We can use DFT to accurately calculate many physical and chemical properties of atoms, molecules, nanostructures, and bulk materials. The main factor that determines the precision that we can obtain using DFT is the XCF, an unknown object for which hundreds of different approximations have been proposed. Some of these approximations work well enough for certain situations, but to this day there is no XCF that can be reliably applied to any arbitrary system. Moreover, there is no clear way for a systematic refinement of these functionals. We propose and explore, for one-dimensional systems, a new way to optimize them, based on establishing a relationship with the electron-electron interaction.

TDDFT is the extension of DFT to time-dependent and excited-states problems, and it is also one of the most popular methods (sometimes the only practical one) in the electronic structure community to deal with them. Once again, the reason behind its popularity is its accuracy/computational cost ratio, which allows us to tackle bigger, more complex systems. It can be used in combination with Ehrenfest dynamics, a non-adiabatic type of molecular dynamics. We have furthermore combined both TDDFT and Ehrenfest dynamics with optimal control theory, a scheme that has allowed us, for example, to predict the shapes of the laser pulses that induce a Coulomb explosion in different sodium clusters. Despite the good numerical performance of TDDFT compared to other methods, we found that these computations were still quite expensive.

Motivated by this fact, we have also dedicated a part of the thesis work to computational research. In particular, we have studied and implemented families of numerical propagators that had not been tested in the context of TDDFT. More concretely, linear multistep schemes, exponential Runge-Kutta formulas, and commutator-free Magnus expansions. Moreover,

we have implemented modifications of these commutator-free Magnus methods for the propagation of the classical-quantum equations that result of combining Ehrenfest dynamics with TDDFT.

Resumen

En esta tesis se presentan avances computacionales y teóricos en la teoría de funcionales de la densidad (DFT) y en la teoría de funcionales de la densidad dependientes del tiempo (TDDFT). Hemos explorado una posible nueva ruta para la mejora de los funcionales de intercambio y correlación (XCF) en DFT, comprobado y desarrollado propagadores numéricos para TDDFT, y aplicado una combinación de la teoría de control óptimo con TDDFT.

En los últimos años, DFT se ha convertido en el método más utilizado en el área de estructura electrónica gracias a su inigualable relación entre coste y precisión. Podemos usar DFT para calcular multitud de propiedades físicas y químicas de átomos, moléculas, nanoestructuras, y materia macroscópica. El factor principal que determina la precisión que podemos alcanzar usando DFT es el XCF, un objeto desconocido para el cual se han propuesto cientos de aproximaciones distintas. Algunas de estas aproximaciones funcionan correctamente en ciertas situaciones, pero a día de hoy no existe un XCF que pueda aplicarse con certeza sobre su validez a un sistema arbitrario. Más aún, no hay una forma sistemática de refinar estos funcionales. Proponemos y exploramos, para sistemas unidimensionales, una nueva manera de estudiarlos y optimizarlos basada en establecer una relación con la interacción entre electrones.

TDDFT es la extensión de DFT a problemas dependientes del tiempo y problemas con estados excitados, y es también uno de los métodos más populares (a veces el único método que se puede poner en práctica) en la comunidad de estructura electrónica para tratar con ellos. De nuevo, la razón detrás de su popularidad reside en su relación precisión/coste computacional, que nos permite tratar sistemas mayores y más complejos. Puede usarse en combinación con la dinámica de Ehrenfest, un tipo de dinámica molecular no adiabática. Hemos ido más allá y hemos combinado TDDFT y la dinámica de Ehrenfest con la teoría de control óptimo, creando un instrumento que nos permite, por ejemplo, predecir la forma de los pulsos láser que inducen una explosión de Coulomb en clusters de sodio. A pesar del buen rendimiento computacional de TDDFT en comparación con otros métodos, hallamos que el coste de estos cálculos era bastante elevado.

Motivados por este hecho, también dedicamos una parte del trabajo de la tesis a la investigación computacional. En particular, hemos estudiado e implementado familias de propagadores numéricos que no se habían examinado en el contexto de TDDFT. Más concretamente, métodos con varios pasos previos, fórmulas Runge-Kutta exponenciales, y las expansiones de Magnus sin conmutadores. Finalmente, hemos implementado modificaciones de estas expansiones de Magnus sin conmutadores para la propagación de las ecuaciones clásico-cuánticas que resultan de la combinación de la dinámica de Ehrenfest con TDDFT.

Table of contents

Chapter 1

Introduction

In recent years, the ab initio modeling techniques (also called first principles techniques) for Chemistry, Material Sciences and Molecular Physics have grown past the point where the results obtained could only be thought of as a qualitative aid. Simply put, we are entering the age where we can use these techniques as an accurate substitute for otherwise expensive experiments, both for academic endeavors and for industry applications [71–73]. Mainly thanks to the increase in the power and availability of hardware and software, the rise in popularity of first principles modeling can also be attributed to the improvement of the algorithms and theories. Also, the development and consolidation of nanotechnology has allowed the experiments to reach the size scale available to the current first principles simulations.

Already past the base-research-only phase, the field of ab initio modeling has matured and keeps growing. Some examples of this spread within the modeling community are: the study of atomic nuclear structure [8, 151] (in this case, the main advantage of first principles models over phenomenological ones is the generality with which both the nuclear structure and its associated processes can be treated); the modeling of point defects in materials [213, 93]; and even large biological problems like tumor cell populations [46], DNA [162, 135, 177], proteins [223], and viruses [184, 126] (including their symptomatic responses [63]), have also been studied using ab initio techniques.

Looking beyond these individual examples, there are a few indicators that help us to understand the current relevance of ab initio modeling:

1. The number of scientific publications, and their average impact index, is growing faster than the scientific average. Various studies like Refs. [71, 72] show that the growth of the number of papers about electronic structure calculations and its impact is significantly faster than that of the full of science.

2. The number of patents, which are traditionally used as a measure of the return-on-investment of research, has started to grow. These patents are mainly from the field of electronic structure and, to a lesser extent, organic chemistry and related areas. Goldbeck [71] reports a growth from 30 patents in 2002 to 150 in 2011.

3. The number of scientists working on modeling, both developers and users, have also increased in the last years. This increase has happened in both the private sector and the academy, and the number of trained people in simulations grows every year. For example, Dederichs et al. [159] reported more than 22000 authors in the field of ab initio simulation in 2008.

4. The software industry in the field of ab initio modeling has consolidated during the last decades, and has developed numerous commercial and free codes. Nowadays, this industry is well past the "spin-off" phase. It is estimated that there are 30 companies working in ab initio codes [71].

"First principles methods" may be applied to different objects of study; in this thesis the term is mainly referring to the problem of electronic structure (i.e. the many-particle problem for fermions), coupled perhaps to the underlying nuclei, treated classically with Molecular Dynamics techniques. As described above, the field of electronic structure is nowadays an active area of research, and has found practical use in both the academic and private sectors. From a purely theoretical point of view, however, the solution to any problem posed in this field has been known since the decade of the 1920s: write the many-body Schrödinger equation for the system you wish to study, solve it to find the wave function, and then use this result to calculate the desired observables. Sadly, when we take this idea into practice we run into insurmountable technical problems mainly derived from the size of the many-body Schrödinger equation. Quoting Paul Dirac [53], "The underlying physical laws necessary for the mathematical theory of a large part of physics and the whole of chemistry are thus completely known, and the difficulty is only that the exact application of these laws leads to equations much too complicated to be soluble. It therefore becomes desirable that approximate practical methods of applying quantum mechanics should be developed, which can lead to an explanation of the main features of complex atomic systems without too much computation." A straightforward approach to the many-body Schrödinger equation is thus unfeasible from a practical point of view, and for this reason many theories and approximations have been developed. Even with these more sophisticated techniques, we

still find many numerical complications, due to the notorious bad scaling with the size of the system. This motivates scientists all over the world to look for new methods to tackle the many-body problem that are more computational-friendly, and to improve the existing algorithms.

There are three types of necessary work related to first principles modeling: research and improvement of the theories to be used to solve the many-body problem, technical implementation of this theory in a code, and finally the subsequent application to a physical system and problem (which is, ultimately, the main goal). In this thesis we have somehow contributed to all three lines of work. First of all, to contribute to the solution of the long-standing many-electron theoretical problem, in this thesis we present work on the development of ab initio theories, more concretely on the improvement of the exchange and correlation functionals (XCFs) in density functional theory (DFT). Second, from a technical point of view, we have studied and implemented different families of numerical propagators for the equations of motion of time dependent density functional theory (TDDFT). We have also shown how to combine quantum optimal control theory (QOCT) with a non-adiabatic, classical-quantum hybrid molecular dynamics model, the Ehrenfest model (EMD). Finally, we have also worked on applications of these theories and methods: we have used the QOCT+EMD+TDDFT formalism to optimize the ability of a laser pulse subject to a series of restrictions (fluence, duration and frequency) to induce the Coulomb explosion of small sodium clusters. Therefore, the research described in this thesis has somehow required a sample of those three necessary skills in the field of first principles electronic structure. In the remaining of this Introduction, we briefly describe these lines of work.

Let us start by stating the theoretical problem. As we have mentioned before, the main task in the electronic structure field is to find a way to deal with the many-body Schrödinger equation. Although the general theory of quantum mechanics was essentially completed in the 1930s, it was not until the 1960s that computers had enough power and memory to solve the Schrödinger equation for small atoms and molecules with a minimum accuracy. The first general and minimally accurate method that was developed and employed was the Hartree-Fock approximation. This is a variational method that consists of assuming, as an approximation to the full multi-electronic wave function, a single Slater determinant formed by monoelectronic orbitals. This wave function is affected by the external potential generated

by the fixed nuclei of the system, the classic electrostatic repulsion generated by the electrons, and a non-local exchange potential which provides short range repulsion among electrons with the same spin. The variational principle is then applied to this ansatz, and the resulting equations are nonlinear and must be solved self-consistently – which is the reason that this scheme was also called the self-consistent field method. The equations include the exchange operator, which depends on the orbitals of the system, and is non-local. For this reason it was prohibitively expensive for the first half of the XX century. In 1951, Slater proposed to replace the exchange operator with an orbital average which came to be known as the Slater potential, speeding up significantly the computations. This approximation, unfortunately, does not include many correlation effects. Chemists require more complex and accurate choices for the many-electron wave function. Likewise, solid state physicists preferred to use simplified model Hamiltonians borrowed from quantum field theory.

In his Nobel lecture from 1999 [105], Walter Kohn eloquently explains the difficulties of using variational wave function methods that attempt to go beyond the Hartree-Fock approximation. In short, the number of parameters required to reach chemical accuracy grows exponentially with the number of particles involved, a phenomenon dubbed the "exponential wall". Of course, this means that, with the exception of very small atoms or molecules – or situations with an exceptional number of symmetries that we can use to simplify the problem –, the direct, straightforward methods are not feasible for large systems with the current level of technology, and probably will never be.

This prompted the search for better ways to tackle the solution of the many-body Schrödinger equation, looking for reinterpretations of the quantum theory, or less computationally expensive approaches for the calculation of the wave function. Here we cite some of the most popular theories:

- (Full) Configuration interaction [49]: This is, in fact, the *straightforward route*. The first post Hartree-Fock method, used for the first time in 1928. Instead of a single Slater determinant, in configuration interaction the wave function uses more than one determinant weighed with a set of coefficients that can be varied. Its name comes from the fact that one must choose a *configuration* of Slater determinants used to form the wave function, whereas the mix of different electronic states gives us the *interaction*. If all the possible variations of the coefficients are used, it is denominated full configuration interaction, and the result is exact.

- Multi-configuration self consistent field [203]: In this approach, one takes the same idea of configuration interaction, and optimizes not only the coefficients of the trial wave function, but also its orbitals.

- Random phase approximation [44]: Although presented by Bohm and Pines at the beginning of the 1950s in the context of plasma theory, in 1957 Gell-Mann and Brueckner [67] reformulated the random phase approximation in a way that easily extended to nonuniform systems, which is when quantum chemists started to take an interest in this theory. The name of the theory comes from the way it deals with the contribution of the electric potential (the sum of the external perturbing potential and the screening) to the dielectric function, which is averaged out. For some time, random phase approximation and time dependent Hartree-Fock were used as synonyms, because getting rid of the screening term results in the Hartree-Fock method.

- Møller-Plesset perturbation theory [48]: First described by Møller and Plesset in 1934 [150], this approach uses perturbation theory to take into account the correlation missing in the Hartree-Fock method.

- Coupled cluster [231]: Used mainly in computational chemistry and nuclear physics, it was born at the end of the 1950s in the field of nuclear physics and applied to the problem of electronic structure for the first time in the 1960s. This numerical technique uses an exponential ansatz of cluster operators applied the initial wave function, where this initial guess is built from the orbitals found through a Hartree-Fock calculation.

- Quantum Monte Carlo [7]: All the methods based on the Monte Carlo stochastic numerical techniques as applied to the many-electron Schrödinger's equation are united under this label. The common factor among them is the use of random sampling to obtain its results.

Although these theories are improvements over the original Hartree-Fock method in essentially every relevant aspect, all of them still carry the burden of a bad scaling with respect to the size of the system, and thus they become computationally too expensive for problems that involve more than a few atoms.

In any case, the quest for a solution based on the approximation to the many-electron wave function, such as all the methods mentioned above do, was the only alternative until, in 1964 the seminal paper by Pierre Hohenberg and Walter Kohn [90] gave birth to DFT. In this work they proved that the electron density of a system is enough to fully characterize the ground state of a many-electron system, avoiding the use of the wave function. In order to do so, Hohenberg and Kohn showed that the external potential of a system can be written as a unique functional of the density, a result that is nowadays called the Hohenberg-Kohn

theorem. The conceptual origins of DFT, however, can be traced back to the 1920s, to the works of L. H. Thomas [207], E. Fermi [61] and P. A. M. Dirac [52]. They proposed that the kinetic and exchange energy of many-electron systems could be locally modeled using the density. The so called Thomas-Fermi theory [120] thus obtained was an approximation to the electronic structure of a system that only relied on the electronic density. Unfortunately, this theory fails even qualitatively, as it cannot reproduce the atomic shell structure, and is unable to bind molecules. Furthermore, the Thomas-Fermi equations were not based on the firm theoretical grounds demonstrated in 1964 by Hohenberg and Kohn.

The next landmark in this field was set the following year, when in 1965 Walter Kohn and Lu Jeu Sham [106] demonstrated a practical way to compute the density and energy of the exact many-electron problem from a set of one-particle equations, which would come to be known as the Kohn-Sham equations. These equations describe an auxiliary system of non-interacting electrons (the Kohn-Sham system) subject to a certain potential that reproduces the electronic density of the real system. In this way, one can calculate the electronic density from this set of more computer-friendly equations.

Although formally exact, one of the components in the potential of the non-interacting system in DFT is the the exchange-correlation potential, which is derived from the so-called *exchange and correlation energy functional*, a functional of the electronic density. This is an unknown object that has to be approximated to be used in practical applications. The first proposal for this object was already given by Hohenberg and Kohn in their 1964 paper: it is the local density approximation (LDA), an XCF that remains popular today. Many different alternatives have been proposed during the last 50 years, and the search for the exact XCF is still the primary theoretical problem in DFT.

Through the 1970s and 1980s, many simulations on different materials showed that DFT could be used with predictive power. However, it was not until the late 1980s that, with the significant improvement of the XCFs, the degree of accuracy obtained for molecular calculations convinced many quantum chemists, and the first commercial DFT codes appeared. The improvement on the functionals was led by Perdew et al., who developed what we know today as the generalized gradient approximation (GGA) [163, 169]. This helped to spread DFT, and thanks to its relatively low cost/accuracy ratio it became the main tool for the calculation of specific properties for atoms, molecules, liquids, solids, and nanostructures. A crucial date for the popularization of DFT was 1992, when Pople et al. [99] showed that, for 32 different molecules, DFT outperformed the best wave function computations at the time. This fact, and the subsequent inclusion of DFT in the widely used Gaussian computer program, helped many chemists and physicists to recognize the value of DFT. In 1998, Kohn

and Pople received the Nobel Prize in Chemistry for their development of computational methods in quantum chemistry.

Although DFT has a great track of successes, there are still many areas where it fails to give even a qualitatively correct answer. Some of the most challenging problems for DFT are:

1. The underestimation of the fundamental gaps of bulk solids [167].
2. Most XCFs fail to approximate or even include the van der Waals forces [51, 116].
3. It produces poor results for strongly correlated problems [164, 107].
4. DFT, in its standard formultion, is not a good scheme to study excitations [118, 226] (although see below for the solution provided by TDDFT).
5. While it certainly is one of the cheapest computation schemes, it still has problems when dealing with very large problems.
6. It fails for the paradigmatic problem of the stretched Hydrogen molecule [47].
7. DFT cannot be improved by just adding computational power, in contrast to wave function based methods, whose results are improved by simply enlarging the basis sets and variational search space. The accuracy of DFT depends on the quality of the chosen XCF, and there is no recipe to refine these functionals in a systematic manner.

There is no universal solution to solve all these problems, even if there are some good fixes for some of them, individually. This fact implies that the user of DFT has to become an "expert" in the use of the wide array of necessary tools to perform the calculations: XCFs, basis sets, parameters, etc. Therefore, there are no black-box codes that can be easily used. The learning curve of DFT thus becomes one of the greatest obstacles for its spread within the scientific community and the industry. For a more detailed perspective on the last fifty years of DFT, check Refs. [11, 228].

In this thesis we present work dedicated to deal with the issue of finding new and more accurate XCFs, and doing it in a way that permits them to be systematically improved. The key idea behind our approach is that a DFT can be constructed for any system of fermions independently of the particle-particle interaction potential function (IF). Obviously, in the "real world" this IF is the Coulomb function $1/r$, but in fact the main theorems of DFT can be formulated for a large set of *admissible* functions. The key idea is therefore the following: Let us denote the set of admissible IFs by Γ. From the basic DFT theorems, for each IF $\gamma \in \Gamma$ exists a corresponding XCF λ. Let us denote the set of XCFs as Λ, where each $\lambda \in \Lambda$

corresponds to an XCF. With these definitions, we can write the map l between IFs and XCFs established by DFT as:

$$\begin{aligned} l : \Gamma &\rightarrow \Lambda \\ \gamma &\rightarrow l(\gamma) = \lambda \end{aligned}$$

Then, one may ask the inverse question: which is the IF (if it exists) that makes a given XCF exact? And if it does not exist, which is the IF that makes its corresponding XCF as close as possible to the exact one? The goal of this work is to develop a method that performs an optimization procedure over this correspondence between IFs and XCFs. To carry this optimization out, let us consider a given XCF $\lambda \in \Lambda$ for whom we want to find the associated IF $\gamma_0 \in \Gamma$ that makes λ exact (or, if it does not exist, at least the best possible approximation). We define, for each IF γ and external potential v, the ground state density $n_\gamma[v]$ (that we will assume to be non-degenerate). For a given XCF λ and external potential v we also define the ground state density found using DFT as $n_\lambda^{\mathrm{DFT}}[v]$. Now, if $\gamma \in l^{-1}(\lambda)$, both densities coincide for any choice of external potential v. This is also a sufficient condition, and thus if both densities coincide for any choice of external potential, then λ is the exact XCF that corresponds to the IF γ.

Setting up a set of trial external potential v_k, we can now define a distance G between the two densities as a functional of λ, γ and v:

$$G[\gamma;\lambda,v_k] = \sum_k \int \mathrm{dr}\, (n_\gamma[v_k] - n_\lambda^{\mathrm{DFT}}[v_k])^2 .$$

Minimizing this function(al) with respect to γ will yield the corresponding IF for a given XCF. The use of a set of external potentials instead of just one is due to the fact that the solution has to hold for every external potential.

The final step in the procedure consists in finding, out of some pool of possible XCFs $\{\lambda\}$, the one whose corresponding IF γ is as close as possible to the *real* Coulomb one. This can be done with a further optimization step. Compared with previous attempts to the creation and improvement of functionals, our proposal is radically different. Instead of optimizing a set of parameters with respect to results obtained for a diverse set of molecules (an approach that cannot be properly qualified as ab initio, and is limited by the size of the sets of used molecules), we propose an ab initio systematic optimization where the target is the Coulomb interaction. This is a truly universal object, and thus the optimized functional will have similar accuracy for all the systems. In Chapter 3, we report our proof-of-concept results for this scheme, for one-dimensional model systems.

We have seen how, at least from a formal point of view, DFT provides an exact method to compute any ground state property of a system without the need of the wave function: from Hohenberg and Kohn's work we know that given a many-body quantum system one can compute the value of any observable if we know its ground state density. It is natural to consider the same question for the time-dependent case, that is, if the evolution of the electronic density can be used instead of the many-body wave function to determine the values of whatever magnitude. Although there were several previous time-dependent calculations using density functionals, like Bloch's time-dependent expansion of the Thomas-Fermi theory [16] (thirty years before the foundation of DFT), the formal answer to that question was found by Erich Runge and Hardy Gross in 1984 [179]. They proved that all the time-dependent properties of a system can be determined with the help of the time-dependent density $n(r,t)$, and thus TDDFT was born. Analogous to the Hohenberg-Kohn theorem, the Runge-Gross theorem states that there is a one-to-one correspondence between the time evolving density of a system and its external potential (up to a purely time-dependent function, as it only contributes to the wave function with a time-dependent phase factor that cancels when we calculate expectation values from Hermitian observables). Now, one may then wonder if there exists a Kohn-Sham system that reproduces the evolution of the density of a real system, a problem denominated the question of non-interacting v-representability. In 1999 van Leeuwen [212] showed that for a given interacting system there exists a unique time-dependent Kohn-Sham potential whose associated Kohn-Sham non-interacting system has a density identical to that of the real system. The proof only demands that both the potential and the density are time analytic (which in fact can can be a quite restrictive constraint in some cases of interest).

The TDDFT theorems are also *existence* theorems, and therefore do not provide the full recipe for the time-dependent many-electron problem solution. The existence of a Kohn-Sham formulation, however, permits to work in an analogous manner than in the ground-state case: work with the non-interacting system of electrons, that can be managed with a single Slater determinant. These electrons evolve, therefore, following the time dependent Kohn-Sham (TDKS) equations, a set of nonlinear, one-particle Schrödinger-like equations. These fictitious electrons are under the effect of a potential consisting in the sum of the real external potential of the system (for example, the one generated by the nuclei and/or a laser pulse), a Hartree potential (the *classical* electrostatic potential due to the electron charge), and the time-dependent exchange and correlation potential, the unknown piece that must be approximated. This introduces the same problem as in DFT, that is, the precision of the simulations will be determined by the approximated XCF.

The problem is, unfortunately, harder than in standard DFT. First of all, formally speaking the XCF is also now a functional of the initial state of the real system, and of the initial Slater determinant chosen to start the evolution of the fictitious system. Normally (and this will be the case in all the calculations shown below), one uses first ground-state DFT to obtain the ground-state Slater determinant of the Kohn-Sham system (and the density), and starts the TDDFT calculation from there. This eliminates this state-dependence problem. A more severe problem is the *memory dependence*: the XC potential at a given time t depends on all the past densities $n(t')$, $t' < t$. In practical applications it is common to neglect the time dependence, and so the XCF only takes into account the instantaneous density $n(t)$, i.e., one assumes the *adiabatic approximation*. A more exhaustive description of the history and fundamentals of TDDFT can be found in Ref. [209, 141, 136].

Even with the problems that we have just outlined, TDDFT is one of the leading methods for the simulation of time-dependent many-electron systems, thanks to its great balance between computational cost and accuracy. It is widely spread in the field of spectroscopy [157] and real-time non-perturbative dynamics [220]. It is applied nowadays in the limits of its supposed applicability range, such as for example the study of charge transfer processes [137], nuclear collisions [194, 133] or out of equilibrium effects that require a non-adiabatic approach (like those deriving from the effect of a short laser pulse) [225, 227].

Our work on TDDFT in this thesis has focused on its combination with optimal control theory (OCT), in particular on the application of this combination to one particular problem: the *optimal* Coulomb explosion of clusters. In the following, we briefly introduce the basics of this combination.

DFT takes care of the questions related to the ground state of a many-electron system; TDDFT gives us the tools to compute their evolution and reaction to any external perturbation. A natural question is then the following: can we solve the *inverse problem*, i.e, find an external perturbation capable of steering the system in a predefined way?

The preferred mathematical tool for this type of inverse problems is OCT. Born from the general theory of calculus of variations, OCT is the branch of mathematics that studies the optimization of a given objective functional through the steering of a dynamical system with the purpose of driving the system in a desired way. There is some controversy about when to date the exact origin of OCT: while some believe the formal theory was started by the "Pontryagin Maximum Principle", established by the soviet mathematician L. S. Pontryagin and his group [17, 102], it is true that in some sense, already since ancient Greece times many

mathematicians have been concerned with optimization problems. The oldest one of them may be the search for the shortest path between two points (the *geodesic*). One pivotal point in the history of optimization problems was Johann Bernoulli's challenge in 1696 to solve the problem of the *brachystocrone*, that is, to find the curve that minimizes the time that takes a point object to travel from point A to point B, subject only to its own weight. This problem was first posed by Galileo in 1638 along with the catenary problem (i.e., which shape would take a heavy chain suspended between two points), but it was not until Bernoulli's challenge that it was correctly solved. Besides Johann Bernouilli, five mathematicians answered the challenge: Leibniz, Johann's brother Jakob Bernoulli, Tschirnhaus, l'Hopital and Newton (who submitted his solution anonymously). These works were published in 1697 in *Acta Eruditorum*, and caused a significant increase in the popularity of this kind of problems. This fact makes 1697 a good choice as the starting point for the theory of calculus of variations, and derived from it, OCT. For a deeper historical review of OCT, check Refs. [202, 183].

Although similar at first glance, there is a key difference between the usual problem solved by calculus of variations and OCT. The former deals with optimization problems typically defined as the minimization of a functional such as

$$J = \int_a^b \mathrm{d}t\, L(\dot{q}(t), q(t), t)\,,$$

with respect to q, where L is called the Lagrangian of our dynamical system, which is constrained by some conditions $q(a) = q_a$ and $q(b) = q_b$. The minimization in OCT is done over a certain set of curves C, determined by some given dynamical constraints. For example, C could be defined as the set of all the curves $t \to q(t)$ that satisfies

$$\dot{q} = f(q(t), u(t), t)\,,$$

where $u(t)$ are a set of "control" parameters over which the optimization is carried over. Within this framework we have two objects to study, the functional to minimize J and the dynamical control function f. This perhaps makes the search for the brachystochrone problem the true starting point for OCT, as it is the first optimization problem with pure dynamical constraints where the selection of an optimal path is the objective.

We are interested in the application of OCT to quantum systems, that is, those whose evolution is given by Schrödinger's equation, governed by an hermitian Hamiltonian. This branch of OCT is called *quantum optimal control theory*. The corresponding experimental discipline is usually called *coherent control*. With the advent of the ultrafast laser, it is an area of physics that has grown rapidly in the last decades. More concretely, with the access to very short laser pulses (in the range of femtoseconds), and the possibility of giving them

complex shapes, the "real-time" laser control of chemical reactions was first realized in the 90s (see for example Ref. [4]). The preferred experimental technique is the "adaptive feedback control"[101]: the yield of a given reaction is obtained at the end of the experiment, and a computer analyzes the results, and modifies the pulse to optimize the yield. QOCT may lend theoretical support, suggesting possibilities to carry out the modifications of the pulse. Mathematically, the problem consists in the optimization of the parameters that control the shape of the laser, subject to dynamical constraints, in the form of a control function. One of the key theoretical results is a formula for the gradient of the functional to optimize with respect to the control parameters. If this formula can be efficiently computed, it opens the door to the use of all the gradient-based optimization algorithms.

In Chapter 4, we demonstrate the use of OCT to optimize the ionization, and subsequent Coulomb explosion, of small sodium clusters irradiated with laser pulses with a duration of a few tens of femtoseconds. The process is modeled with TDDFT, coupled with Ehrenfest dynamics in order to account for the ionic movement. Ehrenfest dynamics differs from the classical Born-Oppenheimer approach in that it treats both the nuclei and the electrons at the same time, i.e., it is a non-adiabatic form of molecular dynamics. One of the advantages of this kind of approach is that we can deal with far-from-equilibrium systems (like those irradiated by a very short laser pulse, or when two molecules collide with each other). Ehrenfest dynamics combine a quantum treatment of the electrons with classical, point particle nuclei, which is why it is a form of hybrid dynamics.

Obviously, if the problem is how to induce a Coulomb explosion, an easy solution, for any system, is to apply a very high intensity laser pulse that does away with the electrons. The same problem, however, becomes difficult if one wants to get the same result, but with a limited energy input. As a proof of the practicality of the QOCT+EMD+TDDFT model, we placed restraints on the intensity of the pulse, and restricted its duration to a few femtoseconds in order to avoid this trivial solution to the problem. Naively, one could think that the optimal solution is however still obvious: just apply an harmonic pulse with frequency equal to the main excitation frequency of the cluster, which would maximize the energy absorption, and consecutively, the ionization. However, due to the fast nature of the process, it is unclear what should be chosen as the *main excitation frequency*: the separation of the nuclei during the pulse causes a redshift in this frequency, while the escape of electrons results in a blueshift. Therefore, the optimal shape of the pulse is hard to approximate intuitively. In order to assess the relevance of the ionic movement in this very fast process, we compared the results that we found using the full hybrid propagation scheme with those where the nuclei remained fixed during the application of the pulse, and came to the conclusion that even for short pulses of ≈ 30 fs, the nuclear movement plays an important role during the application of the pulse, as

some of the solutions found for the static simulations were unable to induce the Coulomb explosion of the full moving system.

Although we managed to find successful solutions for all the studied systems, the calculations were long and heavy. QOCT requires a high degree of precision in the time-dependent simulations of the model. Even with a relatively cheap computational scheme as the EMD+TDDFT combination, the size of the clusters that we could treat in practice was rather limited. This motivated us to initiate the third line of work within this thesis, centered in the development and implementation of new algorithms to ease the application of the theories described above. In particular, we have searched and implemented new propagation algorithms. In this thesis we focused first on numerical integration methods for the TDKS equations (electronic-only systems), and then we adapted some of them to the EMD+TDDFT model (electrons + nuclei).

When the Hilbert space is discretized, the TDKS equations turn into a system of ordinary differential equations (ODEs). Since the inception of the differential equations (a work already pioneered by Newton and Leibniz in the XVII century), hundreds if not thousands of methods have been developed for the numerical propagation of the systems described by ODEs. Nowadays, a rich body of literature dealing with this problem exists, but the creation and development of numerical integrators is still an active area of research, as the problems approached increase in size, and the computers used to solve them also change their architecture and performance.

There are many different ways to categorize these propagators. For example, depending on the number of previous steps required for the propagation: if the state of the system at a given time step is computed using the state of the system at one previous step only, we have one-step methods; otherwise we have multistep methods. If the equations of the integrator involve the solution of an algebraic system of equations, we have an implicit method; otherwise we talk about explicit propagators. If they preserve the (possible) symplecticity of the ODE, we say that the integrator is symplectic. Likewise, the methods may (or not) preserve other underlying *geometric* structures of the ODE system – e.g. the norm, the energy...

One of the most widespread family of one-step propagators is the Runge-Kutta (RK) family [27]. The explicit order four integrator ("RK4") is the most commonly used (to the point that it is usually simply referred as *the* Runge-Kutta method). The full family, however, also has implicit propagators like the Gauss-Legendre collocation methods, which are also

symplectic. Besides the standard RK integrators, many extensions and variations of the base propagators exist, like RK methods with variable time-step, extrapolation coupled with RK, partitioned RK...

Regarding the multistep methods, the most famous are the formulas of Adams [10]. This family also encompasses explicit and implicit methods, and its main advantage is that the computational cost is independent of the order of the propagator, although this comes at a price: there is a trade of computation cost for memory (as higher order integrators require to store a higher number of previous steps) and stability. Another important family of multistep methods is the one of the backwards differentiation formulas, a family of implicit integrators that use the previous steps of the propagation to approximate the derivative of the system equations.

If the system of ODEs that must be solved is linear and autonomous (as in a quantum problem where the Hamiltonian is time independent), simply applying the exponential of the operator that defines the system (the Hamiltonian in our case) to the initial state is enough to carry out the time propagation. The problem then reduces to the efficient implementations of the exponential of the operator. Many alternatives exist, such as truncations of the Taylor expansion [62], Leja and Padé's interpolations[28] or Krylov [85] and Chebychev's [45] polynomial expansions. For systems with time-dependent Hamiltonians, i.e., for non-autonomous systems of ODEs, we need to take the time-ordered exponential of the Hamiltonian. If the time interval is small enough, we can approximate the Hamiltonian as a constant and use the aforementioned methods for the computation of the exponential operator. If that is not the case, the Magnus expansion [134] is one of the most popular methods to deal with this kind of ODE systems.

There are also methods that attempt to take advantage of the structure of the equations of motion. In our case, our target are the TDKS equations of TDDFT. The Kohn-Sham Hamiltonian can be divided into a linear part, where the kinetic term is included, and a nonlinear part, where the Hartree and XC potentials belong. Usually the kinetic operator is the main source of trouble for the numerical integrators due to its unbounded nature. Therefore, designing integrators with a more careful approach for that linear part can help to alleviate the problems deriving from this term. As an example of this approach, the family of exponential integrators [104] use this division into linear and nonlinear parts.

Unfortunately, the previous quick revision of propagator alternatives just starts to describe the huge array of possibilities: for example, we can also cite the semi-global propagator of Schaefer et al. [185], Fatunla's algorithm [58, 59], etc. It becomes clear that the creation and development of propagators is a very active field of research. For this reason, keeping track of the state of the art methods, and identifying the most suitable one for a specific

system can be a difficult task. The careful testing and benchmarking of numerical integrators applied to different situations is an important aid for any type of research that requires ODE systems. In particular, it is crucial for the time-dependent branch of ab initio modeling, as the calculations are very computationally intensive – as we had the opportunity to note for our sodium clusters calculations.

Motivated by this fact, we have contributed to this endeavor, and have studied the accuracy and performance of different families of propagators for the TDKS equations that have been scarcely (or not at all) tested in the context of TDDFT, and then moved onto the implementation of the best methods found to the hybrid EMD+TDDFT model.

First, we studied different families of numerical propagators that previously had not been considered within the field of electronic structure, applying them to the TDKS equations. Namely, linear multistep schemes, exponential Runge-Kutta propagators, and commutator-free formulas. We analyzed both the precision and performance of these methods, and compared them with some well known integrators that we used as a benchmark. From this study we found that the commutator-free Magnus expansion outclassed every other family of propagators, both in accuracy and computational cost.

Then, we moved onto the implementation of the commutator-free methods for a full Ehrenfest dynamics model. In order to do this, we had to reconcile the classical nature of Newton's equations that describe the evolution of the nuclei of the system with the Schrödinger-like form of the TDKS equations for the electrons. The most common way to deal with this kind of problem consists on applying a fast and computationally cheap integration method for the nuclei and another, more precise propagator for the electrons. This approach to the problem stems from the fact that the movement of the nuclei is significantly slower than that of the electrons (around a thousand times slower in the most common situations), so faster but less sophisticated methods are usually enough. However, doing this can potentially destroy the properties of the propagators (symplecticity, time reversibility, unitarity...), and thus it is preferable to use a single propagation method for the whole system. We found that we could rewrite the equations of movement for the nuclei in a nonlinear Schrödinger-like form, and then apply the same propagator to both the classical and quantum parts of the system. This methodology not only assures the conservation of the propagator features, but from a practical point of view simplifies the code implementation of the method. We analyzed various commutator-free Magnus expansions, once again benchmarking the accuracy and performance of the methods.

This thesis is structured in the following way: chapter 2 presents the theoretical basis for the works developed in this work. It starts with a review of DFT and TDDFT, and introduces the hybrid classical-quantum Ehrenfest model. We provide some general notions about ordinary differential equations and numerical propagators. It continues with QOCT and its combination with TDDFT, and finally there is a brief introduction of the density matrix renormalization group (DMRG) theory. Chapter 3 details the project on the study of the XCFs and their relation to the electron-electron interaction potential, and presents a proof of concept on the functional optimization scheme mentioned above. Then, in chapter 4 we show an application of QOCT+TDDFT: a laser pulse under fluence, time and frequency restraints is optimized to induce the Coulomb explosion of small sodium clusters. Chapter 5 presents the work that we developed about numerical propagators for the TDKS equations: we prove the symplecticity of the TDKS equations, study different families of integrators that had not been tested in the context of TDDFT, and present a new method for the propagation of hybrid classical-quantum systems. Finally, chapter 6 presents the conclusions of this thesis.

Chapter 2

Theory

2.1 Density Functional Theory

The objective of DFT is to solve the static many-body electronic problem, which can be enunciated as the search for solutions of the Schrödinger equation for a system of N interacting non-relativistic electrons:

$$\hat{H}\Psi_I(x_1, x_2, ..., x_N) = E_I\Psi_I(x_1, x_2, ..., x_N), \tag{2.1}$$

where $\hat{H}$ is the many-electron Hamiltonian, Ψ_I is an N-electron antisymmetric wave function and the I-th eigenstate of $\hat{H}$, and E_I is its corresponding energy. We will use the notation $x_i = (r_i, \sigma_i)$ for the spacial and spin coordinates of the electron i.

The N-electron Hamiltonian (in the absence of relativistic effects such as magnetic fields, spin-orbit coupling, etc.) is given by

$$\begin{aligned}
\hat{H} &= \hat{T} + \hat{V} + \hat{W}, \\
\hat{T} &= \sum_{i=1}^{N} -\frac{1}{2}\nabla_i^2, \\
\hat{V} &= \sum_{i=1}^{N} v(\hat{r}_i), \\
\hat{W} &= \frac{1}{2}\sum_{\substack{i,j \\ i\neq j}}^{N} w(|\hat{r}_i - \hat{r}_j|),
\end{aligned} \tag{2.2}$$

where $\hat{T}$ and $\hat{V}$ are the kinetic and potential operators respectively, and $\hat{W}$ is the electron-electron interaction operator, the usual choice being the Coulomb interaction $w(r) = 1/r$,

i.e.:

$$\hat{W} = \frac{1}{2} \sum_{\substack{i,j \\ i \neq j}}^{N} \frac{1}{|\hat{r}_i - \hat{r}_j|}, \tag{2.3}$$

because it is the true interaction among electrons, relativistic considerations aside. We are also interested in the expression of this Hamiltonian in the second quantization formalism, as it is more fitting when dealing with lattice systems, that we will use later. The electronic Hamiltonian takes the form

$$\begin{aligned} \hat{H} = & \sum_{\sigma} \int \mathrm{dr}\ \hat{\psi}^{\dagger}_{\sigma}(r) \left[-\frac{1}{2} \nabla^2 \right] \hat{\psi}_{\sigma}(r) + \int \mathrm{dr}\ v(r) \hat{n}(r) \\ & + \frac{1}{2} \sum_{\sigma\tau} \int \mathrm{dr} \int \mathrm{dr}'\ w(|r - r'|) \hat{\psi}^{\dagger}_{\sigma}(r) \hat{\psi}^{\dagger}_{\tau}(r') \hat{\psi}_{\tau}(r') \hat{\psi}_{\sigma}(r)\,, \end{aligned} \tag{2.4}$$

where $\hat{\psi}^{\dagger}_{\sigma}(r)$ and $\hat{\psi}_{\sigma}(r)$ are the creation/annihilation field operators at position r with spin projection σ, respectively, and the density operator is defined by $\hat{n}(r) = \sum_{\sigma} \hat{\psi}^{\dagger}_{\sigma}(r) \hat{\psi}_{\sigma}(r)$. We can identify the first term of Eq. 2.4 with the kinetic operator $\hat{T}$, the second one with the external potential operator $\hat{V}$ and the last term with the electron-electron interaction operator $\hat{W}$.

If we know the wave function Ψ_I associated with the I-th eigenstate of the system we can compute the expectation value O_I of any physical observable $\hat{O}$, in that state. For example, for the lowest energy eigenstate $I = 0$, and for the Hamiltonian $\hat{H}$ we get the ground state energy:

$$E_0 = \langle \Psi_0 | \hat{H} | \Psi_0 \rangle. \tag{2.5}$$

The wave function holds all the information about the state of the quantum system, and therefore on the possible outcomes of the measurement of any observable. From a formal point of view, the many-electron problem is therefore completely solved by finding the eigenstates of the system that we are studying. However, when we tackle problems with a large number of electrons, we find that the number of parameters needed to construct accurate wave functions capable of approximating these eigenstates grows exponentially with N, a problem that has been denominated the "exponential wall". In practical terms, just storing a wave function for some tens of electrons becomes impossible. This is where DFT comes into play. This theory allows us to compute properties of many-electrons systems without having to manipulate the wave function, as we will show in the following sections.

2.1.1 The Hohenberg-Kohn Theorem

The publication in 1964 of the proof of the Hohenberg-Kohn theorem [90] marks the origin of DFT. Let us consider a system of N interacting electrons governed by the Hamiltonian 2.2. The ground state electronic density is defined as:

$$n_0(r) = N \sum_{\sigma} \int \mathrm{dx_2} ... \int \mathrm{dx_N} \, |\Psi_0(r\sigma, x_2, ..., x_N)|^2, \tag{2.6}$$

where we use the notation $\int \mathrm{dx_i} = \sum_{\sigma_i} \int \mathrm{dr_i}$. As the density n_0 comes from the wave function computed through Schrödinger's equation, it follows that the ground state density, at least for non-degenerate cases, is a functional of the external potential $v(r)$, i.e., $n_0(r) = n_0[v](r)$.

The opposite statement is also true, and it is known as the Hohenberg-Kohn theorem:

Hohenberg-Kohn Theorem. *The external potential $v(r)$, and hence the total energy, is a unique functional of the electron density $n_0(r)$.*

For a proof of the theorem, besides the original 1964 paper, check for example Refs. [143, 209]. This is the most basic version of the theorem, where it is assumed that the ground state of the system is not degenerate. It is possible to expand it to include cases with degenerate ground states, as shown for example in Ref. [54].

Since $\hat{T}$ and $\hat{W}$ are fixed, one may conclude from Hohenberg-Kohn theorem that the Hamiltonian 2.2 is a functional of the ground state density, i.e., $\hat{H} = \hat{H}[n_0]$. From Schrödinger's equation 2.1 it follows that all the eigenstates of the system are also functionals of the density, $\Psi_I = \Psi_I[n_0]$. In conclusion, all the properties of a given N-electron system are determined by the ground state electronic density n_0.

For example, from the Hohenberg-Kohn theorem it follows that the energy of the ground state of a N-electron system is a functional of the electronic density n, that we can write as:

$$E_v[n] = \langle \Psi[n] | \hat{T} + \hat{V} + \hat{W} | \Psi[n] \rangle, \tag{2.7}$$

where $\Psi[n]$ is the ground-state wave function of a N-particle system whose ground state density is n. This functional is defined for each choice of external potential v. And note that it can only be defined for densities n for which there exists an external potential such that the ground state density is precisely n (these are called the *interacting v-representable densities*). From the variational principle, we can write:

$$\begin{aligned} E_v[n] &< E_0, \qquad n(r) \neq n_0(r), \\ E_v[n] &= E_0, \qquad n(r) = n_0(r). \end{aligned} \tag{2.8}$$

where E_0 and n_0 are the ground state energy and density that correspond to v. This fact suggests a procedure to obtain the ground state energy and density: minimize $E_v[n]$, which may be done by finding the critical points of the corresponding Euler equation:

$$\frac{\delta}{\delta n(r)}\left[E_v[n] - \mu \int \mathrm{d}r'\, n(r')\right] = 0, \tag{2.9}$$

where μ is a Lagrange multiplier multiplying a term introduce to ensure the conservation of the number of electrons. In principle, from this equation we can find the ground state density n_0 avoiding completely the use of Schrödinger's equation. In practice, however, it is not very helpful since the form of functional $E_v[n]$ is unknown. Even its domain is unclear, as the interacting v-representability has proven to be a difficult mathematical problem.

In their original paper, Hohenberg and Kohn defined E_v by previously defining a so-called *universal* functional F, such that:

$$E_v[n] = F[n] + \int \mathrm{d}r\, n(r)v(r). \tag{2.10}$$

This new functional $F[n]$ is called the universal functional because it is system-independent, i.e., it is the same for any N-electron system with the same electronic interaction. It is defined as the remaining energy of the system without the external potential contribution:

$$F[n] = \langle \Psi[n] | \hat{T} + \hat{W} | \Psi[n] \rangle = T[n] + W[n]. \tag{2.11}$$

Using F, the Euler equation 2.9 takes the form:

$$\frac{\delta F[n]}{\delta n(r)} + v(r) = \mu. \tag{2.12}$$

A reformulation in terms of a universal function will prove its usefulness in the following section, as it circumvents some of the difficulties of the previous energy functional $E[n]$ in Eq. 2.9 – in particular the v-representability issue.

In conclusion, the Hohenberg-Kohn theorem allows us, in principle, to replace the N-body wave function Ψ (a function of $3N$ variables) with the electronic density of the ground state n_0 (a function of 3 variables), since it proves that no two different electronic systems can have the same ground state density. Unfortunately, the theorem does not provide us with a scheme to transform this knowledge into a practical procedure.

2.1.2 Constrained Search Formalism

To ensure the existence of the derivatives in Eqs. 2.9 and 2.12, we need that the density $n(r)$ corresponds to some ground state characterized by its external potential $v(r)$, i.e. we need them to be (interacting) v-representable. As mentioned above, the conditions for v-representability are still unknown, so that the exploration of the domain of $E[n]$ is to this day an unsolved problem.

We can overcome (some of) the difficulties related to the domain of $E[n]$ using the Levy-Lieb constrained search formalism [117, 119]. This is in fact a reformulation of Hohenberg-Kohn theorem, that somehow generalizes it. From the Rayleigh-Ritz method, we know that we can express the ground state energy E_0 as

$$E_0 = \min_{\Psi \to n} \langle \Psi | \hat{T} + \hat{V} + \hat{W} | \Psi \rangle, \tag{2.13}$$

where $\Psi \to n$ means that we have to trudge through the set of all the antisymmetric N-particle wave functions Ψ that have n as its corresponding density, until we minimize $\langle \Psi | \hat{H} | \Psi \rangle$. We can approach this search in a sequential way: first, we look for the Ψ that produces a given density $n(r)$ and minimizes the expectation value of the Hamiltonian, and then search for the density that minimizes the density, that will correspond to the ground state density $n_0(r)$. We can write this sequential process to find the ground state density as:

$$E_0[n] = \min_{n} \left\{ \min_{\Psi \to n} \langle \Psi | \hat{T} + \hat{V} + \hat{W} | \Psi \rangle \right\}. \tag{2.14}$$

This expression suggests a new way to define the energy functional $E_v[n]$:

$$E_v[n] = \min_{\Psi \to n} \langle \Psi | \hat{T} + \hat{V} + \hat{W} | \Psi \rangle, \tag{2.15}$$

where the minimization is carried over all the wave functions Ψ that produce the density n. This also suggests a new definition for a universal functional $F[n]$, as:

$$F[n] = \min_{\Psi \to n} \langle \Psi | \hat{T} + \hat{W} | \Psi \rangle. \tag{2.16}$$

Note that these definitions do not rely on the v-representability problem – only on the so-called N-representability: a density is N-representable if there exists at least one many-electron wave function that corresponds to it. This is a much easier condition, and any reasonable density is in fact N-representable.

The constrained search formalism based on these definitions also permits to demonstrate the Hohenberg-Kohn theorem [117], and arrive to the idea of a variational search to find

the minimum of E_v as a way to find the ground state energy and density. Unfortunately, the functional form for F is unknown, and therefore one has to find a different route to solve the problem in practice.

2.1.3 The Kohn-Sham Equations

Consider a non-interacting system ($\hat{W} = 0$), described by the Hamiltonian

$$\hat{H}_S = \hat{T}_S + \hat{V}_S = \sum_{i=1}^{N} \left(-\frac{1}{2}\nabla_i^2 + v_S(\hat{r}_i) \right). \tag{2.17}$$

The demonstration of the Hohenberg-Kohn theorem does not rely on a particular form for the electron-electron interaction potential function w, and can also be applied to this non-interacting case, in which $w = 0$. We therefore know that there is a one-to-one correspondence between $v_S(r)$ and the ground state density of the non-interacting system. We may then write the associated energy functional as

$$E_S[n] = T_S[n] + \int \mathrm{d}r\, n(r) v_S(r). \tag{2.18}$$

In this non-interacting case, the functional F is conventionally represented by $T_S[n]$. Eq. 2.9 then becomes:

$$\frac{\delta E_S[n]}{\delta n(r)} = \frac{\delta T_S[n]}{\delta n(r)} + v_S(r) = \mu, \tag{2.19}$$

and thus solving this equation we can obtain the ground-staet density n_{0S}. In practice, T_S is not known explicitly as a functional of the ground state, and therefore this solution to the problem would be limited by the accuracy of the approximations used for this term.

However, we do know how to solve the problem of a non-interacting system of electrons. We recall that the many-body wave function of a non-interacting system is given exactly by a single Slater determinant:

$$\Psi_S(x_1, ..., x_N) = \frac{1}{\sqrt{N}} \left| \begin{pmatrix} \varphi_1(x_1) & \varphi_2(x_1) & ... & \varphi_N(x_1) \\ \varphi_1(x_2) & \varphi_2(x_2) & ... & \varphi_N(x_2) \\ \vdots & \vdots & & \vdots \\ \varphi_1(x_N) & \varphi_2(x_N) & ... & \varphi_N(x_N) \end{pmatrix} \right|. \tag{2.20}$$

Here, the single-particle orbitals $\{\varphi_i\}$ are the lowest energy solutions to the single-particle Schrödinger's equation:

$$\left(-\frac{1}{2}\nabla^2 + v_S(r)\right)\varphi_i(r\sigma) = \varepsilon_i\varphi_i(r\sigma), \tag{2.21}$$

Since v_S is a functional of the ground state density, the orbitals are also functionals of the density. Inversely, one we can find n_S from the orbitals as:

$$n_{0S}(r) = \sum_{\sigma}\sum_{i=1}^{N} |\varphi_i(r\sigma)|^2. \tag{2.22}$$

The Kohn-Sham procedure [106] to approach the (interacting) many-electron problem consists now of imagining a fictitious system of non-interacting electrons – the Kohn-Sham system – such that its ground state density coincides with the one of the real interacting system. Since the non-interacting system can be solved in an easy way as shown above, the problem is translated to finding the appropriate external potential v_S (the Kohn-Sham potential). It turns out that this method to calculate n_0 has proved more convenient and precise than attempting to directly solve Eq. 2.12. This single-particle picture is at the basis of most of the current DFT applications.

It remains to see in which way to approach the problem of obtaining a working approximation for v_S. The road starts with the following expression for the total energy functional, already given by Kohn and Sham:

$$\begin{aligned} E[n] &= T[n] + W[n] + \int \mathrm{d}r\, n(r)v_S(r) \\ &= T_S[n] + \int \mathrm{d}r\, n(r)v_S(r) + E_{\mathrm{H}}[n] + E_{\mathrm{XC}}[n], \end{aligned} \tag{2.23}$$

where E_{H} is the Hartree energy given by

$$E_{\mathrm{H}}[n] = \frac{1}{2}\int \mathrm{d}r \int \mathrm{d}r'\, \frac{n(r)n(r')}{|r-r'|}, \tag{2.24}$$

and E_{XC} is the exchange and correlation energy functional, defined as:

$$\begin{aligned} E_{\mathrm{XC}}[n] &= T[n] - T_S[n] + W[n] - E_{\mathrm{H}}[n] \\ &= F[n] - T_S[n] - E_{\mathrm{H}}[n]. \end{aligned} \tag{2.25}$$

Inserting Eq.2.23 into the Euler equation 2.9 and comparing the result with Eq. 2.19, we can see that they are formally identical identifying

$$v_S[n](r) = v(r) + v_{\mathrm{H}}[n](r) + v_{\mathrm{XC}}[n](r), \tag{2.26}$$

where v_{H} is the Hartee potential

$$v_{\mathrm{H}}[n](r) = \frac{\delta E_H[n]}{\delta n(r)} = \int \mathrm{d}r' \, \frac{n(r')}{|r - r'|}, \tag{2.27}$$

and we define the exchange and correlation potential v_{XC} as

$$v_{\mathrm{XC}}[n](r) = \frac{\delta E_{\mathrm{XC}}[n]}{\delta n(r)}. \tag{2.28}$$

The exchange and correlation energy potential constitutes a small but important fraction of v_S, and is the only unknown piece. Therefore, the problem of DFT reduces to finding a good way to approximate E_{XC}, and therefore, v_{XC}.

Summarizing, the Kohn-Sham scheme consists of solving the single-particle Schrödinger-like Kohn-Sham equations:

$$H_{\mathrm{KS}}[n](r)\varphi_i(r\sigma) = \varepsilon_i \varphi_i(r\sigma)\,, \tag{2.29}$$

where H_{KS} is the Kohn-Sham Hamiltonian defined by

$$H_{\mathrm{KS}}[n](r) = -\frac{1}{2}\nabla^2 + v_S(r) = -\frac{1}{2}\nabla^2 + v(r) + v_{\mathrm{H}}[n](r) + v_{\mathrm{XC}}[n](r)\,, \tag{2.30}$$

and then compute the density from the lowest N occupied orbitals:

$$n_0(r) = \sum_{\sigma} \sum_{i=1}^{N} |\varphi_i(r\sigma)|^2\,, \tag{2.31}$$

By construction, this will also be the density of the interacting system. The main advantage of the Kohn-Sham equations is that they treat T_S exactly, leaving only the unknown $E_{\mathrm{XC}}[n]$ to be approximated. The contribution of $E_{\mathrm{XC}}[n]$ to the total energy is significantly smaller than the rest of the terms in Eq. 2.23, and so is the error derived from the approximation.

2.1.4 The Exchange and Correlation Functional

In this subsection, we summarize the most important approximations to the exchange and correlation functional, since one of the projects addressed in this thesis has been in fact the analysis of this important object.

Local Density Approximation

Already proposed by Kohn and Sham in their 1965 article [106], the local density approximation (LDA) expresses the exchange and correlation (XC) energy $E_{\mathrm{XC}}[n]$ using the XC energy per volume of a homogeneous electron gas e^h_{XC}

$$E^{\mathrm{LDA}}_{\mathrm{XC}}[n] = \int \mathrm{dr}\, e^h_{\mathrm{XC}}(\bar{n})|_{\bar{n}=n(r)}. \tag{2.32}$$

The homogeneous electron gas is an ideal system formed by an infinite electron system extended over all space, such that the density is equal everywhere. One cannot define a total XC energy, but the XC energy per volume $e^h_{\mathrm{XC}}(\bar{n})$, a function of the (constant) density of the homogeneous gas. It is usually split into its exchange part e^h_{X}, which can be calculated exactly, and its correlation part e^h_{C}, for which there exists highly accurate parameterizations. The XC potential is then given by

$$v^{\mathrm{LDA}}_{\mathrm{XC}}[n](r) = \frac{de^h_{\mathrm{XC}}}{d\bar{n}}|_{\bar{n}=n(r)}. \tag{2.33}$$

In short, the LDA means that, at each point of space r, we approximate $e_{\mathrm{XC}}(r)$ with the one found from the homogeneous electron gas that has a constant density $n(r)$. In practical implementations, instead of LDA a more general form called local spin-polarized density approximation (LSDA) is used, where

$$E^{\mathrm{LSDA}}_{\mathrm{XC}}[n_\sigma] = \int \mathrm{dr}\, e^h_{\mathrm{XC}}(n_\sigma(r)), \qquad v^{\mathrm{LSDA}}_{\mathrm{XC},\sigma}[n_\sigma](r) = \frac{de^h_{\mathrm{XC}}}{d\bar{n}_\sigma}|_{\bar{n}_\sigma=n_\sigma(r)}. \tag{2.34}$$

In this case, the functionals depend on the two separate spin-densities, rather than on the total.

While in the uniform limit LDA becomes exact, it is natural to think that for inhomogeneous systems LDA will only provide an accurate approximation if the density $n(r)$ is smooth enough. A scale to measure whether these variations of the density are slow enough

can be found with the help of Fermi's wave vector k_F:

$$\begin{aligned} k_F &= \frac{1}{r_S}\left(\frac{9\pi}{4}\right)^{1/3}, \\ r_S &= \left(\frac{3}{4\pi\bar{n}}\right)^{1/3}, \end{aligned} \tag{2.35}$$

where r_S is the Wigner-Seitz radius, the radius of a sphere which on average contains one electron, and $\bar{n} = N/V$ is the average electronic density for system with N electrons and a volume V. With this we can write

$$\frac{|\nabla n(r)|}{n(r)} \ll k_F. \tag{2.36}$$

This condition is rarely met. For example, close to the nuclei $|\nabla n(r)|/n(r) \gg k_F(r)$. We should expect to be able to apply LDA only to simple metals, like bulk sodium where the density variations are small. However, the LDA provides a great approximation for a wide range of physical and chemical properties. For example, the ground state energies are usually within 1-5% of the experimental values. The molecular geometries and bonding distances typically agree within a 3% error.

We can partially explain the success of LDA looking at the homogeneous electron gas that is used as its base. This system satisfies some exact conditions like the sum rules and scale properties [143]. In contrast, LDA does not have the correct asymptotic behavior when $r \to \infty$. Instead of going like $-1/r$, the LDA XC potential behaves as

$$\lim_{r\to\infty} v_{\mathrm{XC}}^{\mathrm{LDA}} \to\sim e^{-\alpha r}. \tag{2.37}$$

The reason for this wrong behavior is that LDA is not free from self-interactions, which leads to the following problems:

1. The Kohn-Sham energy eigenvalues are too low, with the energy of the highest occupied Kohn-Sham orbital differing around 30-50% with the ionization energy.

2. LDA fails to predict many stable negative ions.

3. $v_{\mathrm{XC}}^{\mathrm{LDA}}$ lacks a discontinuity in its derivative. As a consequence, the band gaps in solids are predicted rather poorly and the predicted dissociation limits in molecules are not accurate.

As a final recap about LDA, we can say that while it generally predicts the correct physical and chemical behavior of the systems, it lacks the accuracy required for most

practical applications, specially in Chemistry. This fact motivated the search for new, more accurate XC functionals.

Generalized Gradient Approximation

One obvious way to try to improve upon then LDA is to make the XC functional depend not only on the density, but also on its gradient. The naive implementation of this idea results in the gradient expansion approximation [106, 131] (GEA), where one assumes that the condition 2.36 holds, allowing one to use the density gradient as a small parameter to expand XC functionals in powers of the density. A popular choice to quantify the density gradient is to use the *reduced density gradient*:

$$s(r) = \frac{|\nabla n(r)|}{2n(r)k_F(r)}. \tag{2.38}$$

This results in energy functionals with the form

$$E_{\mathrm{XC}}^{\mathrm{GEA}}[n] = \int \mathrm{dr}\, \left(e_{\mathrm{XC}}^{h}(n) + C_{\mathrm{XC}}^{(2)}(n)s^2 + ... \right), \tag{2.39}$$

where e_{XC}^{h} is the XC energy per particle of the homogeneous electron gas and the terms $C_{\mathrm{XC}}^{(i)}(n)$ are suitable functions of the density. Sadly, although a great deal of work has been invested to find these functions [54, 143] the results are often even worse than those obtained using LDA. The main reason behind this is the fact that the addition of these terms cause the functional to violate sum rules and exact properties that are however respected by the LDA.

Fortunately, despite the failure of GEAs, a new class of gradient-based approximations to the XC functional appeared, the general gradient approximation [169] (GGA):

$$E_{\mathrm{XC}}^{\mathrm{GGA}}[n_\sigma] = \int \mathrm{dr}\, e_{\mathrm{XC}}^{\mathrm{GGA}}(n_\sigma(r), \nabla n_\sigma(r)). \tag{2.40}$$

Instead of trying to build the functional going through the expansions in terms of the reduced density, what GGA searches for are explicit mathematical expressions for $e_{\mathrm{XC}}^{\mathrm{GGA}}$ that satisfy exact known properties of the functional. With this approach we lose the systematic methodology of the GEAs, as there is no road map to the formulation of $e_{\mathrm{XC}}^{\mathrm{GGA}}$ expressions. This has resulted in the spawn of hundreds of GGAs functionals, many of them quite successful [166, 165, 222].

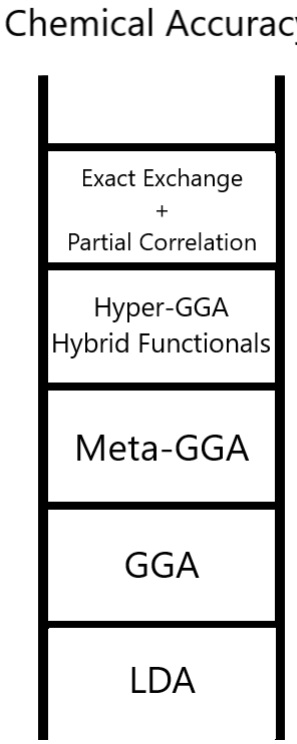

Fig. 2.1 Jacob's Ladder for DFT. Starting from the LDA, each rung represents a new family of XCFs that takes us one step closer to the "heaven" of chemical accuracy.

Jacob's Ladder for the Exchange and Correlation Functionals

These two approaches to approximate the XC functionals, LDA and GGAs, permit to see the pattern that was used for most later developments: add further ingredients, besides the density and the gradient of the density, to the set of dependencies of the functional, in order to increase its accuracy. This suggested John Perdew the metaphor of a "Jacob's Ladder" [168] of approximations. At each step of this ladder we get closer to the desired chemical accuracy – the accuracy considered to be necessary to properly predict chemical properties of materials and molecules, that conventionally is considered to be around 1 kcal/mol. Besides the LDA and GGA that we have just presented, at the moment this ladder has three more rungs. The current steps, from lower to higher are:

1. The local density approximation represents the lower level of the ladder, being determined by n_σ.

2. For the second rung we have the General Gradient Approximation, which includes ∇n_σ.

3. Meta GGA adds $\nabla^2 n_\sigma$ and extra semi non-local functionals of the occupied Kohn-Sham orbitals τ_σ:

$$E_{\mathrm{XC}}^{\mathrm{MGGA}}[n_\sigma] = \int \mathrm{dr}\, e_{\mathrm{XC}}^{\mathrm{MGGA}}(n_\sigma, \nabla n_\sigma, \nabla^2 n_\sigma, \tau_\sigma), \tag{2.41}$$

$$\tau_\sigma(r) = \frac{1}{2}\sum_{i=1}^{\mathrm{occ}} |\nabla \varphi_{i\sigma}|^2. \tag{2.42}$$

4. The hyper-GGA and hybrid functionals add the exact exchange energy density, which is a fully non-local functional of the occupied Kohn-Sham orbitals:

$$e_{\mathrm{X}}^{\mathrm{exact}} = -\frac{1}{2}\sum_{\sigma}\sum_{i,j=1}^{N}\int \mathrm{dr}'\, \frac{\varphi_{i\sigma}^*(r')\varphi_{j\sigma}(r')\varphi_{i\sigma}(r)\varphi_{j\sigma}^*(r)}{|r-r'|}. \tag{2.43}$$

While the whole class of functionals dependent on $e_{\mathrm{X}}^{\mathrm{exact}}$ (besides the dependence on the density and its gradient) is labeled as hyper-GGAs, there is a subclass within it that has seen a widespread use, the hybrid functionals. They are constructed using a fraction $0 < a < 1$ of the exact exchange energy functional and mixing it with LDA or some GGA, like in this example:

$$E_{\mathrm{XC}}^{\mathrm{hybrid}} = aE_{\mathrm{X}}^{\mathrm{exact}} + (1-a)E_{\mathrm{X}}^{\mathrm{GGA}} + E_{\mathrm{C}}^{\mathrm{GGA}}. \tag{2.44}$$

5. Exact exchange coupled with partial correlation, making use of both occupied and non-occupied Kohn-Sham orbitals.

Exchange and Correlation Functionals in Lattice DFT

The XC functionals presented until now were devised for the "normal" DFT, built on the real, continuous space. In this work, however, we will also consider the so-called "lattice models". The branch of DFT that deals with this kind of systems is called site-occupation DFT [78], or simply lattice DFT. In purity, it is the same DFT after all, but it departs from the second quantization Hamiltonian 2.4, and considers a basis change from the continuous creation and annihilation operators to a new discrete set of site operators $d^{\dagger}_{n\sigma}$, $d_{n\sigma}$, corresponding to some chosen basis – the *sites* of the lattice:

$$\begin{aligned}\hat{H} &= \sum_{mn\sigma} t_{mn}\hat{d}^{\dagger}_{m\sigma}\hat{d}_{n\sigma} + \sum_{n} v_n\hat{n}_n + \sum_{mn\sigma\tau} \gamma_{|m-n|}\hat{d}^{\dagger}_{m\sigma}\hat{d}^{\dagger}_{n\tau}\hat{d}_{n\tau}\hat{d}_{m\sigma} \\ &= \sum_{mn\sigma} t_{mn}\hat{d}^{\dagger}_{m\sigma}\hat{d}_{n\sigma} + \sum_{n} v_n\hat{n}_n + \sum_{m\neq n} \gamma_{|m-n|}\hat{n}_m\hat{n}_n + \sum_{m} \gamma_0\hat{n}_{m\uparrow}\hat{n}_{m\downarrow}\,.\end{aligned} \tag{2.45}$$

Here n runs over the number of sites of the lattice, σ corresponds to the spin projection of the operator and the site operators $\hat{d}^{\dagger}_{n\sigma}$, $\hat{d}_{n\sigma}$ fulfill the anti-commutation relations:

$$[\hat{d}_{m\sigma}, \hat{d}^{\dagger}_{n\tau}]_+ = \delta_{mn}\delta_{\sigma\tau}\,, \qquad [\hat{d}^{\dagger}_{m\sigma}, \hat{d}^{\dagger}_{n\tau}]_+ = [\hat{d}_{m\sigma}, \hat{d}_{n\tau}]_+ = 0\,. \tag{2.46}$$

We have considered one-dimensional lattice models, as a starting point for our study of the XC functional problem. One paradigmatic example is the Hubbard model (HM) [121], for its simplicity and popularity. This model was originally proposed to describe solids where the electrons are heavily localized around the atomic nuclei, neglecting the electronic interaction between electrons pertaining to different nuclei. Consequently, in this model the electron-electron interactions only occur when both electrons are in the same site. The one dimensional model takes the form of a chain of length L (that can go up to infinity) with p equidistant sites, and it has the following Hamiltonian:

$$\hat{H} = -t \sum_{\langle m,n\rangle\sigma} \hat{d}^{\dagger}_{m\sigma}\hat{d}_{n\sigma} + \sum_{n} v_n\hat{n}_n + U_{\mathrm{HM}} \sum_{n} \hat{n}_{n\uparrow}\hat{n}_{n\downarrow}\,, \tag{2.47}$$

where $\langle m,n\rangle$ denotes summation over nearest neighbors only and $\hat{n}_{n\sigma} = \hat{d}^{\dagger}_{n\sigma}\hat{d}_{n\sigma}$ is the density operator for the site n with spin σ. The first term corresponds with the kinetic operator in a lattice $\hat{T}$ and it is determined by the parameter t, the second one describes the external potential $\hat{V}$ as a function of the values v_m on each site of the lattice, and the last term describes

the electron-electron interaction on the sites, defined by the parameter U_{HM}. Depending on the form of the kinetic term on the extremes of the lattice, we can have periodic boundary conditions or open boundary conditions.

The 1DHM can be solved (under certain conditions) using the Bethe ansatz [13]. This fact is used in the construction of the Bethe ansatz local density approximation (BALDA), an XC functional that departs from the same idea of using the homogeneity as the LDA, but substitutes the electron gas system for the 1DHM accurately solved with the Bethe ansatz. The homogeneity is ensured if $\hat{V} = 0$, and the parameters t and U_{HM} are the same for every site of the (infinite) chain. This results in the following expressions for the BALDA XC energy functional $E_{\mathrm{XC}}^{\mathrm{BALDA}}$:

$$E_{\mathrm{XC}}^{\mathrm{BALDA}}(n,U) = \sum_n (\varepsilon^{\mathrm{hom}}(n_n,U) - \varepsilon^{\mathrm{hom}}(n_n,0)), \tag{2.48}$$

where $\varepsilon^{\mathrm{hom}}(n_n,U)$ denotes the energy per site of an infinite 1DHM with interaction parameter U and constant density n_n, and the sum is carried over the p sites of the lattice. As we can see from Eq. 2.48, to compute the XC energy we subtract the energy of the non interacting 1DHM from that of the interacting one with $U_{\mathrm{HM}} = U$. Using Lima et al.'s [124] parameterization of BALDA, the energy per site for the homogeneous infinite 1DHM with constant density $\tilde{n}$ is expressed as

$$\varepsilon^{\mathrm{hom}}(\tilde{n},U) = \theta(1-\tilde{n})\varepsilon_{<}^{\mathrm{hom}}(\tilde{n},U) + \theta(\tilde{n}-1)\varepsilon_{>}^{\mathrm{hom}}(\tilde{n},U), \tag{2.49a}$$

$$\varepsilon_{<}^{\mathrm{hom}}(\tilde{n},U) = -\frac{2\beta(U)}{\pi}\sin\left(\frac{\pi\tilde{n}}{\beta(U)}\right), \tag{2.49b}$$

$$\varepsilon_{>}^{\mathrm{hom}}(\tilde{n},U) = (\tilde{n}-1)U + \varepsilon_{<}^{\mathrm{hom}}(2-\tilde{n},U), \tag{2.49c}$$

where the subindexes $\lessgtr$ denote whether $\tilde{n} \lessgtr 1$, θ is the Heaviside function and $\beta(U)$ is an auxiliary function found solving the equation

$$-\frac{2\beta(U)}{\pi}\sin\left(\frac{\pi}{\beta(U)}\right) = -4\int_0^\infty \mathrm{dx}\,\frac{J_0(x)J_1(x)}{x[1+\exp(Ux/2)]}, \tag{2.50}$$

where $J_0(x)$ and $J_1(x)$ are the zero-th and first order Bessel functions.

From Eq. 2.49a one can see that the functional presents a cusp appearing at $\tilde{n} = 1$. This implies a discontinuity in its derivative, that in turn results in a discontinuity in the Kohn-Sham potential. Although this feature of the BALDA functional has in fact proven be useful for some purposes (for example, in order to calculate the Mott gap [31]), the exact XC functional does not have this discontinuity. Furthermore, this cusp can make the Kohn-Sham

calculations difficult to converge when we are dealing with densities close to the discontinuity. The solution that we chose for this problem was suggested by Kurth et al. [114], and consists on the use a smoothing function around the conflicting range of densities.

2.2 Time Dependent Density Functional Theory

In the previous section we reviewed the DFT formalism for an interacting nonrelativistic electron system. This formalism is only valid to study ground-state problems. For the project presented in chapter 4, however, we have required the simulation of time-dependent phenomena, i.e. clusters irradiated with laser fields. For this reason, we briefly describe now the expansion of the DFT formalism to include the time evolution of this class of systems. The extension of the theory valid for this purpose is called time dependent density functional theory (TDDFT).

To take into account this new situation, we modify the external potential $\hat{V}$ of the Hamiltonian 2.23 making it time dependent:

$$\hat{V}(t) = \sum_{i=1}^{N} v_i(\hat{r}_i, t). \tag{2.51}$$

Neither the kinetic operator $\hat{T}$ nor the interaction operator $\hat{W}$ change. Now we can write the Hamiltonian as

$$\begin{aligned} \hat{H} &= \hat{T} + \hat{V}(t) + \hat{W} \\ &= -\frac{1}{2}\nabla^2 + \sum_{i=1}^{N} v_i(\hat{r}_i, t) + \frac{1}{2}\sum_{\substack{i,j \\ i\neq j}}^{N} \frac{1}{|\hat{r}_i - \hat{r}_j|}. \end{aligned} \tag{2.52}$$

For an N-electron system with an initial state Ψ_0, the many-body time-dependent Schrödinger equation describes its evolution:

$$i\frac{\partial}{\partial t}\Psi(x_1, x_2, ..., x_N, t)(t) = \hat{H}(t)\Psi(x_1, x_2, ..., x_N, t). \tag{2.53}$$

Once again, as it happens in the static case, the solution of this equation, despite its formal simplicity, becomes numerically impossible due to the large size of the wave function as soon as the number of particles is not very small.

2.2.1 Runge-Gross van Leeuwen Theorems

At the core of TDDFT there are two theorems which we will briefly recall in this section. The first one is the fundamental existence theorem for TDDFT and was demonstrated by Runge and Gross in 1984 [179] (check section 3.2 from Ref. [209] for a detailed proof):

Runge-Gross theorem. *Two densities $n(r,t)$ and $n'(r,t)$ evolving from a common initial many-body wave function Ψ_0 under the influence of two different external potentials $v(r,t)$*

and $v'(r,t) \neq v(r,t) + C(t)$ (both of them assumed Taylor-expandable around t_0), will start to become infinitesimally different after t_0. Therefore, there is a one to one correspondence between densities and potentials for any fixed initial state Ψ_0.

This one to one correspondence implies that the time-dependent density is a functional of the external potential, $n(r,t) = n[v](r,t)$, and the converse is also true: the external potential v is also a functional of the time-dependent density. If $v(r,t) = v[n](r,t)$, then the full Hamiltonian $\hat{H}(t)$ and the many-body wave function $\Psi(t)$ are also functionals of $n(r,t)$. In conclusion, the expectation values of all the observables $\hat{O}(t)$ become functionals of the density:

$$O[n,\Psi_0](t) = \langle \Psi[n,\Psi_0] | \hat{O}(t) | \Psi_0[n,\Psi_0] \rangle \,, \tag{2.54}$$

where here we have also explicitly considered the dependence on the initial state Ψ_0.

From the Runge-Gross theorem we learn that, if we know the time-dependent density of a system, we could in principle evaluate any observable of a many-body system. The setback of this theorem is, of course, that it does not tell us a way to write the observables as a function of the time-dependent density.

Other caveats of Runge-Gross theorem are the fact that the external potentials have to be expandable in a Taylor series around t_0, and the requirement for the externals potentials to be scalar (leaving out the important situations where we have vector potentials). The first problem is more a theoretical nuisance than a practical issue, but to tackle the second problem, and being able to encompass magnetic perturbations, etc., one needs to expand the theory to the so-called *time-dependent current-DFT*, which is out of the scope of this thesis. For a more detailed explanation of these problems, check Ref. [209].

In any case, now that we know that we can express any many-body observable as a functional of the time-dependent density, the next step is to find a practical way to compute this functional. The obvious route to follow is to attempt a Kohn-Sham route similar to the one of ground-state DFT, i.e. to substitute the interacting system with a non interacting one that reproduces the same density like we did in DFT. The question of the existence of this non interacting ("Kohn-Sham") system is answered by the van Leeuwen theorem [212]:

van Leeuwen theorem. *For a time-dependent density $n(r,t)$ associated with a many-body system with particle-particle interaction $w(|r-r'|)$, external potential $v(r,t)$ and initial state Ψ_0, there exists a different many-body system with an interaction $w'(|r-r'|)$ and a unique external potential $v'(r,t)$ (up to a purely time-dependent $C(t)$) which reproduces the same time-dependent density $n(r,t)$. The initial state Ψ_0' in this system must be chosen such that it correctly yields the given density and its time derivative at the initial state.*

If we make $w = w'$ and $\Psi_0 = \Psi'_0$, the van Leeuwen theorem states that there exists a unique potential $v'(r,t)$ that generates the time-dependent density $n(r,t)$, i.e., we recover the Runge-Gross theorem as a consequence of this one.

The new theorem, however, contains more information, if we now consider $w' = 0$, i.e., a non interacting system. Assuming the existence of an initial non interacting state $\Psi'_0 \equiv \Phi_0$ with the appropriate $n(r,t_0)$ and its first time derivative, there is a unique potential $v_S(r,t)$ in a non interacting system that produces the same time-dependent density $n(r,t)$ of the real system, at times $t > t_0$. Therefore, the theorem of van Leeuwen is a positive answer to the question of the non-interacting time-dependent v-representability problem. Of course, it is an *existence* theorem, and it provides no recipe to the construction of the Kohn-Sham potential. For an in depth analysis of these issues, check [209].

2.2.2 Time-Dependent Kohn-Sham Equations

From the van Leeuwen theorem we know that the time evolution of a density $n(r,t)$ from an interacting system can be reproduced by a non-interacting system evolving under the effective potential

$$v_S = v_S[n, \Psi_0, \Phi_0](r,t), \tag{2.55}$$

where Ψ_0 is the initial state of the real, interacting system, and Φ_0 is the initial state of the non-interacting system. This notation stresses the fact that, in general, the time-dependent Kohn-Sham potential v_S is a functional of those two objects.

This dependency on Ψ_0 and Φ_0 can be safely ignored, however, in the case in which the system departs at t_0 from the ground state – in fact, the most common scenario. In that case, both initial wave functions are in fact functionals of the ground state density. Therefore, most TDDFT calculations start in fact with a previous ground-state DFT calculation, i.e. the solution of the Kohn-Sham equations, in order to find a single Slater determinant, as described in section 2.1.3, formed by the Kohn-Sham orbitals φ_i^0.

From $t = t_0$ on, the evolution of the *real* system is driven by the action of $v(r,t)$, whereas the evolution of the *fictitious* Kohn-Sham system is driven by the action of $v_S(r,t)$. Both gives rise to the time-dependent density $n(r,t)$, that can be computed from the Kohn-Sham orbitals:

$$n(r,t) = \sum_{i=1}^{N} |\varphi_i(r,t)|^2, \tag{2.56}$$

These time-dependent Kohn-Sham orbitals $\varphi_i(r,t)$ follow the time-dependent Kohn-Sham (TDKS) equation:

$$\begin{aligned}\left[-\frac{1}{2}\nabla^2 + v_S[n](r,t)\right]\varphi_i(r,t) &= i\frac{\partial}{\partial t}\varphi_i(r,t),\\ \varphi_i(r,t_0) &= \varphi_i^0(r)\,,\end{aligned} \tag{2.57}$$

where the time-dependent Kohn-Sham Hamiltonian is defined by

$$H_{\mathrm{KS}}[n](r,t) = -\frac{1}{2}\nabla^2(r) + v_S(r,t)\,. \tag{2.58}$$

The time-dependent effective potential for this equation, also known as Kohn-Sham potential, is unknown. In analogy to the ground-state case, it is typically split into some known pieces, and a remaining exchange and correlation potential:

$$v_S[n](r,t) = v(r,t) + v_{\mathrm{H}}[n](r,t) + v_{\mathrm{XC}}[n](r,t), \tag{2.59}$$

where $v_{\mathrm{H}}[n](r,t)$ is the time-dependent Hartree potential:

$$v_{\mathrm{H}}[n](r,t) = \int \mathrm{d}r'\,\frac{n(r',t)}{|r-r'|}. \tag{2.60}$$

Eq. 2.59 serves as the definition of the time-dependent Kohn-Sham exchange and correlation potential.

Once again, from a formal point of view the TDKS equation produces the exact density $n(r,t)$ for a N-electron system evolving under the influence of an external potential $v(r,t)$ starting from the ground state. However, one requires multiple approximations to turn this formalism into a practical method: the ground-state $v_{\mathrm{XC}}[n_0](r)$ for the calculation of the initial state, the time-dependent $v_{\mathrm{XC}}[n](r,t)$ for the time evolution of the system, and probably a further approximation to relate the evolving density to the required observable.

A typical TDDFT review would include now a reformulation of the TDDFT equations shown above in the linear response case, i.e. in the case in which the perturbation applied to the system is weak. The linear response formalism of TDDFT [33, 224, 77, 95] has been the most successful, and it allows to compute linear response properties of atoms, molecules, and materials (polarizabilities, susceptibilities, ...). However, in this thesis work we have not used it, requiring only the real-time equations shown above.

2.2.3 Adiabatic Local Density Approximation

Just like in DFT, we need suitable approximations for the time-dependent Kohn-Sham functional $v_{\mathrm{XC}}[n](r,t)$. Note, however, that this is in principle a much more difficult task, because v_{XC} depends in fact on the full history of the density: the value of v_{XC} depends on the value of the density at all times $t' \leq t$. The memory-dependence problem of TDDFT is one of the most pressing and difficult ones [138].

Most applications of TDDFT have however ignored this issue, assuming the *adiabatic approximation*. In this way, the most straightforward way to create TDDFT XC functionals is to take those from DFT and apply them to the TDKS equation, evaluating them with the time-dependent density $n(r,t)$ instead of with the ground n_0.

The most basic one would be the adiabatic local density approximation (ALDA), one of the most widely spread XC functionals and the one that we have used for the TDDFT calculations presented in this thesis. This functional uses the LDA from DFT as its basis. The XC potential is therefore given by:

$$v_{\mathrm{XC}}^{\mathrm{ALDA}}(r,t) = \frac{de_{\mathrm{XC}}^{h}(\bar{n})}{d\bar{n}}|_{\bar{n}=n(r,t)}, \tag{2.61}$$

where $e_{\mathrm{XC}}^{h}(\bar{n})$ is the XC energy of a homogeneous electron electron gas with particle density $\bar{n}$. In other words, ALDA is constructed taking the XC potential at the point r and time t corresponding to the homogeneous electron gas of density $n(r,t)$.

Let us briefly discuss the applicability of ALDA. First, of all, it should only work for systems and situations for which the LDA is already valid. After all, the errors present in the underlying ground state functional (in this case the ALDA) are carried on to the adiabatic extension (the exponential decay of the XC potential instead of the $-1/r$ behavior of the exact potential, for example). In addition, any adiabatic extension of a static DFT functional should only work for systems that fulfill the adiabatic theorem of quantum mechanics, that is, those where the perturbations affecting them are slow enough. Another way to put it is saying that using adiabatic functionals means that we are ignoring any possible memory effect. It turns out that in many circumstances, in particular when high intensity fields are used as perturbations, this requirement is not met. Nonetheless ALDA has proved to be a good solution, even for problems that are apparently far removed from its theoretical range of applicability [82, 23, 214, 210].

2.3 Ehrenfest Dynamics

Now that we know how to approach the electronic part of a system (both its ground state with DFT and its time evolution with TDDFT), we turn to the problem of a full system formed by both electrons and nuclei.

Molecular Dynamics (MD) is the discipline that considers the atoms as classical particles moving in force fields that take into account the effect of the electrons. Therefore the main computational task required for MD is the integration of the classical Hamiltonian equations of motion. If these force fields are pre-established, we are talking about "classical" MD, but when the forces that act on the nuclei are computed at the time of the propagation, we have an "ab initio" or first principle MD. In both cases, one is only concerned with the dynamics of the classical nuclei: the electrons, considered in the adiabatic approximation, are always in the ground state corresponding to the nuclear configuration at each time. However, if one needs to consider excited states of the electrons, a non-adiabatic version of MD is needed. This implies the use of truly hybrid classical-quantum models, where the mixed degrees of freedom of the classical part and the quantum part of the system evolve simultaneously, and coupled to each other. This section is dedicated to one of this models: the so-called Ehrenfest Molecular Dynamics, sometimes also called "mean-field Ehrenfest dynamics", or simply "quantum-classical MD" [18].

We have used this variant of non-adiabatic MD – in combination with TDDFT to describe the electronic part of the system – to tackle the problems presented in this thesis (chapter 4) for several reasons:

1. It is a non-adiabatic form of molecular dynamics: this means that the treatment of phenomena like electron emission or excited states arise naturally within this formalism, unlike in the adiabatic Born-Oppenheimer approximation. It should be stressed that the term *adiabatic* here does not relate to the adiabatic approximation of the XC functions, described previously. In this case, a system behaves adiabatically if the electrons are constantly in the ground state corresponding to each instantaneous nuclear configuration.

2. It is a mixed classical-quantum approximation: the nuclei are treated as classical objects while the electrons receive a full quantum approach, which allows the description of (some) quantum effects while keeping our simulations at a relatively low computational cost. The first application of Ehrenfest dynamics that we could find in the literature was presented by Mittleman in 1961 [148].

3. The mix of Ehrenfest dynamics and TDDFT has proven to be a popular and useful tool for the electronic structure and quantum chemistry communities [206, 2].

The derivation of EMD is based on two approximations: 1) first, one separates the electronic and nuclear parts of the system, obtaining the "time-dependent self-consistent model" [68]; and 2) then, one takes the classical limit for the nuclear equations using the short wave asymptotics idea [216, 110, 21]. Check Ref. [18] for a rigorous discussion of this procedure. In its basic implementation the state of the system is determined by a set of classical position and momentum variables $\{R,P\} = \{R_\alpha, P_\alpha\}_{\alpha=1}^{M}$ for the nuclei, and the many-electron wave function Ψ for the electrons. This results in the following equations of motion:

$$-i\frac{\mathrm{d}}{\mathrm{dt}}|\Psi(t)\rangle = \hat{H}(R(t),t)|\Psi(t)\rangle\,, \tag{2.62a}$$

$$\dot{R}_\alpha = \frac{1}{m_\alpha}P_\alpha\,, \tag{2.62b}$$

$$\dot{P}_\alpha = F_\alpha[R(t),\Psi(t),t]\,, \tag{2.62c}$$

where the latin indexes run over the N electrons, the greek ones run over the M nuclei, m_α is the mass of the α-th nucleus, $\hat{H}$ is the Hamiltonian of the electronic system, and F_α is the force that it experiments, given by:

$$F_\alpha[R(t),\Psi(t),t] = -\langle\Psi(t)|\frac{\partial\hat{H}}{\partial R_\alpha}(R(t),t)|\Psi(t)\rangle\,. \tag{2.63}$$

Usually, the derivative of the Hamiltonian with respect to the nuclear positions is given by a one-body multiplicative potential in real space:

$$\frac{\partial H}{\partial R_\alpha}(R(t),t) = \sum_{i=1}^{N}\frac{\partial v(\hat{r}_i;R(t),t)}{\partial R_\alpha} \tag{2.64}$$

where v is the external potential that the electrons see, i.e. it includes the nuclear interaction and possibly an external field. The expectation value that provides the force can then be written explicitly in terms of the density:

$$F_\alpha[R(t),\Psi(t),t] = -\int\mathrm{dr}\, n(r,t)\frac{\partial v(r;R(t),t)}{\partial R_\alpha} \tag{2.65}$$

As we can see from Eqs. 2.62, the classical description of the nuclei is carried out by Newton's equations while the Schrödinger equation deals with the electrons. Here, the interplay between classical and quantum components of the system is codified in the forces

F_α experimented by the nuclei – as they take into account the effect of the electrons through its dependence on Ψ –, and in the electronic Hamiltonian $\hat{H}$, that depends on the nuclear position coordinates.

EMD is non-adiabatic: if one casts the equations written above into the *adiabatic basis* (the R-dependent eigenstates of the electronic Hamiltonian), it is easy to see that the coefficients change in time due to the presence of non-adiabatic couplings between the different excited states).

The previous equations use the wave function as the fundamental object to describe the electrons; in the previous subsection we have seen how one can do away with it and substitute it with the electronic density. Here, one may also combine TDDFT with EMD, in order to arrive to a model that is computationally easier. These are the equations that we have used when dealing with time evolving systems:

$$-i\frac{\mathrm{d}}{\mathrm{dt}}|\varphi_i\rangle = \hat{H}_{\mathrm{KS}}(R(t),t)|\varphi_i\rangle\,, \tag{2.66a}$$

$$\dot{R}_\alpha = \frac{1}{m_\alpha}P_\alpha\,, \tag{2.66b}$$

$$\dot{P}_\alpha = -\int \mathrm{dr}\; n(r,t)\frac{\partial v(r;R(t),t)}{\partial R_\alpha}\,, \tag{2.66c}$$

where, as usual, $\{\varphi_i\}$ are the Kohn-Sham orbitals, and $\hat{H}_{\mathrm{KS}}$ is the Kohn-Sham Hamiltonian. Note that it is the fact the the force is an explicit functional of the density what permits to use, without further approximation, the Kohn-Sham system as a substitute for the real one, and do EMD with it.

2.4 Numerical propagators for Systems of Ordinary Differential Equations

Up to this point we have studied formalisms to find the ground state of a many electron system, and describe its evolution in time. Then, we have seen how to couple this quantum system to a classical one representing the nuclei, thus creating a hybrid classical-quantum, non-adiabatic molecular dynamics model. Now we turn our attention to the practical implementation of this theory. In particular, how to actually propagate the TDKS and Ehrenfest equations (2.57 and 2.66, respectively).

In order to do this we will have to use a numerical propagator suitable for these equations of motion. There is a great variety of families of propagators to choose from, and ample room for improvement. That is the reason that has motivated our work in the subject. In this section, we will first present the generalities about the methods to solve ordinary differential equations (ODEs). Then, we will present the four families of numerical propagators that we have studied, implemented and used in this thesis work (see chapter 5) . For a more detailed discussion about ODEs and their numerical propagation, check Refs. [80, 81].

2.4.1 General Properties of Numerical Propagators

Hamilton's equations of motion for a set of classical variables make up a system of ODEs; Schrödinger's and the TDKS equations are partial differential equations (PDEs) that, however, upon discretization, are converted into a set of ODEs, too. The combination of both, therefore, is also a set of ODEs. In general, a set of ODEs has the form:

$$\dot{y}(t) = f(y(t),t)\,, \tag{2.67}$$

$$y(t_0) = y_0\,. \tag{2.68}$$

Notice that in this definition, the so-called *dynamical function* f depends on the system state at time t only, and not on previous states. In consequence, the TDKS equations actually belong to the more general group of *time delayed differential equations* if the XC functional takes into account memory effects, but as we will only use ALDA (an adiabatic functional) in this thesis, the study of ODEs will suffice. A great amount of literature about how to propagate this kind of equations has been written since the times of Newton, Euler or Lagrange, and we can apply all that knowledge to our problem.

There are many ways to categorize the approaches to the propagation of ODEs, but we will split the numerical integrators following these two criteria:

1. Number of previous steps required: If a propagation method only needs the knowledge of the previous solution at time $t-\Delta t$ to approximate the function y at time t, we say that it is a one-step method. Conversely, if it needs the solutions at times $t-\Delta t, t-2\Delta t, ..., t-s\Delta t$ it falls in the category of multistep methods, with s being the number of previous steps required.

2. Solution of a nonlinear algebraic system of equations: If an integration method implies the solution of a possibly nonlinear algebraic system of equations to approximate $y(t)$, it is an implicit method. On the other hand, if no such system is present, we have an explicit method.

This last division is important when we deal with "stiff equations". The definition of what is a stiff equation is up to debate even nowadays, and so we just settle with the pragmatic "a stiff equation is one for which implicit methods of propagation notably outrank the explicit ones". This is important because the kinetic operator $\hat{T}$ of the Kohn-Sham Hamiltonian is often considered a source of stiffness in the TDKS equations, and we often find problems where the explicit methods break down for this reason. Another advantage of the implicit methods is that they are generally better than their explicit counterparts at preserving the structural properties of a system, a very desirable quality as it improves the accuracy of the conserved magnitudes for long propagations. On the other hand, the use of implicit propagators implies the need to solve a nonlinear algebraic system of equations, an overhead that the explicit methods do not have, and that considerably hurts their performance.

The solution to an ODE system such as the one given by Eqs. 2.67, can be written in terms of a nonlinear evolution operator, denominated "flow", defined as

$$\Phi_t(y(t-\Delta t)) = y(t)\,. \tag{2.69}$$

This is the operator that one has to approximate, i.e. the propagating algorithm effectively defines a *numerical flow*:

$$\tilde{\Phi}_t(y(t-\Delta t)) = y(t)\,. \tag{2.70}$$

For the multistep methods, one actually must use a more general numerical flow definition, one that depends on several previous time steps.

To clarify some ideas, let us restrict the problem for the moment to linear equations with the form

$$\dot{\varphi}(t) = -iH(t)\varphi(t), \tag{2.71}$$

where $H(t)$ is a Hamiltonian and φ is its associated wave function. As it is linear, we can write its solution as:

$$\varphi_i(t) = \hat{U}(t, t-\Delta t)\varphi_i(t-\Delta t), \tag{2.72}$$

for a discrete time step Δt (which we will consider constant through this thesis), and where the (time ordered) evolution linear operator $\hat{U}$ is given by:

$$\hat{U}(t, t-\Delta t) = \mathscr{T} \exp\left\{-i \int_{t-\Delta t}^{t} \mathrm{d}\tau\, \hat{H}(\tau)\right\}. \tag{2.73}$$

The symbol $\mathscr{T}$ exp represents the time-ordered exponential. [Note that, as the TDKS equations are nonlinear, a linear evolution operator that drives the orbitals from $\varphi_i(t-\Delta t)$ to $\varphi_i(t)$ does not exist.]

The election of a specific method for the propagation of ODEs in general, and the TDKS equations in particular, is usually conditioned by the performance and stability of the algorithm. By performance we mean the time required by our computers to propagate the equations to a certain point in time. The stability of a propagator is related to whether or not the error in the propagation grows exponentially after a given number of time steps. One can give a simple definition of stability for linear ODEs: a propagator is stable below $\Delta t_{\max}$ if, for any $\Delta t < \Delta t_{\max}$ and $n > 0$, $\hat{U}^n(t+\Delta t, t)$ is uniformly bounded. We can ensure the stability of the integrator by making it contractive, i.e., $||\hat{U}(t+\Delta t)|| \leq 1$. If the propagator is unitary, it follows that it is contractive, but for the schemes that are only approximately unitary it is better if, at least, they are contractive. Unconditional stability is also defined for the cases where the stability of the algorithm is ensured, regardless of both Δt and the spectrum of $\hat{H}$. Although decreasing the time step generally improves the stability of the method (at the cost of decreasing its performance), in some cases certain integrators will never be able to achieve long term stability, specially if the systems are stiff.

Another issue to consider when choosing or developing a propagator is whether or not it preserves some of the properties of the equation that is to be solved. For example, for linear systems with Hermitian Hamiltonians, we know that the propagation should be unitary:

$$\hat{U}^{\dagger}(t, t-\Delta t) = \hat{U}^{-1}(t-\Delta t, t). \tag{2.74}$$

This conditions ensures the orthonormality of the orbitals $\{\varphi\}$ during the propagation. This is important because it ensures that stability mentioned above; a method that does not fulfill this condition would have to orthogonalize regularly the wave functions, and the cost of this operation scales as N^3.

Another useful property that a propagator may or not respect, is time reversibility:

$$\hat{U}(t,t-\Delta t) = \hat{U}^{-1}(t,t-\Delta t). \tag{2.75}$$

This is true for systems that do not contain magnetic fields or spin-orbit couplings.

Finally, another important property that we will pay special attention to is symplecticity. This may be a property of the ODE system, and may or not be respected by the numerical integrators [79]. Part of the work developed in section 5.1.1 is directly related to this concept. The concept is very general, and can be predicated of any differentiable map in an even-dimensional real space: We say that a differentiable map $g : \mathbb{R}^{2n} \to \mathbb{R}^{2n}$ is symplectic if and only if

$$\frac{\partial g}{\partial y}^T J \frac{\partial g}{\partial y} = J\,, \qquad J = \begin{bmatrix} 0 & I_n \\ -I_n & 0 \end{bmatrix}, \tag{2.76}$$

where I_n is the identity matrix in n dimensions. For any system of ODEs, the flow [Eq. 2.69] is a differentiable map. For a flow to be symplectic, first we need that the system is formed by an even number of real equations. Classical Hamiltonian systems have by definition an even number of variables; quantum systems are actually defined in complex spaces and thus the definition would not seem to apply; however, for complex systems we can always divide them into their real and imaginary parts, and the resulting equivalent real ODE system will always fulfill the even number of dimensions condition.

It may then be proved [172, 79] that a differentiable map is Hamiltonian if and only if it is Hamiltonian, i.e. one can find a system of coordinates that makes the equations take the form

$$\dot{y} = J^{-1}\nabla H(y)\,, \tag{2.77}$$

where $y \in \mathbb{R}^{2n}$ and the Hamiltonian H is a scalar function of y. Dividing $y = (q,p)^{\mathrm{T}}$ we get the famous Hamilton equations of motion

$$\dot{q}_i = \quad \frac{\partial H(p,q)}{\partial p_i}\,, \tag{2.78a}$$

$$\dot{p}_i = -\frac{\partial H(p,q)}{\partial q_i}\,, \tag{2.78b}$$

with q_i and p_i being the elements of the vectors q and p respectively. The relevance of the symplecticity resides in its theoretical implications: for example, a symplectic system conserves the volume in phase space.

Regarding the Schrödinger equation

$$i\frac{\mathrm{d}}{\mathrm{d}t}|\Psi(t)\rangle = \hat{H}|\Psi(t)\rangle\,, \tag{2.79a}$$

$$|\Psi(0)\rangle = |\Psi_0\rangle\,, \tag{2.79b}$$

one can prove that it also forms a Hamiltonian system and thus it is symplectic. In order to do so, one expands the wave function into the orthonormal basis set $|\Psi_i\rangle$

$$|\Psi(t)\rangle = \sum_i c_i(t)|\Psi_i\rangle\,, \tag{2.80}$$

where $c_i(t) = \langle\Psi_i|\Psi(t)\rangle$. We can then rewrite Eq. 2.79a as

$$\dot{c} = -iHc\,, \tag{2.81a}$$

$$c_i(0) = \langle\Psi_i|\Psi_0\rangle\,, \tag{2.81b}$$

where the Hamiltonian matrix H is defined by $H_{ij} = \langle\Psi_i|H|\Psi_j\rangle$, and c is the vector formed by the time-dependent coefficients $\{c_i(t)\}$. Now we divide the coefficients into their real and imaginary part

$$c_i = \tfrac{1}{\sqrt{2}}(q_i + ip_i)\,, \tag{2.82}$$

i.e., $q_i = \sqrt{2}\,\Re c_i$, $p_i = \sqrt{2}\,\Im c_i$. This allows us to define the Hamiltonian function

$$H(q,p) = \langle\Psi(q,p)|\hat{H}|\Psi(q,p)\rangle\,. \tag{2.83}$$

Notice that, if $\hat{H}$ is Hermitian, then $H(q,p)$ has to be real. Also, if we denote $\Re H$ and $\Im H$ to the real and imaginary parts of the matrix representation of $\hat{H}$ in the chosen orthonormal basis, the hermiticity implies $\Re H^{\mathrm{T}} = \Re H$ and $\Im H^{\mathrm{T}} = -\Im H$. One may then arrive at:

$$H(q,p) = \tfrac{1}{2}q^{\mathrm{T}}\Re H q + \tfrac{1}{2}p^{\mathrm{T}}\Re H p + p^{\mathrm{T}}\Im H q\,. \tag{2.84}$$

Its partial derivatives are

$$\frac{\partial H(q,p)}{\partial q_i} = \sum_j \left(\Re H_{ij}q_j - \Im H_{ij}p_j\right)\,, \tag{2.85a}$$

$$\frac{\partial H(q,p)}{\partial p_i} = \sum_j \left(\Re H_{ij}p_j + \Im H_{ij}q_j\right)\,. \tag{2.85b}$$

We can now rewrite Eqs. 2.81a as

$$\dot{q}_i + i\dot{p}_i = -i\sum_j (\Re H_{ij} + i\Im H_{ij})(q_j + ip_j)\,, \tag{2.86}$$

Comparing these equations to Eqs. 2.85, we see that the Schrödinger equation indeed forms a Hamiltonian system, and is therefore symplectic.

When we use a propagator to approximate the flow of a system of ODEs, the numerical flow that is effectively defined by the propagator may or may not be also symplectic. These should be preferred for theoretical reasons, but also for practical considerations: for example, the conservation of constant of motions such as the energy is much better with symplectic schemes than with non-symplectic ones [12].

2.4.2 Runge-Kutta Methods

In 1768, Euler proposed a method [57] to solve the initial value problem given by Eqs. 2.67. It consisted in dividing the interval of integration in $n+1$ steps $\{t_0, t_1, ..., t_n\}$, and then replacing the exact solution of the equation with the first term of the Taylor expansion of $f(y,t)$, obtaining

$$\begin{aligned} y_1 - y_0 &= (t_1 - t_0) f(y_0, t_0), \\ y_2 - y_1 &= (t_2 - t_1) f(y_1, t_1), \\ &\cdots \\ y_n - y_{n-1} &= (t_n - t_{n-1}) f(y_{n-1}, t_{n-1}). \end{aligned} \tag{2.87}$$

where y_i approximates $y(t_i)$. Introducing the notation for the steps $h_i = t_{i+1} - t_i$, we can write the Euler method as

$$y_{i+1} = y_i + h_i f(y_i, t_i). \tag{2.88}$$

In the following, we will only consider constant subdivisions of the integration interval: $h_i = h$.

Euler's method is a first order integrator, which means that its error is directly proportional to the step size h, and thus it is highly inefficient if we need high accuracies. Let us consider the case where $\dot{y}(t) = f(t)$, i.e., when f is independent of y. The solution is then simply given by the quadrature problem

$$y(t_n) = y_0 + \int_{t_0}^{t_n} \mathrm{dt}\, f(t). \tag{2.89}$$

In order to integrate this problem numerically, we can for example use the first Gauss formula (or midpoint rule), defined by

$$\begin{aligned} y_1 &\sim y_0 + hf\left(t_0 + \frac{h}{2}\right), \\ y_2 &\sim y_1 + hf\left(t_1 + \frac{h}{2}\right), \\ &\dots \\ y_n &\sim y_{n-1} + hf\left(t_{n-1} + \frac{h}{2}\right). \end{aligned} \tag{2.90}$$

This is an order 2 integrator, i.e. the global error is of order $\mathscr{O}(h^2)$. In 1895, C. Runge [178] wondered if this method could be extended to deal with the more general problem 2.67. For our first step one would have

$$y_1 \sim y_0 + hf(y(t_0 + \frac{h}{2}), t_0 + \frac{h}{2})), \tag{2.91}$$

but we don't know the value of $y(t_0 + h/2)$. The idea is to use Euler's method with step size $h/2$ to compute it. In this way, one obtains the following method:

$$\begin{aligned} k_1 &= f(y_n, t_n), \\ k_2 &= f(y_n + \frac{h}{2}k_1, t_n + \frac{h}{2}), \\ y_{n+1} &= y_n + hk_2. \end{aligned} \tag{2.92}$$

Although we are using Euler's method to find k_2, the error is not linear for the the computation of y_{n+1}, but quadratic thanks to the extra h factor that multiplies it. By comparing the Taylor expansion of 2.92 with the corresponding expansion of the exact solution, one can find that the error at each step grows proportionally to h^3, and therefore the general error of this method grows as h^2, i.e., it is an order 2 method.

The generalization of the previous process was presented by W. Kutta in 1901 [115], giving birth to what is now called the family of Runge-Kutta (RK) methods:

Runge-Kutta Methods. *Let s be an integer (the number of stages), and let $\{a_{ij}\}_{i,j=1}^{s}$, $\{b_i\}_{i=1}^{s}$ and $\{c_i\}_{i=2}^{s}$ be sets of real coefficients. The s-stages Runge-Kutta method is defined*

by:

$$\begin{aligned}
k_1 &= f(y_n + h\sum_{j=1}^{s} a_{1j}k_j, t_n + c_1 h),\\
k_2 &= f(y_n + h\sum_{j=1}^{s} a_{2j}k_j, t_n + c_2 h,),\\
&\ldots,\\
k_i &= f(y_n + h\sum_{j=1}^{s} a_{ij}k_j, t_n + c_i h),\\
&\ldots,\\
y_{n+1} &= y_n + h\sum_{i=1}^{s} b_i k_i.
\end{aligned} \tag{2.93}$$

The choice of the number of stages s, and the coefficients a_{ij}, c_i and b_i determine the precise method among all the (infinite) possibilities of this family. Since Butcher's paper from 1964 [26], it is customary to present these methods using what has come to be called Butcher's tableau:

$$\begin{array}{c|cccc}
c_1 & a_{11} & a_{12} & \ldots & a_{1s}\\
c_2 & a_{21} & a_{22} & \ldots & a_{2s}\\
\vdots & \vdots & \vdots & \ddots & \vdots\\
c_s & a_{s1} & a_{s2} & \ldots & a_{ss}\\
\hline
 & b_1 & b_2 & \ldots & b_s
\end{array} \tag{2.94}$$

As we commented at the beginning of the section, numerical propagators can be divided into explicit and implicit methods. In the case of RK, from a look at its Butcher's tableau we can immediately know whether the method is implicit or explicit: For explicit RK propagators, the coefficients $\{a_{ij}\}_{j\geq i} = 0$, which results in a Butcher's tableau where the diagonal terms and all those above it disappear.

For example, the most famous explicit RK method, usually known as RK4, or simply "the" RK method, is an explicit fourth order formula, and is defined by:

$$\begin{array}{c|cccc} 0 & & & & \\ \frac{1}{2} & \frac{1}{2} & & & \\ \frac{1}{2} & 0 & \frac{1}{2} & & \\ 1 & 0 & 0 & 1 & \\ \hline & \frac{1}{6} & \frac{1}{3} & \frac{1}{3} & \frac{1}{6} \end{array} \tag{2.95}$$

By increasing the number of stages, one may obtain higher order methods (at the cost of larger computational cost). However, the number of stages is not equal to the order; in fact the order four marks an important threshold for explicit RK methods: one only needs four stages to obtain an order four method, but one needs a number of stages strictly greater than five in order to construct an order five formula [26]. Likewise, for higher orders. This makes these explicit propagators become inefficient, as we have to compute extra auxiliary functions k_i. Beyond this issue, a more important shortcoming of the explicit RK methods is their failure when dealing with stiff equations (a problem for all explicit methods), and the fact that it can be proven [182] that that no explicit RK method can be symplectic.

In order to find a way to solve those problems, the implicit RK methods were developed. From the system 2.93 we can see that if $\{a_{ij}\}_{j\geq i} \neq 0$, we will have to solve an algebraic system of equations to find the auxiliary functions k_i. This makes the implicit methods generally slower when we compare them with the explicit ones, but what is lost in computational time is won in stability and conservation of magnitudes through the propagation.

In particular, one can build implicit symplectic methods: Sanz-Serna [182] showed that if the matrix M with coefficients

$$m_{ij} = b_i a_{ij} + b_j a_{ji} - b_i b_j \,, \tag{2.96}$$

is equal to zero, the RK method is symplectic. Looking at this expression, we can see that no explicit method can fulfill it.

There is another family of integrators related to the RK methods that came to our attention during the development of this thesis, the exponential RK propagators (ERK) [104]. Let us assume that our function $f(y,t)$ can be divided into a lineal part A and a nonlinear one B:

$$\dot{y}(t) = Ay(t) + B(y(t),t) \,. \tag{2.97}$$

In the systems that we study, the linear part would correspond to the kinetic operator, and is considered the main responsible for the possible stiffness, whereas the nonlinear part would be the rest of the Hamiltonians. The ERK propagators are defined as

$$\begin{aligned} k_i &= e^{c_i hA} y_n + h \sum_{j=1}^{s} \overline{a}_{ij}(hA) B[k_j, t_n + hc_j] k_j \,, \\ y_{n+1} &= e^{hA} y_n + h \sum_{i=1}^{s} \overline{b}_i(hA) B[k_i, t_n + hc_i] k_i \,, \end{aligned} \tag{2.98}$$

where the new coefficients $\overline{a}_{ij}$ and $\overline{b}_i$ are now functions of the operators, whose value coincides with the corresponding RK coefficients a_{ij} and b_i when $A = 0$. This means that if we get rid of the stiff part of the equation we retrieve the RK methods. Of course, we can have both implicit and explicit ERK methods. These propagators are better suited than the regular RK methods when they face stiff equations as the stiff part of the equation A is treated "exactly" (i.e. approximated by a very precise formula), and the rest of the equation B is approximated by a quadrature formula.

The general expression for the coefficients $\overline{a}_{ij}(A)$ and $\overline{b}_i(A)$ can be written as a linear combination of some auxiliary functions $\phi(z)$ defined as:

$$\phi_k(z) = \sum_{i=0}^{\infty} \frac{z^i}{(k+i)!}. \tag{2.99}$$

As an example, let us write the exponential version of the Euler method:

$$y_{n+1} = y_n + h\phi_1(hA) B[y_n, t_n] y_n \,. \tag{2.100}$$

Just like with the regular RK integrators, the ERK schemes cannot be symplectic if they are explicit. Furthermore, if we want a symplectic ERK method, the coefficients $\overline{a}_{ij}$ and $\overline{b}_i$ must fulfill [147]:

$$\begin{aligned} \overline{a}_{ij}(hA) &= a_{ij} e^{h(c_i - c_j)A} \,, \\ \overline{b}_i(hA) &= b_i e^{h(1-c_i)A} \,. \end{aligned} \tag{2.101}$$

2.4.3 Multistep Methods

We have also considered multistep methods, i.e. numerical methods that require the knowledge of a number s of previous steps to propagate the equations. They were first presented in 1883 within the context of fluid dynamics by Adams and Bashforth [10] to solve a problem related with the capillary action (although this is the first documented paper where the

multistep methods are used, in an application for a Royal Society grant from 1855 Bashforth thanked John Couch Adams for showing him these propagators, and therefore we must consider Adams as the original creator of these schemes).

As they need s previous values of the solution to compute a new one, the multistep algorithms consist of two parts: first, we need a starting procedure to generate the $y_1, \ldots, y_n$, and then we apply the multistep formula to find y_{n+1}. There are many choices for the starting procedure: Adams initially proposed using a Taylor series expansion, but one can also simply use any one-step RK method.

Explicit Adams Methods

Let $t_i = t_0 + ih$, and let us assume that we know the values $y_{n-s+1}, ..., y_n$ of the s previous approximations to the exact solution of the differential equation 2.67. Adams considered this equation in its integral form

$$y_{n+1} = y_n + \int_{t_n}^{t_{n+1}} \mathrm{dt}\, f(y(t),t). \tag{2.102}$$

On the right part of this equation we have the unknown solution $y(t)$. We can find $f_i = f(y_i, t_i)$ from the previous known values $y_{n-s+1}, ..., y_n$, and then approximate the exact function $f(y(t),t)$ with an interpolation polynomial calculated from the points $\{t_i, f_i\}_{i=n-s+1}^{n}$. We can compute this interpolation polynomial $p(t)$ as a function of backward differences using Newton's interpolation formula

$$\begin{aligned} p(t) = p(t_n + kh) &= \sum_{i=0}^{s-1} (-1)^i \binom{-k}{i} \nabla^i f_n, \\ \nabla^0 f_n = f_n, \qquad & \nabla^{i+1} f_n = \nabla^i f_n - \nabla^i f_{n-1}. \end{aligned} \tag{2.103}$$

With this result, we can write the numerical approximation to Eq. 2.102 as

$$y_{n+1} = y_n + h \sum_{i=0}^{s-1} \gamma_i \nabla^i f_n, \tag{2.104}$$

where the coefficients γ_i fulfill:

$$\gamma_i = (-1)^i \int_0^1 \mathrm{dk} \binom{-k}{i}, \tag{2.105a}$$

$$\gamma_m + \frac{1}{2}\gamma_{m-1} + ... + \frac{1}{m+1}\gamma_0 = 1\,. \tag{2.105b}$$

i	1	2	3	4	5
γ_i	1	$\frac{1}{2}$	$\frac{5}{12}$	$\frac{3}{8}$	$\frac{251}{720}$

Table 2.1 Coefficients for the explicit Adams methods.

In Table 2.1 we show the coefficients that we have required for the methods used in this thesis. Formula 2.104 is attributed to both Adams and Bashforth, and therefore this explicit variant of the multistep methods is also known as the Adams-Bashforth (AB) method.

In practice, one normally writes the AB formulas directly in terms of the f_i values, as in:

$$y_{n+1} = y_n + h\sum_{i=0}^{s-1} \beta_i f_{n-s+i} \tag{2.106}$$

The coefficients β_i can be written in terms of the γ_i ones given above.

Implicit Adams Methods

In the construction of the explicit Adams methods we have integrated the interpolation polynomial outside of its interpolation range (t_{n-s+1}, t_n) to find an approximation to $y(t_{n+1})$. It is well known that interpolation polynomials present problems outside of this interval. Because of this, Adams also considered formulas for the interpolation polynomial that included the point (y_{n+1}, t_{n+1}):

$$p^*(t) = p^*(t_n + kh) = \sum_{i=0}^{s} (-1)^i \binom{-k+1}{i} \nabla^i f_{n+1}. \tag{2.107}$$

When we insert this expression in Eq. 2.102 we get the implicit Adams methods

$$y_{n+1} = y_n + h\sum_{i=0}^{s} \gamma_i^* \nabla^i f_{n+1}, \tag{2.108}$$

where the new set of coefficients γ_i^* is given by

$$\gamma_i^* = (-1)^i \int_0^1 \mathrm{dk} \binom{-k+1}{i}, \tag{2.109a}$$

$$\gamma_m^* + \frac{1}{2}\gamma_{m-1}^* + \ldots + \frac{1}{m+1}\gamma_0^* = 0 \qquad (m \geq 1), \qquad \gamma_0^* = 1\,. \tag{2.109b}$$

The coefficients that corresponds to the propagators that we will use in this thesis appear in Table 2.2.

i	1	2	3	4	5
γ_i^*	1	$-\frac{1}{2}$	$-\frac{1}{12}$	$-\frac{1}{24}$	$-\frac{19}{720}$

Table 2.2 Coefficients for the implicit Adams methods.

Formula 2.108 is attributed to Adams and F. R. Moulton, so these methods are also known as the Adams-Moulton (AM) methods. We can rewrite this formula just like we did with the Adams-Bashforth method:

$$y_{n+1} = y_n + h\sum_{i=0}^{s} \beta_i^* f_{n-s+1+i}. \tag{2.110}$$

Predictor-Corrector Methods

As we know, when we have an implicit propagator, generally we have to solve a nonlinear system of equations due to the presence of y_{n+1} in both sides of the equation that defines the propagator. This may significantly slow down the procedure. This can be avoided by approximating the solution, using the following algorithm:

- P: using an explicit method (Adams-Bashforth, for example) compute a "predictor" approximate solution $\hat{y}_{n+1}$.
- E: evaluate with $\hat{y}_{n+1}$ the function $\hat{f}_{n+1} = f(\hat{y}_{n+1}, t_{n+1})$
- C: apply the following "corrector" formula to find y_{n+1}

$$y_{n+1} = y_n + h(\beta_s \hat{f}_{n+1} + ... + \beta_0 f_{n-s+1}). \tag{2.111}$$

- E: evaluate with y_{n+1} the function $f(y_{n+1}, t_{n+1})$ and store it for the next iteration of the propagator.

This kind of schemes are known as predictor-corrector (PC) methods, and the one outlined ("PECE") is the most common one. Another possibility is just doing the PEC steps, and using $\hat{f}_{n+1}$ for the next step of the propagator.

Backwards Differentiation Formula

To finish this brief survey of the multistep propagators, let us present the Backwards Differentiation Formulas (BDF), presented in 1952 by Curtiss and Hirschfelder [50] and popularized by Gear in 1971 [66]. Both the AB and AM methods are based on approaches

by quadrature to the integral in Eq. 2.102. The BDF are based on the numerical differentiation of a given function. We will use a polynomial $q(t)$ which interpolates in the range $\{(t_{n+1},y_{n+1}),(t_n,y_n),...,(t_{n-s+1},y_{n-s+1})\}$ and that we can express as a function of backwards differences:

$$q(t) = q(t_n + kh) = \sum_{i=0}^{s} (-1)^i \binom{-k+1}{i} \nabla^i y_{n+1}. \tag{2.112}$$

We determine the value of y_{n+1} forcing the polynomial $q(t)$ to reproduce the differential equation at a point:

$$q'(t_{n+1-r}) = f(y_{n+1-r}, t_{n+1-r}). \tag{2.113}$$

The case $r = 1$ gives us explicit formulas, and for $k > 3$ these methods are unstable. We are interested in the case where $r = 0$, where we find the BDF:

$$\sum_{i=0}^{s} \delta_i \nabla^i y_{n+1} = h f_{n+1}. \tag{2.114}$$

The coefficients $\{\delta_i\}$ are given by

$$\delta_i = (-1)^i \frac{d}{dk} \binom{-k+1}{i} |_{k=1}\,, \tag{2.115a}$$

$$\delta_i = \frac{1}{i} \quad (i \geq 1), \qquad \delta_0 = 0\,. \tag{2.115b}$$

As a final remark about these methods, they have been shown to be unconditionally unstable for $s > 6$ (check section III.3 from Ref. [81]).

2.4.4 Magnus Expansion

In 1954 Wilhem Magnus presented a family of integration methods that would come to be known as the Magnus expansion (ME) [134]. We find the motivation for the development of the ME in physics, more concretely on the theory of linear operators from quantum mechanics. For this reason, we will work with an ODE with the form of the Schrödinger equation:

$$y'(t) = A(t)y(t), \qquad y(t_0) = y_0. \tag{2.116}$$

Continuing with the quantum mechanics analogy, we can write $y(t)$ as a function of the evolution operator $U(t,t_0)$

$$y(t) = U(t,t_0)y(t_0). \tag{2.117}$$

We can make $t_0 = 0$ without loss of generality and simplify $U(t,t_0) \equiv U(t)$. The evolution operator obeys the differential equation

$$U'(t) = A(t)U(t), \qquad U(0) = I, \tag{2.118}$$

where I is the identity matrix.

The ME is based on the substitution of this evolution operator $U(t)$ with the exponential of a new operator $\Omega(t)$ that is given as a series expansion:

$$U(t) = e^{\Omega(t)}, \qquad \Omega(t) = \sum_{k=1}^{\infty} \Omega_k(t). \tag{2.119}$$

These Ω_k operators can be found using the following recursive relation:

$$\begin{aligned}
&\hat{\Omega}_k(t) = \sum_{j=0}^{k-1} \frac{B_j}{j!} \int_0^t \mathrm{d}\tau\, \hat{S}_k^j(\tau), \\
&\hat{S}_1^0(\tau) = A(\tau), \qquad \hat{S}_k^0(\tau) = 0, \qquad (k > 1), \\
&\hat{S}_k^j(\tau) = \sum_{m=1}^{k-j} [\hat{\Omega}_m(t), \hat{S}_{k-m}^{j-1}(\tau)], \qquad (1 \leq j \leq k-1),
\end{aligned} \tag{2.120}$$

where B_j are the Bernoulli numbers. As we can see from these equations, the computation of the Ω_k operators involve commutators of the operator $A(t)$, a computationally expensive operation in the usual situations. In order to obtain a practical propagator, we have to cut the expansion in Eq. 2.119 at some point. When we cut at the $2k$ term we get a $2k-2$-th order propagator, except for the case where we cut at the first term which produces an order 2 method. For a review of the ME and its application to numerical propagation, check Ref. [14].

As an example of the Magnus expansion, let us write the simplest possible one, obtained when we cut the sum in Eq. 2.119 at its first term. The resulting method is denominated the exponential midpoint rule (EMR), a second order, one-step method:

$$y(t) = \exp\left(hA(t-h/2)\right) y(t-h)\,. \tag{2.121}$$

The Magnus expansions are, in principle, only valid for linear systems. However, we will apply them to the solution of the TDKS equations, that are nonlinear: the operation $A(t)y(t)$ has the form $-iH[y(t)]y(t)$, where $H[y(t)]$ is a Hermitian operator that depends on the state

of the system. This turns the EMR into an implicit method:

$$y(t) = \exp\left(-ihH[y(t-h/2), t-h/2]\right) y(t-h)\,. \tag{2.122}$$

As we can see from expression 2.122, the Hamiltonian depends on $y(t-h/2)$, which is unknown. One can approximate it, for example, with $\frac{1}{2}(y(t)+y(t-h))$, and then the EMR turns into a nonlinear algebraic system to find $y(t)$.

In our implementation, however, we turn this implicit method into an explicit one

$$y(t) = \exp\left(-i\Delta t H^{\text{extr}}_{t-\Delta t/2}\right) y(t-\Delta t)\,, \tag{2.123}$$

where $H^{\text{extr}}_{t-\Delta t/2}$ is the Hamiltonian at time $t-\Delta t/2$, that we compute using extrapolation from previous time steps.

One can modify the EMR to design other propagators with the objective of improving its properties. The enforced time reversal symmetry [38] (ETRS) propagator, for example, defined by

$$y(t) = \exp\left(-i\frac{h}{2}H(y(t),t)\right) \exp\left(-i\frac{h}{2}H(y(t-h),t-h)\right) y(t-h)\,, \tag{2.124}$$

was built with the idea of improving the conservation of the time-reversal symmetry. The idea departs from the the following fact: propagating a system from $y(t)$ backwards by $\Delta t/2$ has to lead to the same result than propagating forwards from $t(t-\Delta t)$ by $\Delta t/2$. This can be enforced by the following equation

$$\exp\left(+i\frac{h}{2}H(y(t),t)\right) y(t) = \exp\left(-i\frac{h}{2}H(y(t-h),t-h)\right) y(t-h), \tag{2.125}$$

which, rearranged, gives us the ETRS method 2.124. Although this is once again an implicit method, following the example of the EMR propagator we can use the extrapolated Hamiltonian $\hat{H}^{\text{extr}}$ to turn it into an explicit method. This results in the so called approximated enforced time reversal symmetry (AETRS) propagator.

2.5 Quantum Optimal Control Theory

The application of TDDFT and EMD that we present in this thesis work [Chapter 4] is not limited to the calculation of the response of a piece of matter to an external laser field, but attempts to answer the inverse question: what is the optimal perturbation, subject to some constraints, in order to induce a given system reaction? As mentioned in the introduction, this type of question is addressed, from a general mathematical point of view, by optimal control theory (OCT) [5].

When applied to a quantum problem, the theory is called quantum optimal control theory [217, 20] (QOCT). To fix ideas, consider for example the time evolution of a quantum system described in its ground state by a Hamiltonian $\hat{H}_0 = \hat{T} + \hat{V}$. Then, it is subjected to a perturbation $\varepsilon(t)\hat{\mu}$:

$$\hat{H}(t) = \hat{H}_0 - \hat{\mu}\varepsilon(t) \tag{2.126}$$

We may think of $\hat{\mu}$ as the dipole operator of the system, perturbed by a laser field in the dipole approximation.

In a typical experimental setup, the control field will be $\hat{H}_1 = -\hat{\mu}\varepsilon(t)$: the experimentalist has some liberty in the election of the temporal shape $\varepsilon(t)$ and can therefore tamper with it using different laser pulses. The goal would be to search for the one that produces a desired outcome. Theoretically, this can be codified as the optimization of some functional of the system trajectory. For example, one may attempt the transfer of the system from the ground to an excited target state, and the functional would in this case be the population of the target state at the final time of the propagation.

The first thing that one may wonder is about the feasibility of the idea. Mathematically speaking, this is the so-called problem of controllability, which is a complex mathematical issue. As we are only interested in the practical application of QOCT, we just refer the reader to Refs. [91, 217], for example, for more in-depth information about this issue.

2.5.1 Optimal Control for the Schrödinger Equation

Let us think of a simple, standard formulation of QOCT: our objective is to find the laser pulse $\varepsilon(t)$ which conducts our system from its initial state $\Psi(t_0)$ to a state $\Psi(T)$ that maximizes the expectation value of some hermitian operator $\hat{O}$. We can write this statement in terms of an objective functional that is to be maximized:

$$J_1[\Psi] = \langle \Psi(T)|\hat{O}|\Psi(T)\rangle. \tag{2.127}$$

Since ε fully determines the behavior of the system, $\varepsilon \to \Psi_\varepsilon$, one may define a functional

$$G[\varepsilon] = J_1[\Psi_\varepsilon], \tag{2.128}$$

and the basic problem of QOCT reduces to its maximization.

Note that this statement of the QOCT problem restricts it to the case in which the target only depends on the state at the end of the propagation, and not on the full trajectory: We wish to drive the system to a final state, no matter how – in OCT jargon, it is a "terminal" target. The theory can be generalized, but for the sake of simplicity we describe this restricted formulation here, since this it is the only one that we have needed for our applications.

In practice, one often must somehow restrict the search space to find a solution for $\varepsilon(t)$. For example, we are not interested in too large amplitudes, as they would not be experimentally feasible. One may enforce these restrictions to the problem by adding *penalty* functions, such as:

$$J_2[\varepsilon] = -\alpha \int_0^T \mathrm{dt}\, \varepsilon^2(\mathrm{t}), \tag{2.129}$$

so that $G = J_1 + J_2$. The positive constant α is a penalty factor. This penalty function has been defined as $(-\alpha)$ times the *fluence* of the laser pulse: If the amplitude of the laser pulse is large, so is the fluence, that averages it over time. The total value of G, therefore, would be reduced in the regions of pulse space with large amplitudes, and the optimal solution would not be found there.

The maximization of $J_1 + J_2$ defined as above, without further considerations, would not lead to a valid solution, as one must ensure an obvious extra constraint: the wave function must satisfy the time-dependent Schrödinger equation. This can be ensured through the addition of an extra functional term that acts as a Lagrange multiplier:

$$J_3[\varepsilon, \Psi, \chi] = -2\Im \int_0^T \mathrm{dt}\, \langle \chi(t) | (i\partial_t - \hat{H}[\varepsilon] | \Psi(t) \rangle, \tag{2.130}$$

where the auxiliary field $\chi(t)$ has been introduced as a Lagrange multiplier. Putting together the three contributions defined above, we have:

$$J[\varepsilon, \Psi, \chi] = J_1[\Psi] + J_2[\varepsilon] + J_3[\varepsilon, \Psi, \chi]. \tag{2.131}$$

Now, we want to find the laser pulse (the "control") that optimizes this functional. In order to do that, we have to compute the variation δJ of the full functional and make it zero. In the definition of J, the variable ε, Ψ and χ are treated as independent, and therefore this

variation takes the form

$$\begin{aligned}\delta J &= \delta_\Psi J + \delta_\chi J + \delta_\varepsilon J, \\ &= \int_0^T \mathrm{d}\tau \int \mathrm{d}r \left[\frac{\delta J}{\delta \Psi(r,t)}\delta\Psi(r,\tau) + \frac{\delta J}{\delta \chi(r,\tau)}\delta\chi(r,\tau)\right] + \int_0^T \mathrm{d}\tau \, \frac{\delta J}{\delta \varepsilon(\tau)}\delta\varepsilon(\tau)\,. \end{aligned} \tag{2.132}$$

Here, the variation with respect to the conjugated Ψ^* and χ^* are omitted as they result in the complex conjugate equations of their counterparts.

Let us look at each individual term. For the functional derivative with respect to Ψ we find

$$\begin{aligned}\delta_\Psi J_1 &= \hat{O}\Psi^*(r',\tau)\delta(T-\tau), \\ \delta_\Psi J_2 &= 0, \\ \delta_\Psi J_3 &= -i(i\partial_\tau + \hat{H}(\tau))\chi^*(r',\tau) - [\chi^*(r',\tau)\delta(T-\tau)]|_0^T. \end{aligned} \tag{2.133}$$

where partial integration has been used to find the last expression. This results in the following expression for the variation of J with respect to the wave function Ψ

$$\delta_\Psi J = \langle\Psi(T)|O|\delta\Psi(T)\rangle + i\int_0^T \mathrm{d}\tau \, \langle(i\partial_\tau + \hat{H}(\tau))\chi(\tau)|\delta\Psi(\tau)\rangle - \langle\chi(T)|\delta\Psi(T)\rangle + \langle\chi(0)|\delta\Psi(0)\rangle. \tag{2.134}$$

The last term of this expression vanishes because we have fixed the initial condition $\Psi(t_0)$, and thus $\delta\Psi(t_0) = 0$). We repeat the same process for the auxiliary field χ, and find

$$\begin{aligned}\delta_\chi J_1 &= 0, \\ \delta_\chi J_2 &= 0, \\ \delta_\chi J_3 &= i(i\partial_\tau + \hat{H}(\tau))\Psi^*(r',\tau). \end{aligned} \tag{2.135}$$

Here we do not have boundary terms, so the variation of J with respect to χ is

$$\delta_\chi J = i\int_0^T \mathrm{d}\tau \, \langle(i\partial_\tau + \hat{H}(\tau))\Psi(\tau)|\delta\chi(\tau)\rangle. \tag{2.136}$$

Finally, the variations with respect to ε are given by:

$$\begin{aligned}\delta_\varepsilon J_1 &= 0, \\ \delta_\varepsilon J_2 &= -2\alpha\varepsilon(\tau), \\ \delta_\varepsilon J_3 &= -2\Im\langle\chi(\tau)|\hat{\mu}|\Psi(\tau)\rangle, \end{aligned} \tag{2.137}$$

so we have

$$\delta_\varepsilon J = \int_0^T \mathrm{d}\tau \, [-2\Im\langle\chi(\tau)|\hat{\mu}|\Psi(\tau)\rangle - 2\alpha\varepsilon(\tau)]\delta\varepsilon(\tau). \tag{2.138}$$

In order to find the extrema of J, we set all these variations to zero. This leads to the following set of "control equations":

$$(i\partial_t + \hat{H}(t))\chi(t) = i(\chi(t) - \hat{O})\delta(t-T)\,, \tag{2.139a}$$

$$0 = (i\partial_t + \hat{H}(t))\Psi(t)\,, \tag{2.139b}$$

$$\alpha\varepsilon(t) = -\Im\langle\chi(t)|\hat{\mu}|\Psi(t)\rangle\,. \tag{2.139c}$$

If we impose continuity at $t = T$ to χ, we can replace Eq. 2.139a by

$$\begin{aligned}(i\partial_t - \hat{H}(t))\chi(t) &= 0\,,\\ \chi(r,t) &= \hat{O}\Psi(r,t)\,.\end{aligned} \tag{2.140}$$

This means that the Lagrange multiplier $\chi(t)$ (sometimes called *costate* in the optimal control literature) behaves like the original wave function but, instead of having an initial condition for the propagation of its Schrödinger equation, we have a *final conditions*: one therefore needs to do a backward propagation for its calculation.

The wave function Ψ, costate χ and control field ε that simultaneously solve Eqs. 2.139a, are a solution to the control problem. The equations are nonlinearly coupled, and therefore it is not a trivial task to solve them: in fact, various algorithms have been designed *ad hoc* to carry out the computation of these objects. [232, 233, 96].

Note however that one could also approach the problem in a slightly different way: from the previous derivations, one can also find the gradient of G with respect to ε is:

$$\frac{\delta G}{\delta\varepsilon(t)} = -2\Im\langle\chi(t)|\hat{\mu}|\Psi(t)\rangle - \alpha\varepsilon(t)\,. \tag{2.141}$$

In fact, Eq. 2.139c merely states that, at the solution point, the gradient should be zero. Armed with the gradient, one can use any standard algorithm for the optimization of functions, such as conjugate gradients, etc.

2.5.2 QOCT + TDDFT

The previous section presented the basic equations of QOCT, assuming that one directly deals with the quantum problem though its full wave function and corresponding Schrödinger equation. As we know, this is not normally the case when dealing with many electron

problems. For example, we have used TDDFT for the project described in Chapter 4. Therefore, one must modify the previous approach, and substitute the use of Schrödinger's equation by the ones of Kohn-Sham.

The combination of QOCT and TDDFT was presented in Ref. [40]; we summarize here the key equations. Compared with a quantum system described by the Schrödinger equation, in TDDFT we have the TDKS equations 2.57, which we will rewrite for simplicity in a spin-restricted situation with N electrons ($N/2$ spatial orbitals):

$$\dot{\varphi}(r,t) = -i\hat{H}_{\mathrm{KS}}(n,u,t)\varphi_i(r,t), \tag{2.142}$$

$$n(r,t) = \sum_{i=1}^{N/2} 2\varphi_i^*(r,t)\varphi_i(r,t). \tag{2.143}$$

The Kohn-Sham Hamiltonian is the one described in Eq. 2.58. We will assume the adiabatic approximation, i.e., the XC potential $v_{\mathrm{XC}}[n]$ will only depend on the density at that time $n(t)$. Furthermore, note the presence of an extra argument u; it is a set of parameters $u_1,\ldots,u_M$. that determine the temporal shape of the control pulse, i.e. $\varepsilon = \varepsilon(u,t)$. While in the previous section we have directly used the full continuous function $\varepsilon(t)$, now we will use a set of *control parameters*, and the task will be to find the optimal set u^0.

Once a particular set u has been chosen, and given the initial conditions, the Kohn-Sham equations fully determine the evolution of the Kohn-Sham orbitals, so we can write $\varphi = \varphi(u)$. One must then codify the objective of the optimization into a functional definition, just as we did before, for example $J_1[\Psi] = \langle\Psi(T)|\hat{O}|\Psi(T)\rangle$. However, Ψ is the real many-electron wave function, and within a TDDFT formalism, we do not have that object. Therefore, in an ideal system we should try to define the target functional in terms of the density, $J_1 = J_1[n]$. In this way, we can manipulate the Kohn-Sham system, and use its density – that approximates the one of the real one. One may then add a penalty functional J_2 if necessary, and then define the functional to optimize, G, as

$$G[u] = J_1[n_u] + J_2(u)\,. \tag{2.144}$$

as the density is also determined by the choice of u: $u \to n_u$.

One may then use a similar derivation to the one outlined in the previous section, but considering the Kohn-Sham equations, instead of the Schrödinger one. The nonlinearity makes it a little more involved – the details can be consulted in Ref. [40]. The final expression

for the gradient is given by:

$$\frac{\partial G}{\partial u_m} = \frac{\partial J_2}{\partial u_m} + 2\Im\left[\sum_{i=1}^{N/2}\int_0^T \mathrm{dt}\ \langle\chi_i[u]|\nabla_u V_{ext}[u](t)|\varphi_i[u](t)\rangle\right]. \tag{2.145}$$

This expression depends on a set of *costate* orbitals χ, that can be obtained through the solution of the following equations of motion:

$$i\dot{\chi}_i(t) = [\hat{H}_{\mathrm{KS}}[n[u](t),u,t] + \hat{K}[\varphi[u](t)]\chi_i(t), \tag{2.146a}$$

$$\chi_i(T) = i\frac{\delta(J_1+J_2)}{\delta\varphi_i^*(T)}. \tag{2.146b}$$

The main difference between these equations and its analogous in 2.139a is the presence of the nonlinear operator matrix $K[\varphi[u](t)]$, caused by the dependence of $\hat{H}_{\mathrm{KS}}$ with the Kohn-Sham orbitals. The definition of K is:

$$\langle r|K_{ij}[\varphi]|\varphi\rangle = -4i\varphi_i(r)\Im\left[\int \mathrm{dr}\ \varphi^*(r')f_{\mathrm{HXC}}[n](r,r')\varphi_j(r')\right], \tag{2.147}$$

where $f_{\mathrm{HXC}}[n](r,r')$ is the kernel of the Kohn-Sham Hamiltonian

$$f_{\mathrm{HXC}}[n](r,r') = \frac{1}{|r-r'|} + \frac{\delta v_{\mathrm{XC}}[n](r)}{\delta n(r')}. \tag{2.148}$$

2.6 Density Matrix Renormalization Group

In section 2.1 we have discussed the reason behind the popularity of DFT: its great accuracy/cost ratio that allows the simulation of systems that otherwise would be out of reach for the current hardware level. However, we have also seen how there are other first principles alternatives, each of them with its own niche of applicability. In this section we briefly introduce one of them, density matrix renormalization group (DMRG), a theory that is specially suitable for one-dimensional quantum systems. The motivation for our use of DMRG will be apparent in Chapter 3, as we will need to calculate exact electronic densities for the one-dimensional Hubbard chain [121, 31, 32]. DFT cannot be used to obtain exact densities, since it cannot be systematically improved increasing the basis set, etc. in contrast to other electronic structure methods. For small chains, we used the straightforward diagonalization of the Hamiltonian, but this method is dragged by its cubic scaling with the size of the system. Therefore, we turned to DMRG, which has a linear scaling, and may yield quasi-exact densities.

Steven R. White presented the DMRG theory in 1992 [218]. The concept of renormalization first appeared in physics in the area of quantum electrodynamics [55], where it was applied to solve the divergences that stem from the fine structure of the electron at small distances/large energy scales. Inspired by this, Wilson [219] used the numerical renormalization group concept to solve the Kondo problem. His method (which is very successful for systems with impurities) fails however for real-space lattice systems. White realized that the problem originates from the selection of the degrees of freedom: instead of simply keeping the ones with the lowest energy, one must select the most relevant degrees of freedom in a different way.

In 1995, the matrix product state (MPS) variational ansatz was found by Östlund and Rommer [158, 176], which led to the reformulation of DMRG theory in terms of MPSs. Also, the new developments led to the understanding of DMRG in terms of quantum information theory. The reason behind the interest in MPSs applied to DMRG lies in the practical implementation: carrying out the DMRG algorithm using the language of MPS is more efficient than the previous algorithms. As we mentioned above, DMRG is a very efficient tool for the treatment of one-dimensional quantum systems, a fact that was proved by Hastings [83] in 2007. These two factors led us to choose an MPS based implementation of DMRG for some of the calculations that will be presented in Chapter 3. For an introduction to the MPS ansatz applied to ab initio theories check Ref. [42].

To expand on this topic, check the reviews [221, 187, 188].

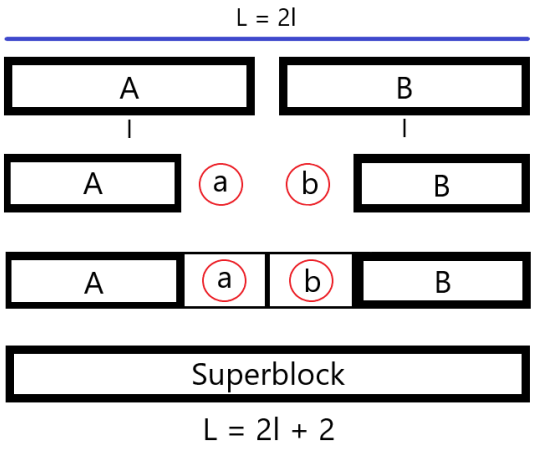

Fig. 2.2 One iteration of the DMRG algorithm for infinite systems: Starting with a superblock of length $L = 2l$, it is split into the blocks A and B, both of length l. Then, one adds between them the sites a and b, which are then absorbed into the nearest block. The two enlarged blocks Aa and bB are then merged into a "superblock" of length $L = 2l + 2$.

2.6.1 Infinite-System DMRG

DMRG is naturally derived for Hamiltonians in second quantization in a discrete basis, i.e. lattice Hamiltonians, such as:

$$H = \sum_{mn\sigma} t_{mn} \hat{d}^{\dagger}_{m\sigma} \hat{d}_{n\sigma} + \frac{1}{2} \sum_{ijmn;\sigma\tau} v_{ijmn} \hat{d}^{\dagger}_{i\sigma} \hat{d}^{\dagger}_{j\tau} \hat{d}_{n\tau} \hat{d}_{m\sigma} \,. \tag{2.149}$$

DMRG is essentially an algorithm to find the best possible truncation of the number of states needed to describe a system, in order to keep the Hilbert space tractable. The key assumption of this process is the existence of a reduced Hilbert space the captures the relevant physics of the system. We will consider that our system consists of a one-dimensional chain described by the Hamiltonian 2.149, with a variable length L, that in the infinite-length version of the algorithm, is iteratively grown to infinity. Each site in the chain is associated to a d-dimensional Hilbert space (for example, we may have a chain of spin 1/2 particles, and d=2).

In essence, the DMRG algorithm for an infinite chain, sketched in Fig. 2.2, is as follows:

1. One starts with two blocks of sites, A (left) and B (right), containing l sites each. The normal choice is to start with $l = 1$. Each block can be described by a Hamiltonian, $\hat{H}_A$ and $\hat{H}_B$, containing all the internal interactions of each block. The dimension of the blocks, when l=1, is d: $m_1 = d$. In the next iterations, this dimension may grow, but the algorithm establishes a pre-defined limit D.

2. We add an extra site to each block, forming the "extended blocks" Aa and bB (second row of Fig. 2.2). An extended block has dimension dm_l.

3. We now consider the "superblock" $AabB$, and build its Hamiltonian $\hat{H}_{AabB}$ (that must contain the interactions between all its elements). The dimension of the superblock space is $m_l^2 d^2$. An arbitrary state of this superblock may be written as:

$$|\psi\rangle = \sum_{a_A \sigma_A \sigma_B a_B} \psi_{a_A \sigma_A \sigma_B a_B} |a_A\rangle |\sigma_A\rangle |\sigma_B\rangle |a_B\rangle \,, \tag{2.150}$$

   where a_A runs over a basis of block A, σ_A runs over a basis the extra added site a, and likewise for a_B and σ_B for the block B and site b. The variational principle allows us to compute the ground wave function by minimizing the energy defined by Hamiltonian of the superblock $\hat{H}_{AabB}$:

$$E = \frac{\langle\psi|\hat{H}_{AabB}|\psi\rangle}{\langle\psi|\psi\rangle}. \tag{2.151}$$

4. We now consider the reduced density operator for Aa, by taking the partial trace over the bB component:

$$\hat{\rho}_{Aa} = \mathrm{Tr}_{\mathrm{Bb}} |\psi\rangle\langle\psi| \,. \tag{2.152}$$

5. We diagonalize $\hat{\rho}_{Aa}$, and keep the D eigenstates with the largest associated eigenvalues w_α. We set $m_{l+1} = D$. If $m_l d$, the dimension of $\hat{\rho}_{Aa}$, is smaller than D, we just keep all the eigenstates, and $m_{l+1} = m_l d$.

6. We define the new block for the next iteration, formed by $l+1$ sites, to be Aa, but on the truncated subspace spanned by the previously defined m_{l+1} eigenstates. All operators are projected on this subspace. Likewise for block Bb. We may now return to point 1 and proceed to the next iteration.

7. The cycle is repeated until convergence is reached, i.e. the properties determined by the ground state of the superblock no longer change significantly at each iteration.

The gist of the algorithm lies in the selection of the states to truncate the Hilbert space of the superblock. The reason for the choice of this specific set of eigenstates stems from the demand that the distance $|||\psi\rangle - |\psi\rangle_{\mathrm{trunc}}||$ between the exact ground state $|\psi\rangle$ and its projection onto the truncated state $|\psi\rangle_{\mathrm{trunc}}$ be minimal. This distance happens to be proportional to the total weight of the discarded eigenvalues of the reduced density matrix, $\varepsilon = 1 - \sum_{a \leq D} w_a$, which justifies the choice made by the DMRG algorithm.

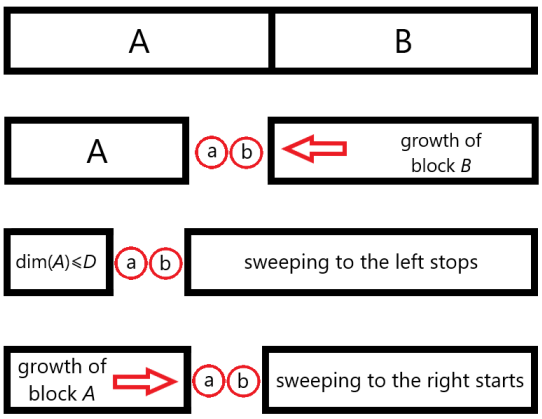

Fig. 2.3 Illustration of the DMRG algorithm for finite systems.

The maximum superblock dimension D serves as a parameter which controls the error. If D is increased, the error can be reduced to any required threshold, making the results quasi-exact.

2.6.2 Finite-System DMRG

The previous algorithm is designed for infinite chains. If the objective is to describe a finite chain, one could think of repeating the same procedure that increases the length iteratively, and stopping when the target length is reached. However, the results can be improved by performing further steps, that define the finite-system version of the DMRG algorithm. This is the version that we have needed to use for our work.

Therefore, the finite-system algorithm uses the infinite-system DMRG as a starting point, growing the chain up to the required size of the system. This provides a first approximation to the wave function of the lattice. Then, the process is illustrated in Fig. 2.3: One takes one of the blocks (for example, the right block B), and performs once again a DMRG step: add a site to form an enlarged block bB; form a superblock with the corresponding A block, find the ground state of this superblock, compute the reduced density operator, diagonalize, and use the most relevant D eigenstates to truncate the bB block. The difference now is that the growth of B comes at the expense of block A, which shrinks the number of sites that B grows. This is repeated until A has a Hilbert space of dimension smaller than D (or until A is of size $l = 1$). Then, the direction of this so-called "sweep" is inverted, once again until B is small enough to have a full Hilbert space smaller than D. These sweeping cycles continue until convergence.

2.6.3 DMRG and Entanglement

Up to this point, we have seen how DMRG avoids the exponential growth of the basis dimension using a truncation of the Hilbert space. However, in principle we do not know if this truncation will be of practical use, i.e., if we can get good accuracy for the magnitudes computed for a truncation dimension D small enough. Or, in other words, if the convergence towards exact results with the size of D is fast, or not. The answer is conditional (roughly speaking, it is fast if it is used for one-dimensional systems, and it is not fast otherwise), and is linked to the concept of entanglement.

As we have seen from the description of the DMRG algorithm, it rests on the idea of considering the blocks Aa and bB the components of a bipartite system. As mentioned above, the quality of approximating the ground state $|\psi\rangle$ of the superblock by making use of a truncated Hilbert space with only D states, is determined by the magnitude of the eigenvalues of the reduced density matrix $\hat{\rho}_{Aa}$ associated to the eigenstates that are discarded. If these eigenvalues decrease fast with D, the algorithm is effective.

This question has been studied for one dimensional systems in Refs. [170, 156]. The answer can be summarized as follows: The value of the eigenvalues of the reduced density matrix is linked to the von Neumann entanglement entropy:

$$S_{A|B} = -\mathrm{Tr}\rho_{\mathrm{A}} \log_2 \rho_{\mathrm{A}} = -\sum_{\mathrm{a}} \mathrm{w_a} \log_2 \mathrm{w_a}. \tag{2.153}$$

We may now apply general scaling laws about the entanglement entropy [171, 56, 211]. Considering the bipartite system $A|B$, where AB is in the thermodynamic limit and A is of size L^q (where q is the spatial dimension), the area laws for ground-state short-ranged Hamiltonians with a gap state that the entanglement entropy is not extensive but proportional to the surface:

$$S_{A|B} \sim L^{q-1}. \tag{2.154}$$

From this expression, we can see that for one-dimensional systems $S \sim$ cst, and therefore it does not grow with L, which places a limit on the magnitude of the eigenvalues that is independent on the size of the system.

With this result we can make a connection between DMRG and the area laws of quantum entanglement. If A and B are two D-dimensional spaces, their maximal entanglement entropy is $S_{A|B} = \log_2 D$ in the case where every eigenvalue w_a is equal to D^{-1}. This means that we need at least a state of dimension $D = 2^S$ to encode all the information of the full system. This implies that for gaped one-dimensional systems increasing the size would not lead to a strong increase in D. In order to have maximal entanglement, we need that the eigenvalue spectra is

close to flat, but for the typical one-dimensional many-body systems the exponential decay of the eigenvalues assumption is valid even if only qualitatively [191]. In practice, for gapped one-dimensional systems the decay of the discarded eigenvalues is exponential, which makes DMRG very successful when dealing with this kind of systems.

Chapter 3

A new route for the Exact Functional

Nowadays, DFT is the most popular theory in the electronic structure community, thanks to its good accuracy/computational cost relation. Chemistry, Condensed Matter Physics, Material Sciences... in all of these areas it has been successfully applied, and many tools and codes have been developed based on DFT. Despite its many merits, however, DFT is still an intrinsically approximated theory: independently of the computational resources available, it never returns exact results, and there are many systems for which DFT even fails qualitatively [47, 24].

The quality of the calculation is determined by the exchange and correlation functional (XCF), by how well it reproduces the density of the real, interacting electron system. Hundreds of functionals [142] have been proposed, but the form of the exact XCF is still elusive. These approximations are not universally successful, and the development of quality XCFs is a complicated problem [190]. Therefore, the research about this object is of great relevance in the field of electronic structure.

In Ref [75], we presented a numerical scheme that associates electron-electron interaction potential functions (IFs) and XCFs, and studied their relationship. While the real IF in the non-relativistic case is just the Coulomb potential $1/r$, DFT can be formulated for any generic IF. To each given IF corresponds a different XCF. We can then ask the inverse question, that is, for a given XCF X, can we find its corresponding IF? And if it does not exists, can we find the *optimal* IF that better reproduces the results found with this X functional? This association between IFs and XC functionals naturally leads to an *ab initio* method to optimize families of parameterized XCFs: let some algorithm search for the parameters of the XCF that produce the closest IF to the real one.

To test this scheme we have used site-occupation DFT, also known as lattice DFT [78, 186, 189]. We choose the version of lattice DFT based only on the densities and not the full one-particle density matrix [127, 208, 128] (other DFTs based on different variables

are also possible in lattice DFT [189]). The reason behind this election is that lattice DFT provides us with a numerically tractable framework, and there is an abundance of lattice models (Hubbard, Anderson, Pariser-Parr-Pople, Heisenberg) that have been studied and used thoroughly through the years. These models are useful because the limited size of the lattice allows us to control the number of degrees of freedom of the objects we are researching. Moreover, they can be seen as numerical discretizations of the real, continuous 3D systems which we can retrieve in the limit of infinitely fine discretization.

In particular, we have used the one-dimensional Hubbard model (1DHM) [121, 31, 32], and worked on a local density approximation parameterized by Lima *et. al* [124], which uses the exact results from the Bethe ansatz [13] solution [122], called BALDA. In the 1DHM, the BALDA is completely determined by a single parameter, given by the IF, and therefore the BALDA is a family of one-parameter XCFs. We will show that the best parameter to choose for the BALDA, i.e. the one that better reproduces the exact densities of system defined by a certain IF is actually not same that the one that defines the IF itself.

In subsection 3.1, we will present in detail the optimization method and the theoretical background for this work; subsection 3.2 shows the results obtained, and the conclusions are presented in subsection 3.4.

3.1 Method

We depart from the generic electronic Hamiltonian, in the second quantization (Eq. 2.4), given by:

$$\begin{aligned}\hat{H} = &\sum_{\sigma}\int \mathrm{d}\mathbf{r}\ \hat{\psi}^{\dagger}_{\sigma}(\mathbf{r})\left[-\frac{\nabla^2}{2}\right]\hat{\psi}_{\sigma}(\mathbf{r}) + \int \mathrm{d}\mathbf{r}\ v(\mathbf{r})\hat{n}(\mathbf{r}) \\ &+ \frac{1}{2}\sum_{\sigma\tau}\int\mathrm{d}\mathbf{r}\int\mathrm{d}\mathbf{r}'\ w(|\mathbf{r}-\mathbf{r}'|)\,\hat{\psi}^{\dagger}_{\sigma}(\mathbf{r})\,\hat{\psi}^{\dagger}_{\tau}(\mathbf{r}')\,\hat{\psi}_{\tau}(\mathbf{r}')\,\hat{\psi}_{\sigma}(\mathbf{r})\,.\end{aligned}$$

As always, the first term corresponds with the kinetic operator $\hat{T}$, the second one is the external potential $\hat{V}$ determined by the local function v, and the last term is the electron-electron interaction $\hat{W}$, characterized by a local function w, usually the Coulomb interaction: $w(r) = \frac{1}{r}$.

However, DFT does not require that specific definition for w in its theoretical formulation, and so in principle we could develop a DFT based on any IF – at least at long as some basic conditions are met, like the need for the Hamiltonian to have a lower bound. Let us group all these admissible IFs in a manifold Γ, where each $\gamma \in \Gamma$ represents an IF w^{γ}. For each γ the DFT theorems assure the existence of an XCF of the density n, $E^{\gamma}_{\mathrm{XC}} = E^{\gamma}_{\mathrm{XC}}[n]$, which can

be used to predict any ground-state observable through the resolution of the non-interacting Kohn-Sham auxiliary system [106].

The previous reasoning has effectively defined a map from Γ to a manifold Λ, where each of its elements λ represents an XCF:

$$\begin{aligned} l : \Gamma &\rightarrow \Lambda \\ \gamma &\rightarrow l(\gamma) = \lambda \end{aligned} \tag{3.1}$$

This map assigns an XCF λ to the IF γ. Could the inverse be possible, i.e., for a given XCF is there any IF for which the XCF is exact? As we know from the inaccuracies of DFT, the XC functionals in use do not correspond to the Coulomb interaction, but are they exact for some other IF? This kind of questions are denominated "representability questions" in the DFT literature (although usually in the context of the relationship of densities and external potentials).

Instead of finding the theoretical conditions for the correspondence between the IF and its exact XCF, here we present a practical route in the form of a numerical approach to the problem. Let us consider that the objects Γ and Λ are parameter sets that characterize IFs and XCFs respectively. For a given functional $E_{\mathrm{XC}}^{\lambda}$ and IF γ, let $n_\gamma[v]$ be the exact density of the ground state corresponding to the external potential v and the IF γ, and $n_\lambda^{\mathrm{DFT}}[v]$ the ground state density obtained solving the Kohn-Sham equations with the XCF λ. We will have that λ is the exact XCF corresponding to γ ($\gamma \in l^{-1}(\lambda)$) if and only if $n_\gamma[v] = n_\lambda^{\mathrm{DFT}}[v]$ for any choice of v. Otherwise, there will be some distance between the two densities. We define, for a given set of external potentials $\{v_k\}$, a function G of γ that accounts for the distance between the two sets of densities:

$$G(\gamma;\lambda,\{v_k\}) = \sum_k \int \mathrm{dr}\, (n_\gamma[v_k](\mathbf{r}) - n_\lambda^{\mathrm{DFT}}[v_k](\mathbf{r}))^2 . \tag{3.2}$$

G will be minimized at zero if $\gamma_0 \in l^{-1}(\lambda)$. The opposite is not true, however: even if γ_0 is a minimum that makes $G = 0$, it cannot be guaranteed that λ is the corresponding exact XCF, because the set of external potential does not include them all. Even then, it will be the optimal IF found for the XCF λ, where by optimal we mean that the two sets of densities are as close as possible.

By carrying out this procedure, we have defined a function $\gamma^{\min}(\lambda)$ that assigns an IF $\gamma = \gamma^{\min}(\lambda)$ to each XCF:

$$G(\gamma^{\min}(\lambda);\lambda,\{v_k\}) = \min_{\gamma\in\Gamma} G(\gamma;\lambda,\{v_k\}) . \tag{3.3}$$

If we use a sufficiently good sample of external potentials and if $G(\gamma^{\min}(\lambda);\lambda,\{v_k\}) \approx 0$, we know that the XC functional λ is a very good approximation for its corresponding IF. This scheme actually measures the "quality" of a given approximated XCF. First, it tells us whether or not it is close to the the exact XCF for some IF. Furthermore, one can then look at how close this associated IF is to the real one (the Coulomb one, in a typical situation).

These questions beget the following procedure for the search of the optimal XC functional from a given family Λ: given two IFs γ_1 and γ_2, we define a distance between them as

$$d(\gamma_1,\gamma_2) = \left(\int_0^\infty \mathrm{dr}\,(w^{\gamma_1}(r) - w^{\gamma_2}(r))^2\right)^{1/2}. \tag{3.4}$$

If we denote the true IF by γ^{ref}, then the minimization of the function

$$H(\lambda) = d^2(\gamma^{\mathrm{ref}}, \gamma^{\min}(\lambda))\,, \tag{3.5}$$

leads to an XCF λ_0 whose associated IF is as close as possible to γ^{ref}.

We have carried out this program, for the moment, only for one-dimensional model systems, with the goal of assessing its feasibility. In particular, we have implemented this scheme for the N-electron 1DHM [121, 31, 32]. The Hamiltonian in this case is given by:

$$\hat{H} = -t\sum_{\langle m,n\rangle\sigma} \hat{d}^\dagger_{m\sigma}\hat{d}_{n\sigma} + \sum_n v_n\hat{n}_n + U_{\mathrm{ee}}\sum_n \hat{n}_{n\uparrow}\hat{n}_{n\downarrow}\,, \tag{3.6}$$

where $\hat{d}_{m\sigma}, \hat{d}_{n\sigma}$ are the discrete creation and annihilation operators (that substitute the continuous ones from Eq. 2.4), and $\langle m,n\rangle$ denotes summation over nearest neighbors only. Depending on whether the kinetic term couples or not the the limits of the chain, we can have periodic boundary conditions (PBC) or open boundary conditions (OBC) respectively. We have used the latter.

In our case, both the kinetic term and the interaction operator are determined by a single constant (t and U_{ee} respectively). This means that the couplings along the chain are homogeneous. For the rest of this section we will fix the energy unit making $t = 1$, which leaves U_{ee} as the only constant determining the model.

One may then build a DFT for this system. The corresponding Kohn-Sham equations take the form

$$\sum_n \left[t_{mn} + \delta_{mn}(v_m + v_m^{\mathrm{Hxc}(\lambda)}(n))\right]\varphi^\alpha_{n\sigma} = \varepsilon^\alpha\varphi^\alpha_{m\sigma}\,, \tag{3.7}$$

$$n_m = \sum_{\alpha\sigma} |\varphi^\alpha_{m\sigma}|^2\,. \tag{3.8}$$

where $\sigma = \uparrow, \downarrow$ is the spin index, α runs from 1 to the number of occupied orbitals, and n_m is the electronic density of the site m of the chain.

As usual, the key ingredient in the equation is the Hartree, exchange, and correlation (HXC) potential $v_m^{\mathrm{Hxc}(\lambda)}(n)$. The form of the HXC potential is given by the derivative of the HXC energy functional with respect to the density:

$$v_m^{\mathrm{Hxc}(\lambda)}(n) = \frac{\partial E_{\mathrm{Hxc}}^{\lambda}}{\partial n_m}(n)\,. \tag{3.9}$$

We label these objects with λ, to stress the fact that one must make a particular approximate choice for them.

Instead of the usual approach where the Hartree part is separated from the approximation used for the XCF, we preferred to work with the full HXC energy. One possible choice is based on the local density approximation for the 1DHM. This functional is called BALDA (Bethe ansatz local density approximation) because it uses the solution of the Bethe ansatz [13] for the homogeneous infinite Hubbard chain, and it was proposed by Lieb and Wu [122]. For its parameterization we used the one from Lima et al. [124], which establishes that for an infinite homogeneous 1DHM the total energy per site is

$$\varepsilon_{<}^{\mathrm{hom}}(\tilde{n},U) = -\frac{2\beta(U)}{\pi}\sin\left(\frac{\pi\tilde{n}}{\beta(U)}\right), \tag{3.10}$$

where $\tilde{n}$ is the constant density of the chain, U is the interaction parameter of the 1DHM and the function $\beta(U)$ is given by

$$-\frac{2\beta(U)}{\pi}\sin\left(\frac{\pi}{\beta(U)}\right) = -4\int_0^{\infty}\mathrm{d}x\,\frac{J_0(x)J_1(x)}{x[1+\exp(Ux/2)]}\,, \tag{3.11}$$

with J_0 and J_1 are the zero-th and first order Bessel functions. The $<$ subindex in Eq. 3.10 refers to the fact that this expression is only valid for the densities $\tilde{n} \leq 1$. For $\tilde{n} > 1$ one may apply the particle-hole symmetry [122], and get:

$$\varepsilon_{>}^{\mathrm{hom}}(\tilde{n},U) = (\tilde{n}-1)U + \varepsilon_{<}^{\mathrm{hom}}(2-\tilde{n},U)\,. \tag{3.12}$$

Therefore, we can write an expression for the energy per site of the infinite homogeneous Hubbard chain, regardless of $\tilde{n}$, using the Heaviside function θ:

$$\varepsilon^{\mathrm{hom}}(\tilde{n},U) = \theta(1-\tilde{n})\varepsilon_{<}^{\mathrm{hom}}(\tilde{n},U) + \theta(\tilde{n}-1)\varepsilon_{>}^{\mathrm{hom}}(\tilde{n},U)\,. \tag{3.13}$$

At $n = 1$ this formula presents a cusp whose height is a function of the interaction constant U. This means that the derivative is discontinuous at this point, and thus it presents a problem for the calculation of the HXC potential: the Kohn-Sham calculation will be hard to converge for values of the density close to 1. Moreover, the exact functional does not have a cusp at this point (its effect is actually very important to understand why this functional fails in the case of the Hubbard dimer, as we will see in the following section). To avoid the convergence problem, we have used a smoothing function around the cusp, as suggested in Ref. [114]. Although this discontinuity is in fact unphysical, it is worth noticing that it also have its upsides, for example it has been used to compute the Mott gap [123].

We can now write the total energy (or energy per unit cell for PBC) as:

$$E^{\text{hom}}(n,U) = \sum_n \varepsilon^{\text{hom}}(n_n,U)\,. \tag{3.14}$$

Now we define the HXC functional as the total energy for a certain interaction parameter U minus the non-interacting energy:

$$E_{\text{Hxc}}^{\text{BALDA}(U)}(n,U) = E^{\text{hom}}(n,U) - E^{\text{hom}}(n,0)\,. \tag{3.15}$$

This is a uniparametric family of XCFs, with $\lambda \equiv U$.

We will now detail the procedure for the optimization of the XC functionals. First of all, we will re-denote Eq. 3.2 as $G(U_{\text{ee}};U,\{v_k\})$, Eq. 3.3 as $U_{\text{ee}}^{\min}(U)$ and Eq. 3.5 as $H(U)$. For our lattice system, the function G then takes the form

$$G(U_{\text{ee}};U,\{v_k\}) = \sum_k \sum_m (n_{U_{\text{ee}}}[v_k]_m - n_U^{\text{DFT}}[v_k]_m)^2\,. \tag{3.16}$$

The computation of function G requires, therefore, the calculation of the DFT densities (that requires the solution of the corresponding Kohn-Sham equations), and the calculation of the exact densities (that requires to solve the exact many-electron problem).

Then, the goal is to find the minimum of G as a function of U_{ee}. We chose gradient-based algorithms [109, 100] for the search of the minima. For that, we need a procedure to compute the gradient of G with respect to U_{ee}, given by:

$$\frac{\partial G}{\partial U_{\text{ee}}} = \sum_k \sum_m 2(n_{U_{\text{ee}}}[v_k]_m - n_U^{\text{DFT}}[v_k]_m)\frac{\partial}{\partial U_{\text{ee}}} n_{U_{\text{ee}}}[v_k]_m\,, \tag{3.17}$$

$$\frac{\partial}{\partial U_{\text{ee}}} n_{U_{\text{ee}}}[v_k]_m = 2\text{Re}\langle \Psi^k | \hat{n}_m | \frac{\partial \Psi^k}{\partial U_{\text{ee}}} \rangle\,, \tag{3.18}$$

with $\Psi^k = \Psi^k(U_{\text{ee}})$ being the ground state of a system with an external potential v_k and electronic interaction constant U_{ee}. In order to compute these derivatives we used Sternheimer's equation [200]:

$$\left[\hat{H} - E_k\right] |\frac{\partial \Psi^k}{\partial U_{\text{ee}}}\rangle = -[\hat{I} - |\Psi^k\rangle\langle\Psi^k|] \sum_m \hat{n}_{m\uparrow}\hat{n}_{m\downarrow}|\Psi^k\rangle\,, \tag{3.19}$$

where E_k is the ground state energy of the system subjected to the external potential v^k.

Armed with these numerical procedures to compute the function G and its gradient, we may use any gradient-based optimization algorithm to find the minimum, and therefore we can establish the function $U_{\text{ee}}^{\min}(U)$, i.e. the function that provides the optimal electron-electron interaction constant U_{ee} for a given BALDA parameter U.

In order to complete this theory section, we explain now the method that we have used to compute the exact exchange and correlation functional – since we use it as a reference to analyze the results. The definition of the exact HXC functional is:

$$E_{\text{Hxc}}(n) = F(n) - T_{\text{S}}(n)\,, \tag{3.20}$$

with

$$F(n) = \min_{\Psi \in M(n)} \langle\Psi|(\hat{T} + \hat{W})|\Psi\rangle\,, \tag{3.21}$$

$$T_{\text{S}}(n) = \min_{\Psi \in M(n)} \langle\Psi|\hat{T}|\Psi\rangle\,, \tag{3.22}$$

where $M(n)$ is the set that contains all the wave functions that produce a determined density n. We could compute these objects following a direct minimization over $\Psi \in M(n)$, but it is more efficient to do what is called a "density to potential inversion" [97]. The functional F is universal in the sense that it does not depend on the external potential of the system. We can define the potential-dependent functional

$$E(n) = F(n) + \sum_m v_m n_m\,,$$

for some external potential $v \equiv \{v_m\}$. If this potential gives raise to the ground state density n, $E(n)$ is the ground state energy and we can use the previous formula to find F. This implies the computation of the potential whose ground state density is n, which we can do minimizing the following function:

$$K(v) = \sum_m (n(v)_m - n_m)^2\,, \tag{3.23}$$

where $n(v)_m$ is the ground state density that corresponds to v, which can be computed by exact diagonalization of Schrödinger's equation. When $K(v) = 0$ both densities are the same and we have established the map $n \to v$. Now we can use Eq. 3.23 to compute $F(n)$, and the same scheme can be applied to find $T_S(n)$. About the numerical aspects of this minimization, having access to the gradient of K would allow us to use gradient-dependent minimization methods, and simplify the search. Indeed, this gradient can be computed:

$$\frac{\partial K}{\partial v_n}(v) = \sum_m 2(n(v)_m - n_m)\frac{\partial}{\partial v_n}\langle\Psi(v)|\hat{n}_m|\Psi(v)\rangle\,. \tag{3.24}$$

where $\Psi(v)$ is the ground-state wave function corresponding to the external potential v, that can be found through the diagonalization of Schrödinger's equation. We can then once again use Sternheimer's equation with $\hat{n}_m$ as a perturbation to compute $\frac{\partial}{\partial v_n}\Psi(v)$:

$$\left[\hat{H} - E\right]|\frac{\partial\Psi}{\partial v_n}\rangle = -[\hat{I} - |\Psi(v)\rangle\langle\Psi(v)|]\hat{n}_m|\Psi(v)\rangle\,. \tag{3.25}$$

In this way, all the ingredients necessary to compute the gradient of K can be obtained.

3.2 Results

Fig. 3.1 shows the plot of the function $G(U_{ee}; U, \{v_k\})$ for 2 (top), 8 (middle) and 14 (bottom) sites lattices populated with two electrons. The range of values of U studied is $U \in [0,1]$ (recall that the energy scale is set by the kinetic constant $t = 1$). This is the regime of weak interaction (e.g., for the 8 sites lattice with $U = 0.5$, the correlation energy contributes $\sim 0.2\%$ of the total energy). Regarding the external potentials, we used a set $\{v_k\}$ of 10 randomly generated potentials, as we found that those were enough to find converged solutions to the optimization process. These potentials $\{v_k\}$ were generated using a flat random distribution in the interval $[0, 0.01t]$, so they constituted small perturbations on the system which do not deviate much from the ground state with $v = 0$. In Fig. 3.1, we show the minimum found for each value of U; all of them form the red curves $U_{ee}^{\min}(U)$. As we can see, these curves are not diagonal lines crossing the XY plane: this means that the electron-electron interaction parameter U_{ee} that better reproduces the densities created by a BALDA with a parameter U is actually different, i.e., $U_{ee}^{\min}(U) \neq U$. We have tested systems up to 22 sites, and the difference between both parameters seems to grow with the number of sites and the value of U.

Now that we have a correspondence between every optimal electron-electron interaction parameter $U_{ee}^{\min}$ and every value of U, we want to find which one of the BALDA functionals

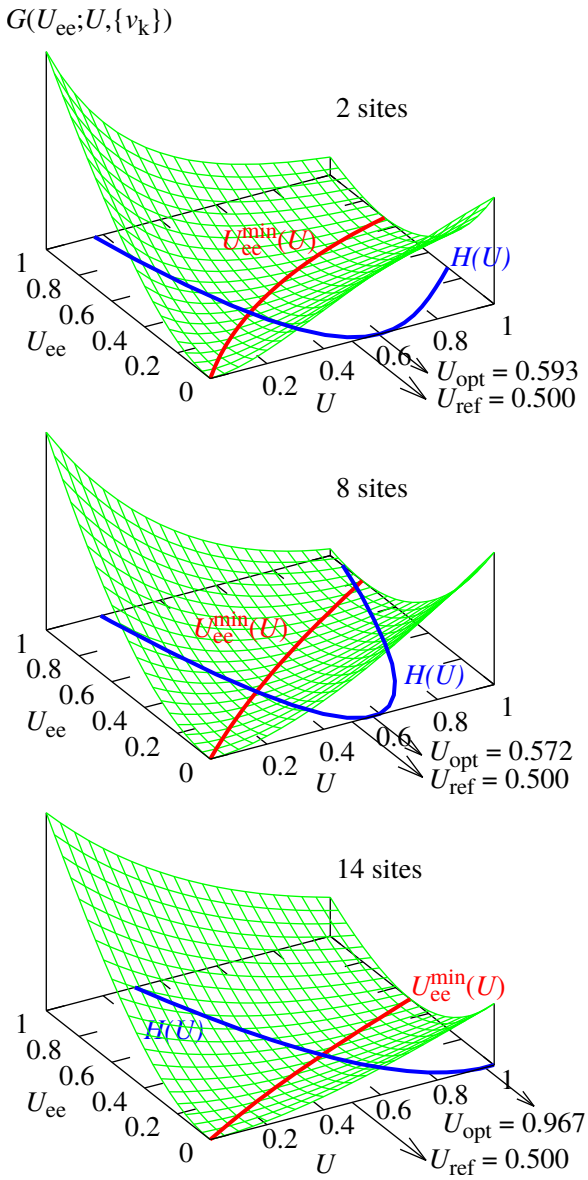

Fig. 3.1 Function $G(U_{ee},U;\{v_k\})$ (surfaces) for a lattice with 2 (top), 8 (middle), and 14 (bottom) sites. Plotted in red over the surface is the curve determined by the minima of this function with respect to U_{ee}, i.e. U_{ee}^{min}. Plotted in blue over the XY plane is the function $H(U)$. Both the reference U_{ref}, and the optimized BALDA parameter, U_{opt} [at the minimum of function $H(U)$], are also marked.

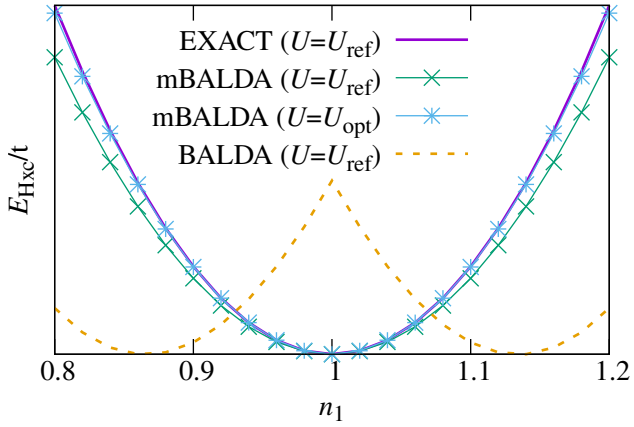

Fig. 3.2 Functional E_{Hxc} (the sum of the Hartree and xc correlation energies), as a function of n_1, the density of one of the sites of a Hubbard dimer. The plot shows the exact and BALDA functional computed with the $U_{\text{ee}}^{\text{ref}}$ interaction (EXACT), and the mBALDA functional (see text its definition) computed with the same reference $U_{\text{ee}}^{\text{ref}}$ and with the optimized U_{opt}.

that U defines is closer to a determined reference value of the electron-electron interaction (in our case we set it to $U_{\text{ee}}^{\text{ref}} = 1/2$). For that purpose, we minimize the function

$$H(U) = (U_{\text{ee}}^{\text{ref}} - U_{\text{ee}}^{\text{min}}(U))^2 . \tag{3.26}$$

This function is also plotted in Fig. 3.1. The argument U_{opt} that minimizes this function is the optimal parameter defining a BALDA XCF for the given reference electron-electron interaction parameter $U_{\text{ee}}^{\text{ref}}$. The resulting U_{opt} values found for each system are indicated in Fig. 3.1. There is a noticeable difference between $U_{\text{ee}}^{\text{ref}}$ and U_{opt}, which grows with the number of sites N_s for $N_s > 2$. From this fact, we conclude that we can find an optimal BALDA parameter U_{opt} for a given electron-electron interaction U_{ee} that minimizes the difference in the densities calculated, but it is different from U_{ee}.

Although we have not plotted all the cases, we observed that U_{opt} grows with the number of sites. However, the case of the two-sites system is exceptional: its optimized U_{opt} is actually larger than the one for eight sites. The reason behind this discrepancy lies in the different approach that we had to take for this case. We did not use the full BALDA (i.e., the one that treats the $n > 1$ and $n < 1$ cases separately), but we have modified the BALDA functional by applying Eq. 3.10 also for $n > 1$. We labeled this approach "mBALDA". When we use the full BALDA for the Hubbard dimer, the optimization process finds $U_{\text{ee}}(U) = 0$ (and, obviously $U_{\text{opt}} = 0$). This means that for a given electron-electron interaction parameter the best approximation is the zero functional. Conversely, it means that for some BALDA XCF the best approximated electron-electron interaction is given by non-interacting electrons.

One can understand this behavior from Fig. 3.2, which shows the E_{HXC} functionals for the two-sites model as a function of the density n_1 (for a two sites model with two electrons, it follows that $n_2 = 2 - n_1$). These functionals are the exact functional, the BALDA functional with $U = U_{\mathrm{ee}}^{\mathrm{ref}}$, the mBALDA functional with $U = U_{\mathrm{ee}}^{\mathrm{ref}}$ and the mBALDA with $U = U_{\mathrm{opt}}$. We are exploring values of the density (both n_1 and n_2) close to 1, and in this region it can be seen how the BALDA functional is in fact a very bad approximation to the Hubbard dimer, because of its discontinuity. This figure also illustrates how the optimization process generates a functional that, for the region explored by the densities that we used, improves over the BALDA with $U = U_{\mathrm{ee}}^{\mathrm{ref}}$. The cusp in the BALDA functional for $n = 1$ is the responsible of the failure of the BALDA: the cusp is a local maximum of the functional, instead of a minimum as it should be, as we can see from the plot of the exact functional. Ref. [64] also discusses how in the regime of weak interaction, and specially near half filling, the BALDA functional fails. For these reasons it is better to make the cusp disappear if we want a good approximation for this region. The height of the cusp depends on the value of U, only disappearing for $U = 0$. But $U = 0$ means that the full functional vanishes.

It becomes clear that the BALDA functional is a bad approximation for the Hubbard dimmer. On the other hand, for the rest of the cases, we have used the unmodified BALDA functional, and it served the purpose of providing a very satisfactory tool to optimize and approximate the exact functional.

3.3 Towards Larger Lattices: Density Matrix Renormalization Group

We have studied Hubbard chains with varying number of sites, and up to 20 sites, we have used a straightforward diagonalization of the Hamiltonian to solve the two-electron Schrödinger equation to get the exact densities needed as a reference for the optimization. This approach has a cubic scaling with the size of the lattice, and thus it quickly becomes the most limiting factor in the optimization process. Furthermore, the available memory of the computer may also become a limiting factor as the size of the system grows: the number of basis required for N electrons in a lattice with P sites grows as $\binom{2P}{N}$. Very soon, the size of the vectors carrying the orbitals, and the matrix for the Hamiltonian become intractable. One needs a more sophisticated scheme.

In our case, these limits restricted us to calculations with lattices of sizes up to 22 sites. To overcome these technical restraints, we used density matrix renormalization group [218] (DMRG), a theory based on the concept of truncation of the full Hilbert space of the system

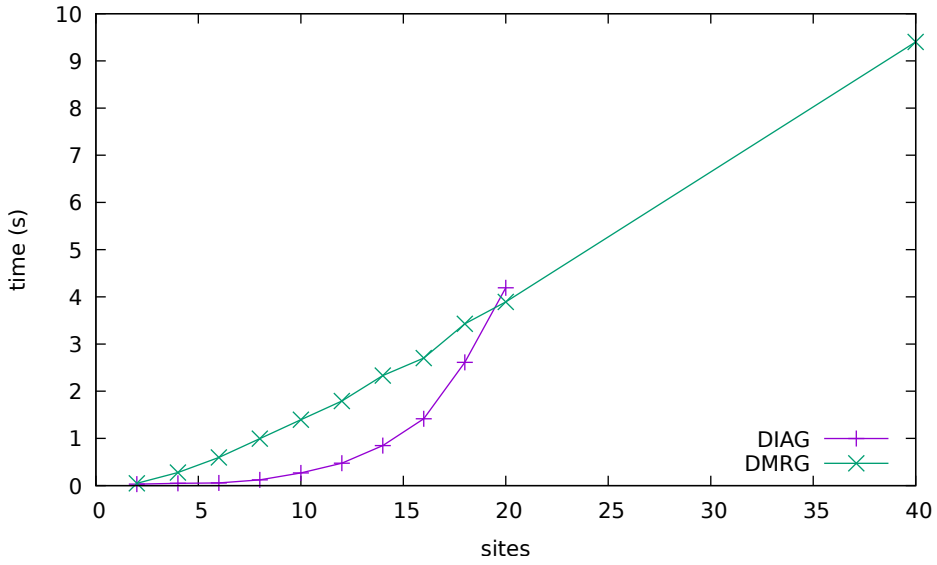

Fig. 3.3 Comparison between the times required to solve Schrödinger's equation using straightforward matrix diagonalization (DIAG) and DMRG, as a function of the number of sites. As we can see, the diagonalization method is faster than DMRG up to 20 sites. Then, the linear scaling of DMRG overtakes the cubic scaling of diagonalization.

that is remarkably efficient for one-dimensional lattice systems (check section 2.6 for a brief review of the theory). Using DMRG allowed us to go well past the initial limit of 22 sites, as the truncation of the Hilbert space not only alleviates significantly the memory problem, but it has a better scaling with the size of the lattice. In this way, we could tackle bigger systems in a reasonable amount of simulation time.

We can see the speed-up of the calculations in Fig. 3.3. While the solution of Schrödinger's equation using diagonalization shows a cubic scaling with the size of the lattice, the DMRG approach presents a linear scaling, which overtakes the other method around the 20 sites mark. For the implementation of DMRG, we used the ITensor Library [145].

The results obtained for the 40 sites lattice appear in Fig. 3.4. As we can see, the value obtained for the optimized U_{opt} parameter follows the previously seen trend (it grows with the size of the lattice).

3.4 Conclusions

We proposed a procedure to associate, numerically, an electron-electron interaction function (IF) to any XCF of DFT. We defined it as the IF for which the XCF performs best: i.e. the Kohn-Sham calculations based on it are the ones that most closely reproduce the ground state

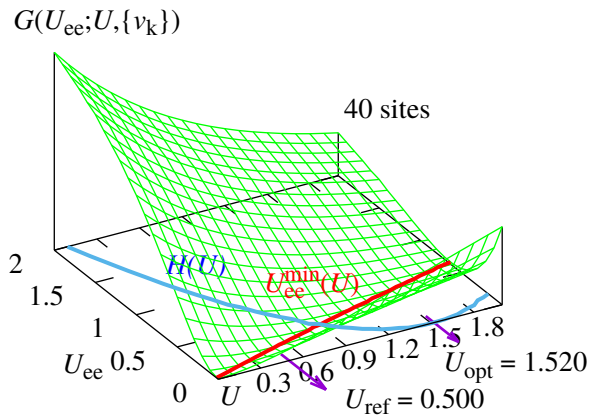

Fig. 3.4 Same as Fig. 3.1, but for a 40 sites lattice. The required exact calculations were done in this case with DMRG.

densities for a set of representative external potentials. Generally, it is not the real IF, i.e., the Coulomb interaction for electrons in 3D. In this work, however, we have not worked in 3D, but we have tested this approach using lattice DFT, concretely for 1DHM chains, as it allows us to work with a manageable number of degrees of freedom.

We have worked using the BALDA XCF as a test bed. It allows us to define a parameterized family of XCFs: the BALDA XCF depends on one parameter, in fact given by the constant defining the electron-electron interaction. We have observed how the parameter that defines the BALDA does not produce the best approximation for a Hubbard chain with the same interaction constant.

From this association process, we can devise a scheme to optimize parameterizated families of XCFs: looking for the XCF whose associated IF most closely resembles the real IF. In fact, optimizing the parameters of families of XC functionals to improve their performance has been used in the past as a method for the creation of new and better functionals. Although the usual approach is to try and improve the ground state energies for a set of external potentials, there could be better options [146]. In Ref. [129], for example, they looked at the densities, also using one-dimensional lattice models, to tune ansatze for the XC functional. Here we build upon this idea, but instead we focus on the associated IF, a smaller object than the full set of densities when considering the same family of external potentials.

The goal now is to take this idea to the 3D world. Ideally, this would allow us to answer many interesting questions, like what kind of screening the IF corresponding to the local density approximation presents, or how far away from the Coulomb interaction is a given XCF. However, by using the 1DHM, we reduced the degrees of freedom that define the IF to

just one, and it is not known how well this concept scales. The optimizations will grow in complexity and computational cost with the number of degrees of freedom, as one needs a way to generate high quality densities. We could overcome the difficulties posed by growing lattice sites in 1D by making use of DMRG, but unfortunately this method is only truly effective in 1D.

Chapter 4

Optimal Control in combination with Non-Adiabatic Molecular Dynamics

TDDFT is one of the most popular methods for the study of the excited electronic structure of atoms, molecules, solids or even complex biological compounds like proteins. The reason behind this success is the great cost/accuracy relation that sports, which translates into the ability to deal with bigger, more complex systems. TDDFT permits to study how the electrons react to perturbations such as the nuclear movements, laser pulses, magnetic fields, etc. It may be combined with some form of Molecular Dynamics to follow the full electron-nuclear movement. In particular, the Ehrenfest equations are well suited for a density-functional treatment, as the expression for the force is only dependent on the electronic density. In addition to studying the reaction of a system to an external perturbation, one may be interested in *controlling* the system by tailoring the perturbation. Thus, TDDFT may be coupled to optimal control theory [40], also in combination with Ehrenfest Molecular Dynamics (EMD) [37].

In this chapter we have combined TDDFT and the Ehrenfest model, with quantum optimal control theory to study and optimize the shape of femtosecond laser pulses that induce a Coulomb explosion on small sodium clusters. The results of this work were published in Ref. [74]. We start with an introduction to the problem and the methodology in section 4.1, present the theory in section 4.2, discuss the numerical implementation of the control method and the dynamics model in section 4.3, show the results obtained in section 4.4, and finish with the conclusions in section 4.5.

4.1 Introduction

Prompted by the rapid development of the laser technology [103], we assisted first to the creation of femtosecond science [230] in the last decades of the past century, and of attosecond science [111] at the beginning of this one. The access to high-intensity, short-duration laser sources allows us to analyze the effect of these pulses on ions and electrons in real time.

The study through simulations of the processes, both in and out of equilibrium, that appear in molecular and condensed matter physics is called Molecular Dynamics (MD) [173]. Usually, the "Molecular Dynamics" term, however, is reserved for the techniques in which the nuclei are approximated as classical point particles, while the electrons keep their quantum nature – the full quantum treatment is usually too computationally expensive for more than a few particles. Even with this approximation, the first principles treatment of quantum electrons in a non-equilibrium situation is still a complex and expensive problem [199]. One then differentiates the "classical" MD schemes in which the electronic problem is integrated out, and a set of force-fields determine the ionic movement, from the "first principles" or "ab initio" MD procedures, that deal explicitly with the electronic structure.

One must also consider whether or not the electronic system is fixed to the ground state determined by the configuration of the classical nuclei. If so, one may use an adiabatic MD. This assumption, unfortunately, does not provide a good framework for the kind of highly excited situations caused by high-intensity short-duration pulses: in general, the electron-nuclear coupling is non-adiabatic. This means that, if we want to model these processes, we need a first principles theory for the many-electron quantum dynamics that is non-adiabatically coupled to the classic nuclear system.

One way to achieve this is by combining TDDFT with EMD (check section 2.3 for a brief description of the model and how it mixes with TDDFT). This combination was first used by Theilhaber [206] and its applicability to laser-matter interaction has been successfully tested in numerous occasions [181, 29, 113, 39, 149, 180].

Besides TDDFT and EMD, the other ingredient of this chapter is control theory. Thanks to the developments of laser sources, controlling quantum dynamics became a reality, and thus the field of coherent quantum control [229, 22, 41, 43, 205, 65, 101, 4, 175, 195, 20] was born. The most complete theory to match these experimental advancements is called quantum optimal control theory (QOCT, check section 2.5 for an introduction, and for a brief description of its combination with TDDFT). This theory studies the diverse methods that can be applied to the following type of problem: given a quantum system, and given a set of parameters that determine its equation of motion, find those that optimize the system behavior with respect to some predefined target, encoded as a functional of the system trajectory. The

first applications of QOCT go back to the 1980s [196, 161, 108, 94], and the following years saw a rapid development of the field [217, 20].

It has also been combined with TDDFT [40] to extend the control to electronic systems. A next logical step is to add to the combination an ab initio non-adiabatic MD model, thus creating a control framework for hybrid classical-quantum systems. The mixture of OCT with classical MD has already been explored [193, 19], whereas for ab initio MD, the EMD+TDDFT scheme has proven to be useful when combined with QOCT. The basic equations for this method were outlined in Ref. [37], and a proof of concept was reported in Ref. [35], in which the the scheme was applied to H_2 and H_3^+ systems.

In this work we expanded the size of the systems treated with the combination of QOCT with EMD+TDDFT: We optimized the laser pulses that induce the Coulomb explosion of small sodium clusters, for a fixed pulse fluence, total duration and cutoff frequency. There are three reasons behind the choice of the Coulomb explosion for sodium clusters as a case study for our scheme: (1) As a violent, far from equilibrium process [60], the regular perturbative approaches fail, requiring a nonperturbative scheme like the one we use; (2) TDDFT has demonstrated its capacity for the treatment of high intensity irradiation of simple metal clusters [30, 220]; (3) The study of the Coulomb explosion of these systems with EMD+TDDFT has been studied [29, 201, 130], showing an interesting interplay between the pulse, the ionic motion and the electrons.

Furthermore, the problem really requires a control theory, as the solution cannot be guessed from physical intuition. One may initially think that the ionization, and subsequent Coulomb explosion, is optimized by setting the laser pulse frequency to the main resonance of the cluster. However, the system undergoes changes during the action of the pulse. First, the ionization produced by the pulse causes a blueshift in the frequency of the plasmon resonance of the cluster. Then, when the nuclei start to separate from each other, this cluster broadening implies a redshift of the resonances [201, 34, 35]. One may therefore wonder then what is the frequency that one should use in order to maximally ionize, and therefore induce the Coulomb explosion: the original resonance, a redshifted, a blueshifted pulse? Predicting the shape of the laser a priori is a complicated, nonintuitive problem. This is precisely the kind of problem for which QOCT was invented.

4.2 Theory

In section 2.5 we presented the basics of QOCT, and of its combination with TDDFT. We will now add to the mixture EMD, the non-adiabatic hybrid classical-quantum scheme described

in section 2.3. We will outline here the key results; for a more detailed discussion, check Ref. [37].

We first recall the basic equations of EMD: In EMD the nuclei are described as classical point particles, characterized by a set of conjugated position and momenta variables $\{R,P\} = \{R_\alpha, P_\alpha\}_{\alpha=1}^{K}$, where α runs over the K nuclei of the system with mass M_α and charge z_α. The state of the N electrons is determined by its many-body wave function Ψ. The forces that drive the nuclear dynamics, when the system is subject, for example, to a laser pulse in the dipole approximation, are given by

$$F_\alpha[R(t),\Psi(t),u,t] = -\nabla_\alpha W^{nn}(R(t)) + z_\alpha \varepsilon(u,t)\pi - \langle\Psi(t)|\nabla_\alpha \hat{H}[R(t),u,t]|\Psi(t)\rangle\,. \quad (4.1)$$

The real-valued function $\varepsilon(u,t)$ is the amplitude of the laser pulse and π is its polarization vector. The set $u = \{u_1,u_2,...,u_M\}$ is formed by the "control parameters" that determine the shape of the pulse. W^{nn} is the nucleus-nucleus interaction that take the usual Coulomb form

$$W^{nn}(R) = \sum_{\alpha<\beta} \frac{z_\alpha z_\beta}{|R_\alpha - R_\beta|}\,, \quad (4.2)$$

and $\hat{H}$ is the electronic Hamiltonian (Eq. 2.2). When using the dipole approximation, it takes the form:

$$\hat{H}[R,u,t] = \sum_{i=1}^{N} \frac{\hat{p}_i^2}{2} + \sum_{i<j} \frac{1}{|\hat{r}_i - \hat{r}_j|} + \varepsilon(u,t)\sum_{i=1}^{N} \hat{r}_i\cdot\pi + \sum_{i=1}^{N}\sum_{\alpha}^{K} v^\alpha(|\hat{r}_i - R_\alpha(t)|)\,, \quad (4.3)$$

where $\hat{r}_i$ and $\hat{p}_i$ are the position and momentum operators for the ith electron, and the electron-nucleus interaction takes the Coulomb form $v^\alpha(r) = -\frac{z_\alpha}{r}$ (although in our implementation we will use pseudopotentials [192]).

We do not use, however, the many-electron wave function Ψ: instead, we employ TDDFT, that substitutes the interacting electronic system with a fictitious non-interacting one which can be described using a single Slater determinant formed by N orbitals. The electronic density is given, in terms of the Kohn-Sham orbitals $\{\varphi_i\}$ that compose that Slater determinant, by

$$n(r,t) \equiv n_t(r) = \sum_{i=1}^{N/2} 2|\varphi_i(r,t)|^2\,, \quad (4.4)$$

where we assume a spin-restricted configuration with an even number of electrons filling doubly occupied orbitals, no magnetic fields and no spin-orbit coupling. The evolution of the

Kohn-Sham orbitals is given by the time-dependent Kohn-Sham (TDKS) equations (2.57):

$$i\frac{\mathrm{d}}{\mathrm{dt}}|\varphi_i(t)\rangle = \hat{H}_{\mathrm{KS}}[R(t),n_t,u,t]|\varphi_i(t)\rangle \qquad (i=1,...,N/2)\,. \tag{4.5}$$

The Kohn-Sham Hamiltonian $\hat{H}_{\mathrm{KS}}$ is:

$$\hat{H}_{\mathrm{KS}}[R(t),n_t,u,t] = \frac{1}{2}\hat{p}^2 + \sum_\beta \hat{v}^\beta(|\hat{r}-R_\beta(t)|) + \varepsilon(u,t)\hat{r}\cdot\pi + \int \mathrm{d}r'\,\frac{n_t(r')}{|r-r'|} + v_{\mathrm{xc}}[n_t](r)\,. \tag{4.6}$$

The last term is the exchange-and-correlation potential; for this work we have simply chosen the adiabatic local density approximation (ALDA), the most basic of all functionals, that is however both well tested in similar situations [201] and a good enough approximation to draw qualitative conclusions (check subsection 2.2.3 for a brief discussion on functionals).

The key now is to consider the last term of Eq. 4.1, that may be exactly rewritten in terms of the density only:

$$\langle\Psi(t)|\nabla_\alpha\hat{H}[R(t),u,t]|\Psi(t)\rangle = \int \mathrm{d}r\, n(r,t)\nabla_\alpha v^\alpha(|\hat{r}-R_\alpha(t)|)\,. \tag{4.7}$$

This fact permits to avoid the use of the true many-body wave function, and use the TDDFT Kohn-Sham system instead. In practice, the equations of motion for the atomic nuclei that are implemented are:

$$\begin{aligned}
\dot{R}_\alpha(t) &= \frac{1}{M_\alpha}P_\alpha\,,\\
\dot{P}_\alpha(t) &= F_\alpha[R(t),\varphi(t),u,t]\\
&= -\nabla_\alpha W^{nn}(R(t)) + z_\alpha\varepsilon(u,t)\pi - \sum_{m=1}^{N/2} 2\langle\varphi_m(t)|\nabla_\alpha v^\alpha(|\hat{r}-R_\alpha(t)|)|\varphi_m(t)\rangle\,.
\end{aligned} \tag{4.8}$$

In these equations, the density is expanded in terms of the Kohn-Sham orbitals φ_m because normally one makes use of non-local pseudo-potentials, that do require the explicit use of the orbitals.

We move now on to the control problem: the search for the particular set of parameters u that optimize a requested behavior of the system – in the case discussed here, the Coulomb explosion. Following section 2.5, one must start by proposing a target functional J_1 in terms of the variables of the system $\{R,P,n,u\}$, whose maximization leads to the desired system behavior:

$$J_1 = J_1[R(T),P(T),n_T,u]\,. \tag{4.9}$$

Note that we restrict the definition by employing only $R(T), P(T)$ and n_T (where T is the time at the end of the propagation), and not the full propagation history: this functional only depends on the state of the system at the end of the propagation (it is a "terminal target"). As we know, the election of each set of parameters u determines the evolution of the system: $u \to R[u], P[u], n[u]$, and thus we may define a real function $G(u)$ as

$$G(u) = J_1[R[u](T), P[u](T), n_T[u], u]\,. \tag{4.10}$$

In the following, we will drop this explicit $[u]$-dependence in the notation.

The purpose of QOCT is, in essence, to find the extrema of this function. One particularly useful information for this task is the gradient of G with respect to its parameters u, since it allows to use the family of gradient-based optimization algorithms. For our EMD+TDDFT model, one may derive the expression [37]:

$$\frac{\partial G}{\partial u_k} = \int_0^T \mathrm{dt}\, \frac{\partial \varepsilon}{\partial u_k}(u,t) g(t)\,, \tag{4.11}$$

$$g(t) = -\sum_\beta z_\beta \tilde{R}_\beta(t) \cdot \pi + 2\mathrm{Im} \sum_{m=1}^{N/2} \langle \chi_m(t) | \hat{r} \cdot \pi | \varphi_m(t) \rangle\,. \tag{4.12}$$

Here, we have introduced a new auxiliary system called the *costate*. This is a hybrid system characterized by the position and momentum variables $\{\tilde{R}, \tilde{P}\}$, and the orbitals $\{\chi_m\}_{m=1}^{N/2}$. The costate is defined though its equations of motion:

$$\dot{\tilde{R}}_\alpha(t) = \frac{1}{M_\alpha} \tilde{P}_\alpha(t)\,, \tag{4.13a}$$

$$\dot{\tilde{P}}_\alpha(t) = \nabla_\alpha \sum_\beta \tilde{R}_\beta(t) \cdot F_\beta[R(t), \varphi(t), u, t] + 2\mathrm{Re} i \sum_{m=1}^{N/2} \langle \chi_m(t) | \nabla_\alpha \hat{H}_{\mathrm{KS}}[R(t), n_t, u, t] | \varphi_m \rangle\,, \tag{4.13b}$$

$$|\dot{\chi}_m(t)\rangle = -i\hat{H}_{\mathrm{KS}}[R(t), u, t]|\varphi_m\rangle - i\sum_{n=1}^{N/2} \hat{K}_{mn}[\varphi(t)]|\chi_n(t)\rangle - 2\sum_\beta \tilde{R}_\beta \cdot \nabla_\beta \hat{v}^\beta(|\hat{r} - R_\beta(t)|)|\varphi_m(t)\rangle\,. \tag{4.13c}$$

The first term in the equation for the evolution of the costate orbitals χ is just the Kohn-Sham Hamiltonian that also moves the Kohn-Sham orbitals, but in addition there are some extra terms. One of them is a non-Hermitian operator K_{mn} defined by:

$$\langle r | \hat{K}_{mn}[\varphi(t)] | \chi_m(t) \rangle = -4\mathrm{i}\varphi_m(r,t)\mathrm{Im} \int \mathrm{dr}'\, \chi_n(r,t) f_{\mathrm{Hxc}}[n_t](r,r') \varphi_n(r,t)\,, \tag{4.14}$$

where the *kernel* f_{Hxc} is the functional derivative of the Hartree and exchange and correlation potential functionals (Eq. 2.148). The presence of these extra terms in the equation of motion for the costate orbitals leads to some numerical difficulties, as described below.

The boundary conditions for these equations are

$$\tilde{R}_\alpha(T) = -\frac{\partial}{\partial P_\alpha} J(R(T), P(T)), \tag{4.15a}$$

$$\tilde{P}_\alpha(T) = \frac{\partial}{\partial R_\alpha} J(R(T), P(T)), \tag{4.15b}$$

$$\langle r|\chi_m(T)\rangle = \frac{\delta J}{\delta \varphi_m^*(r,T)}, \tag{4.15c}$$

which actually are final value conditions, that require knowledge of the real system at the final time T. This means that computing the gradient of G requires a *forwards* propagation of the EMD+TDDFT model, and a *backwards* propagation of the costate with the final value conditions found previously.

4.3 Implementation

To carry out the QOCT+EMD+TDDFT scheme described above, we used the Octopus code, where we have implemented the equations for the real system and for the costate. In this code, the system is contained in a simulation box where the Kohn-Sham orbitals, densities, potentials, etc. are represented in a real space rectangular grid. For our simulations we chose spherical simulation boxes for Na_2 and Na_8 and a cylindrical one for Na_4, with zero boundary conditions. For general information about the numerical techniques used by Octopus, check Refs. [139, 140, 36, 3]. In the following, we briefly comment on some specific issues that affect the calculations described in this chapter in particular:

1. The solution of the equations of motion require the computation of the action of operators in the form

   $$\nabla_{R_a} f(\hat{r} - R_a). \tag{4.16}$$

   In a real-space code like Octopus, it may be advantageous to substitute the numerical derivatives of f with numerical derivatives of the wave function using the identity

   $$\nabla_{R_a} f(\hat{r} - R_a) = -i[\hat{p}, f(\hat{r} - R_a)]. \tag{4.17}$$

   Ref. [84] discusses the advantages and reasons for this procedure.

2. We also have derivatives of the force, present in Eq. 4.13b:

$$\nabla_\alpha \sum_\beta \tilde{R}_\beta(t) \cdot F_\beta[R(t), \varphi(t), u, t]\,. \tag{4.18}$$

As they are a double derivatives of the potential, we have used a finite-difference approach: we compute the forces at neighboring values of the nuclear positions.

3. For the parameterization of the pulse, we have chosen one based on the coefficients a_n, b_n of the Fourier expansion:

$$\varepsilon(u,t) = \sum_{n=0}^{K} \left[a_n(u) \cos\left(\frac{2\pi}{T} nt\right) + b_n(u) \sin\left(\frac{2\pi}{T} nt\right) \right]. \tag{4.19}$$

In this form, we have a clear cutoff frequency $\omega_{\max} = \frac{2\pi}{T} K$ for the shape of the control function. The parameters have to fulfill these conditions:

$$\varepsilon(u,0) = \varepsilon(u,T) = 0\,, \tag{4.20a}$$

$$\int_0^T \mathrm{dt}\; \varepsilon(u,t) = 0\,, \tag{4.20b}$$

$$\int_0^T \mathrm{dt}\; \varepsilon^2(u,t) = F_0\,. \tag{4.20c}$$

The first two equations are natural restraints for an electric field generated by a laser pulse, and the last one fixes the fluence at F_0. This last condition is necessary for our problem because, as we are looking for laser pulses that induce a Coulomb explosion in our system, without it the optimization algorithms would simply raise the intensity of the pulse to infinity. As described in [112], the parameters u and functions $a_n(u), b_n(u)$ are chosen so as to run over the set of Fourier coefficients compatible with the previous constraints.

4. In order to model the ionization of the nuclei caused by the laser pulse, we added an imaginary absorbing potential in the border of the simulation box. In this way we differentiate between two regions: an inner one where there is no absorbing potential and an outer one where, given the imaginary nature of the potential applied, the electron charge will decrease. This potential is defined by

$$V_{\mathrm{abs}}(r) = i\eta \sin^2\left(\frac{d(r)\pi}{2L}\right), \tag{4.21}$$

where L is the width of the absorbing region and $d(r)$ is the distance from the point r to the border between the inner and outer parts of the simulation box. This fact, together with the presence of non-Hermitian operators in the equations of motion of the costate, implies that the norms of the orbitals are not preserved during the propagation.

5. The backwards propagation of the costate, at each time t, requires of the knowledge of the true state at that time t. This could be achieved by storing at every time step the state obtained during the previous forward propagation, but the size of the disk storage required would be enormous and the operations to write to and read from the disk are too slow. For this reason it is more practical to recompute the state of the system at all times, by performing a backwards propagation along with the costate.

   This procedure, however, entails a numerical difficulty: The forward propagation sees a diminishing norm as a consequence of the absorbing boundaries, and thus the numerical error (that is proportional to the norm) decreases: the evolution is thus numerically stable. The opposite effect occurs for the backwards propagation: the increase in the value of the norm leads to a numerically unstable evolution. To ensure that the backwards propagation does not break, we set some "milestone points" during the forward propagation, at which the orbitals are stored. During the backwards propagation, these orbitals are compared with the propagated orbitals and, if the difference overcomes some predefined tolerance, we substitute the backward-propagated orbitals with the stored ones.

6. Regarding the optimization algorithm we have many available options. Some of them were specifically developed for QOCT [232, 233, 204, 198, 132], but many of these approaches lack the generality required by our model (for example, some of them assume a determined parameterization of the laser pulse, or can be applied only to pure QOCT, making them unusable for our hybrid model). We have therefore chosen a general-purpose gradient-dependent optimization algorithm, the low-storage BFGS algorithm [155, 125].

   We need to compute the gradient in a very precise manner, as both the speed and success of the algorithm depend on this. The computation of the gradient, unfortunately, is a complex procedure (propagate the equations of the system and the costate and then the integration of Eq. 4.11), with the time-step Δt being the key parameter of the numerical propagation. We found that we need a precision in the operations of order Δt^4, or else the error scales too fast with the total propagation time T. To assure the order four in

the integration of Eq. 4.11, we use Simpson's rule:

$$\int_0^T \mathrm{dt}\, y(t) = \frac{\Delta t}{3}\left[y(0) + 2\sum_{j=1}^{N/2-1} y(t_{2j}) + 4\sum_{j=1}^{N/2} y(t_{2j-1}) + y(T)\right], \tag{4.22}$$

where $t_j = \Delta t\, j$.

7. Finally, regarding the propagation scheme, we chose the standard order four explicit Runge-Kutta (RK) method (check subsection 2.4.2, for a brief review of the RK methods).

   We have to propagate both the full EMD+TDDFT hybrid system and the costate. For the propagation of the state the RK method requires the evaluation of the Kohn-Sham Hamiltonian, its application on the Kohn-Sham orbitals and the computation of the forces over the nuclei four times for each step. For the costate we have two extra non-local terms for the costate orbitals χ_m. The application of the non-Hermitian operators K_{mn} to each Kohn-Sham orbital results in a bad scaling of the costate propagation with the size of the system (roughly order four with the number of electrons) compared with the order two for the TDKS equations. Also, the last term in Eq. 4.13c makes it inhomogeneous. This complicated structure requires a robust and general propagation method, and despite its computational cost, we found that the chosen RK method was the best option available.

4.4 Results

Using the methodology described in the previous sections, we set out to find the shape of the laser pulse that optimizes the Coulomb explosion of different sodium clusters for a determined duration, fluence and cutoff frequency of the pulse. We have tested this approach for Na_2, Na_4 and Na_8.

The first step is computing the initial state of the system, starting from the geometry of the clusters found in the literature [92, 197, 160], and then using Octopus to find the configuration where the forces among the nuclei vanishes. We found that the final configurations obtained did not differ significantly from the reference ones – only the bond length being slightly shorter, a well known failure of the LDA.

We then define a "reference" pulse with duration T as

$$\varepsilon(t) = A e^{-(t-t_0)^2/2\eta^2} \sin(\omega_0 t)\,, \tag{4.23}$$

where A is the amplitude, $t_0 = T/2$ marks the peak of the pulse, $\omega_0 = 800$ nm is its frequency and $\eta = 0.8\tau_0$ gives us the width of the pulse as a function of its period $\tau_0 = 2\pi/\omega_0$. We explored pulses with a duration T of 6, 12 and 24 periods τ_0 of the reference pulse, which results in $T \approx 16$, 32 and 64 fs. The search space also depends on the total fluence of the pulse (Eq. 4.20c), which is controlled by the amplitude A.

The optimization runs are then started from random pulses having the general shape given in Eq. 4.19, and equal fluence and duration as the reference one. We perform various runs for every case, with several random initial guesses, as there may be many local maxima. One must also specify a cutoff frequency for the Fourier expansion 4.19: we have chosen $\omega_{\text{cutoff}} = 0.5$ Ha. Once the cutoff frequency is given, it determines the number of parameters u that compose the search space.

It remains however to specify the most important object: the target functional for the optimization. It must be chosen according to the physical objective that one wants to achieve. In our case, the goal is to induce the Coulomb explosion of the clusters. Accordingly, we have tried the two following target functionals:

1. A momentum based target, where we try to optimize the difference of momentum among the nuclei at the end of the propagation

$$J[P(T)] = \sum_{i<j} |P_i(T) - P_j(T)|^2 . \tag{4.24}$$

   In a Coulomb-exploding cluster, the nuclei are moving fast apart from each other, and therefore the momenta differences are large.

2. Using the lost charge as a measure of the ionization, we define

$$J[n_T] = -\int_V \mathrm{d}\mathbf{r}\, n_T(r) , \tag{4.25}$$

   with n_T being the electronic density at the end of the propagation. As the ionization of the system is what causes the Coulomb explosion, maximizing the charge escape is also a logical way to define the target.

For the second target, we performed both optimizations with static nuclei (applying only the QOCT on top of TDDFT as described in section 2.5), and with moving nuclei, using QOCT on top of the hybrid model EMD+TDDFT as described above in this chapter.

To check the quality of the obtained pulses, we repeated the propagations in a bigger simulation box, and for longer times. In this way we allow the nuclei to travel far away from their initial positions without reaching the simulation box boundaries, and we can check the

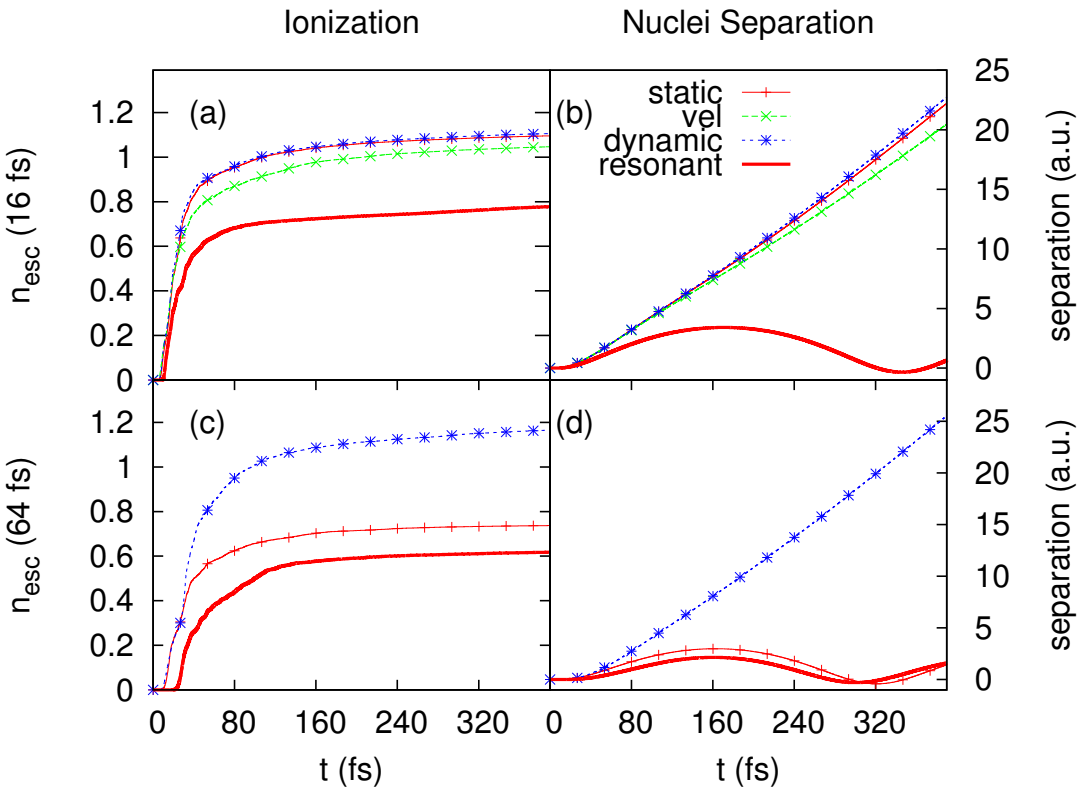

Fig. 4.1 Left panels (a, c): Electrons escaped from the Na_2 molecule after applying the pulses obtained using the three different optimization schemes: the momentum-based target ("vel"), the ionization target with fixed nuclei ("static"), and with moving nuclei ("dynamic"). We also plot the ionization obtained with the laser tuned to the resonance frequency pulse ("resonant"). Right panels (b, d): Separation between the nuclei from their equilibrium position. Top panels (a) and (b) correspond to 16 fs pulses; bottom panels (c) and (d) correspond to 64 fs pulses.

convergence of the solutions with respect to the size of the box. We also used a laser pulse with the shape defined in Eq. 4.23, but tuned to the most relevant excitation frequency of the system to check how much the optimized solutions improve over this naive choice for the pulse.

4.4.1 Na_2

For the Na_2 molecule, Octopus with LDA found a bonding length of 5.48 a.u., shorter than the experimental one of 5.82 a.u. [92], as expected. The laser was polarized along the dimer axis.

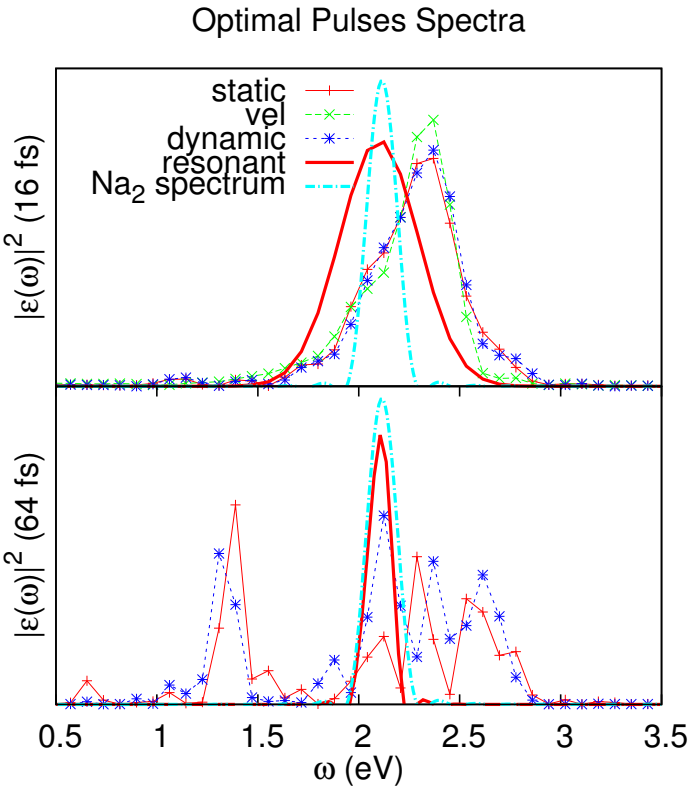

Fig. 4.2 Spectra of the optimized pulses and of the resonant pulse, and absorption spectrum of the Na_2 molecule for light polarized along its axis. Top panel for the 16 fs pulses; bottom panel for the 64 fs pulses.

We present the results for the ionization of the dimer as well as the separation between the nuclei in Fig. 4.1. The three optimization schemes (the momentum based one labeled "vel", the density-based one with fixed nuclei labeled "static", and the density-based one with moving nuclei labeled "dynamic") are compared with the effects of the quasi monochromatic pulse tuned to the resonance frequency $\omega = 2.1$ eV of Na_2 (labeled "resonant"). In the top panels we have the results for the $6\tau_0 \approx 16$ fs pulses, with a peak intensity of the reference pulse 10^{12} W cm^{-2}, while in the bottom ones there are the $24\tau_0 \approx 64$ fs ones where we reduced the intensity to 3×10^{11} W cm^{-2}. The power spectra of the optimal found pulses and of the reference pulse, and the absorption spectrum of the dimer (computed using the linear response formalism of TDDFT) appear in Fig. 4.2.

The top panels of the Fig. 4.1 show that all the schemes managed to find a pulse that induces the Coulomb explosion of the cluster for the 16 fs pulses. As shown in the top panel of Fig. 4.2, the main frequencies of the optimized pulses are a bit higher than the resonance frequency, a blueshift caused by the rapid ionization of the molecule during the application of the pulse. On the other hand, given that both the schemes that consider the nuclei movements and the static one have produced not only the desired Coulomb explosion, but also pulses with very similar shapes, we can conclude that the nuclear movement is not significant during the duration of the pulse. It is worth noting that, in contrast, the simple resonant pulse does not produce a fast enough ionization of the system, and fails to produce the photodissociation.

To investigate the effect of the nuclear movement we tried longer pulses (around 64 fs). The bottom panels of Fig. 4.1 show that, in this case, the "dynamic" target manages to find a pulse that produces the Coulomb explosion of the cluster, while the "static" one fails. In this case, therefore, the nuclear displacement produced during the duration of the pulse is relevant, and ignoring it during the optimization runs prevents us from finding effective pulses. It is clear that for these pulses durations the full QOCT+EMD+TDDFT approach is necessary. Furthermore, we can see in Fig. 4.2 how the the shape of both optimized pulses is quite different – and also different from the simple resonant pulse.

4.4.2 Na_4

The lowest energy configuration for the Na_4 cluster is obtained when its four atoms are arranged as a rhombus. We labeled the short axis as X and the long axis as Y. We have chosen to fix the polarization of the laser along the X axis, for which the Na_4 has a main resonance energy of $\omega_X = 2.7$ eV (for the Y axis the energy is $\omega_Y = 1.9$ eV).

The results for the ionization and total nuclei separation as a function of time, obtained for this Na_4 cluster appear in Fig. 4.3. Fig. 4.4 shows the spectra of the pulses obtained,

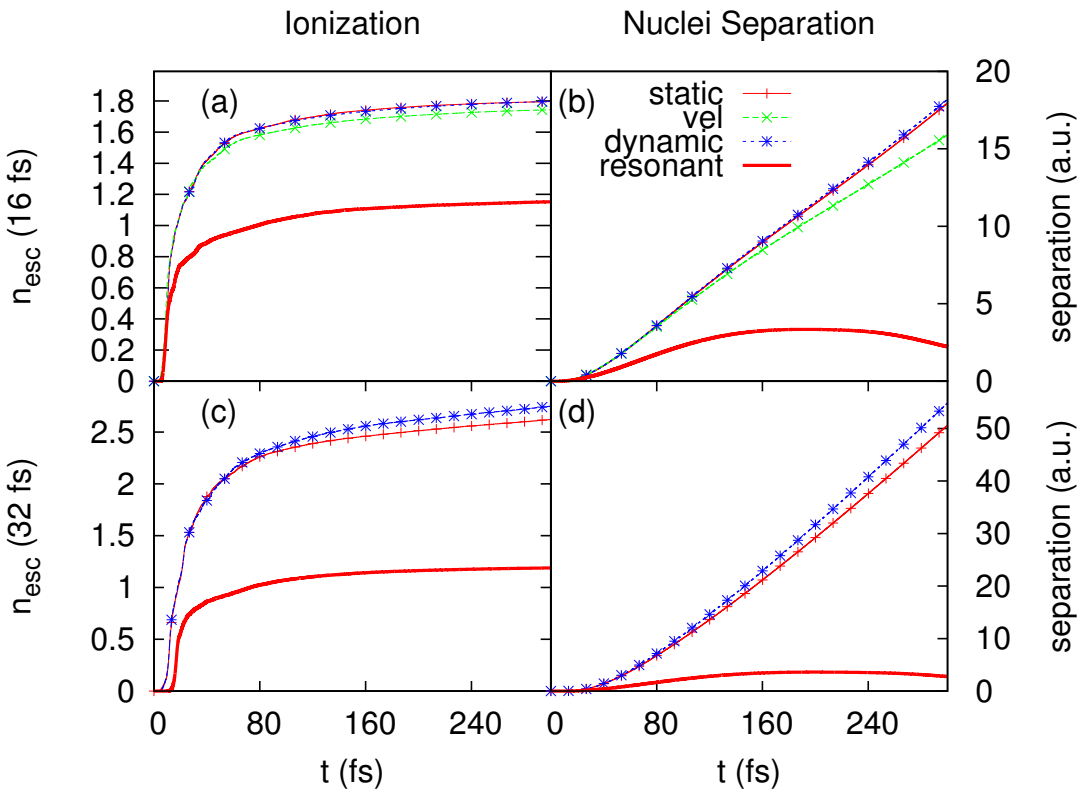

Fig. 4.3 Left panels (a, c): Electrons escaped from the Na_4 cluster after applying the pulses obtained using the three different optimization schemes: the momentum-based target ("vel"), the ionization target with fixed nuclei ("static"), and with moving nuclei ("dynamic"). We also plot the ionization obtained with the laser tuned to the resonance frequency pulse ("resonant"). Right panels (b, d): Overall nuclear separation [Eq. (4.26)]. Top panels (a) and (b) correspond to 16 fs pulses; bottom panels (c) and (d) correspond to 32 fs pulses.

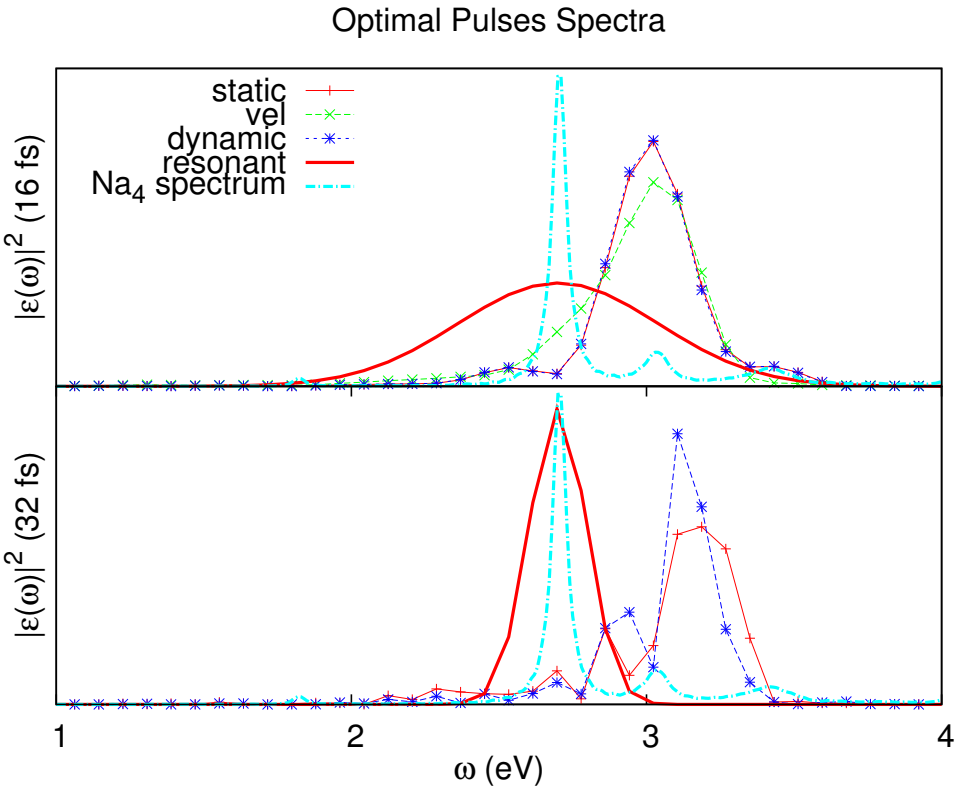

Fig. 4.4 Spectra of the optimized pulses and of the resonant pulse, and absorption spectrum of the Na_4 molecule for light polarized along the X axis. Top panel for the 16 fs pulses; bottom panel for the 32 fs pulses.

together with the reference pulse and the Na_4 absorption spectrum in the X direction. Here, we define the separation as

$$R(t) = \sum_{i<j} |R_i(t) - R_j(t)| - R_{\text{eq}}\,, \tag{4.26}$$

where $R_{\text{eq}} = \sum_{i<j} |R_i(0) - R_j(0)|$ (and therefore $R(0) = 0$).

In this case, we tried 16 and 32 fs pulses. We found optimal pulses for all the optimization targets in both situations. While for the shorter pulses the shape of the lasers obtained barely differ among them, when we look at the 32 fs results we see that the shape of the found pulses differ significantly – although both the static and dynamic optimization schemes manage to Coulomb explode the cluster. This means that the ionic movement starts playing an important role in this range of times. Just like in the Na_2 case, the main frequency of the pulses is slightly blueshifted from the main X axis resonance frequency.

4.4.3 Na_8

For the geometry of the Na_8 cluster we used the D_{4d} symmetry. There is some controversy [160] about which one of the D_{2d}, D_{2h} or D_{4d} geometries is the most stable ground state configuration for this cluster. We chose the D_{4d} geometry because it has a strong absorption peak at 2.55 eV. The pulse was polarized along the Z axis.

As the calculations for this system required long computational times, we only tested the optimization scheme for 16 fs pulses for the static and dynamic ionization based target. In Fig. 4.5 are plotted the ionization and nuclear separation (as defined in Eq. 4.26) for both optimization schemes and for a pulse at the plasmon resonance. Both optimization methods lead to successful laser pulses that manage to Coulomb explode the cluster. In this case the "static" target solution slightly improves over the "dynamic" one, with both of them leading to an ionization that saturates around 2.75 electrons. On the other hand, the ionization induced by "resonant" pulse lies below two electrons, which leads to oscillations of the nuclei around their equilibrium positions.

Fig. 4.6 shows that the spectra of the optimized pulses are similar and, again, blueshifted with respect to the plasmon resonance of the Na_8 cluster caused by the rapid ionization during the pulse. As both the static and the dynamic approaches result in similar pulses, we can conclude that the ionic movement is small in this time frame.

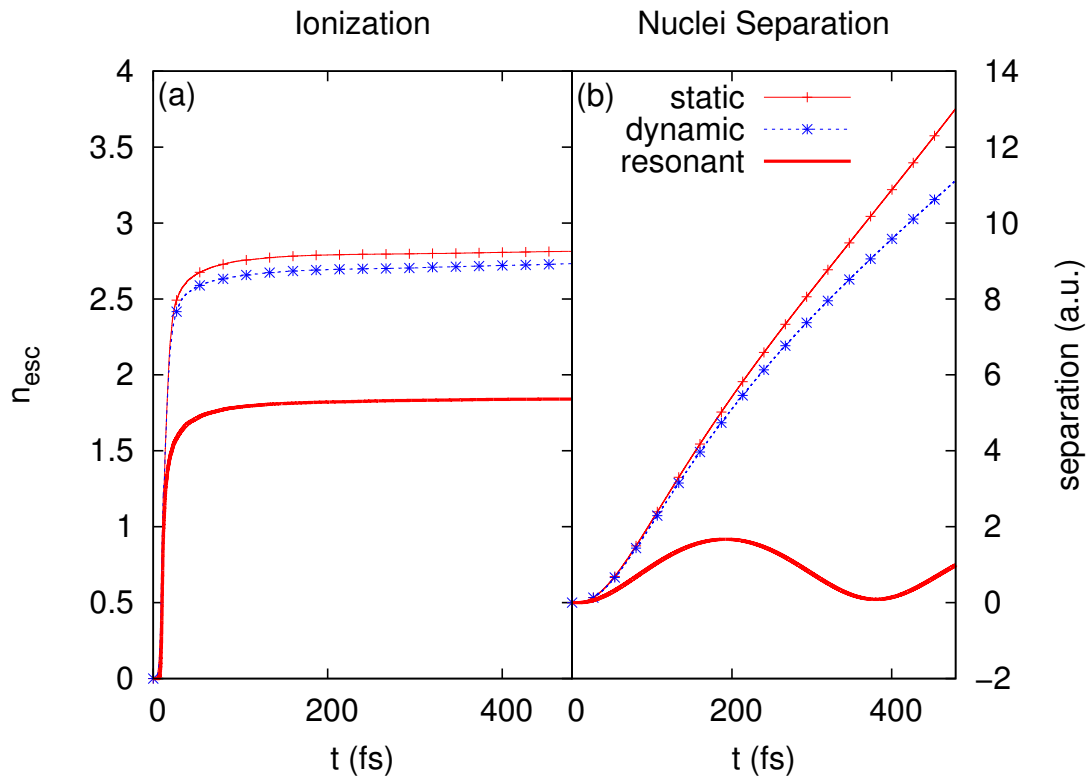

Fig. 4.5 (a) The ionization of the Na_8 cluster after applying the pulses obtained using the static and dynamic nuclei ionization optimization schemes, using light polarized along the Z axis. (b) The overall separation between the nuclei [Eq. (4.26)] that conform the Na_8 cluster calculated with respect to the equilibrium separation.

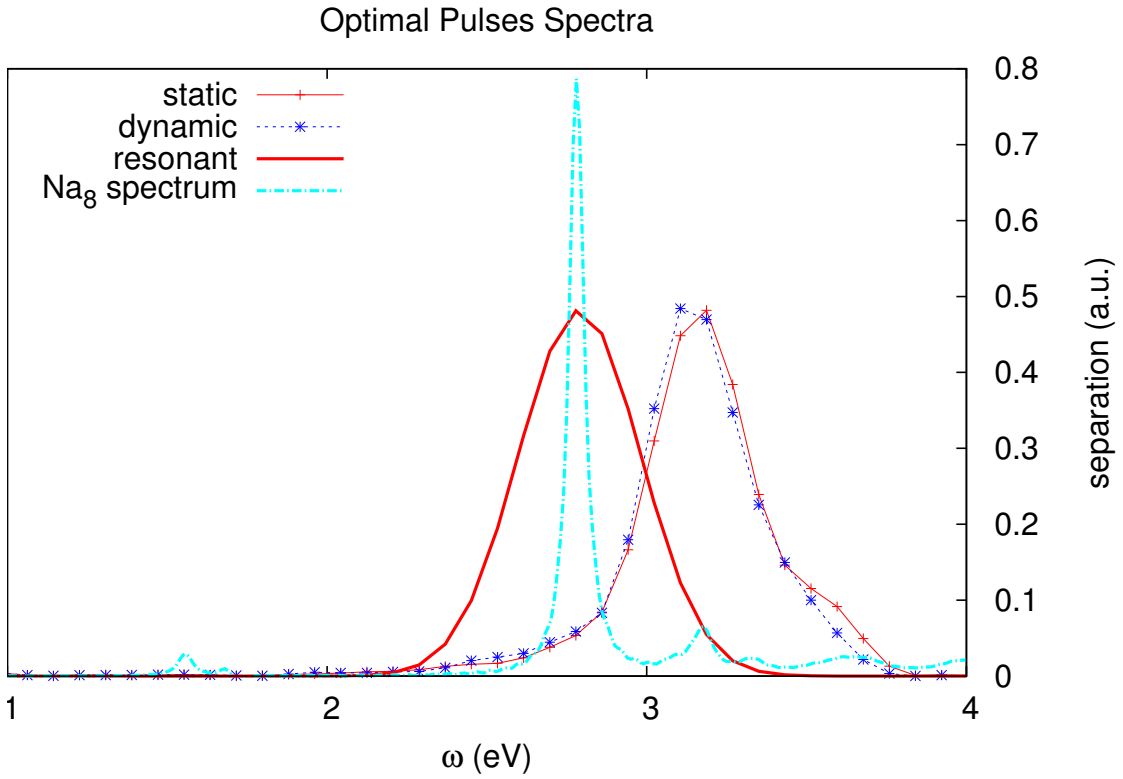

Fig. 4.6 Spectra of the optimized pulses and of the resonant pulses, and absorption spectrum of the Na_8 cluster for light polarized along the Z axis.

4.5 Conclusions

We have applied QOCT techniques to the optimization of the Coulomb explosion of small sodium clusters, where the control mechanisms were laser pulses with a given duration, fluence and cutoff frequency. To describe the dynamics of the sodium clusters we used the EMD+TDDFT model, a non-adiabatic approach which describes our physical system as an hybrid of classical nuclei and quantum electrons. We chose sodium clusters to show that this technique can go beyond simple systems like the hydrogen molecule, already presented in Ref. [35]. The Coulomb explosion for these clusters presents an interesting interplay between the laser pulse, the electronic ionization and ionic movement, a strongly non-adiabatic process not suitable for ordinary adiabatic molecular dynamics. It is also a fitting problem for QOCT because while naively one could think that simply using a laser pulse tuned to the frequency of the plasma resonance of the cluster would trigger the Coulomb explosion, actually some factors affect this frequency during the application of the pulse: the separation of the nuclei induces a redshift in the resonance frequency, while the ionization of the cluster causes a blueshift. Therefore, the choice of the optimal laser pulse for the task is a non-trivial matter.

For the optimization of the laser pulses we used a nonlinear gradient-based function maximization algorithm for a target function dependent on the parameters of the pulse. To compute the gradient of this function we have to propagate both forwards and backwards the EMD+TDDFT equations of motion and its associated costate, an auxiliary system. In the propagation of the costate is where we find the main numerical difficulties of the QOCT scheme: (1) the equations for the costate contain a term that escalates badly with the number of electrons, (2) as we have to propagate them backwards and we are using absorbing boundary conditions to simulate the loss of electrons from the cluster, this implies that the norm of the Kohn-Sham orbitals will grow and the propagation becomes unstable, and (3) for these reasons we have to use an accurate and stable propagator like the fourth order Runge-Kutta, which also means that the integration scheme will be computationally expensive.

For the optimization targets, we proposed two possibilities: the sum of the opposing momenta between pairs of nuclei and the number of escaped electrons. We tested the latter for both static and moving nuclei. We found that for the 16 fs pulses the ionic movement is not relevant, and both static and dynamic optimization schemes arrive at optimal solutions. In the case of 32 fs pulses the pulses start to differ in both cases, most notably in the Na_4 cluster. For the 64 fs pulses the static optimization scheme could not find a solution that induces the Coulomb explosion of the clusters, making the use of QOCT on top of non-adiabatic MD necessary. Even in the case of 16 fs laser pulses the electronic escape is large enough to

induce a shift in the resonance frequencies, so the optimal solutions do not share their main peak at the ground state resonances, but it is slightly blueshifted.

Another important conclusion from this work is that, while TDDFT is one of the most computationally cheap methods for electronic structure calculations, its combination with EMD to tackle realistic molecular systems and the application of QOCT to both results in a fairly expensive scheme in terms of computational cost. This is mostly caused by the numerical problems in the backpropagation needed for the costate, which stem from the non-Hermitian nature of the operators that appear in its equations of motion, and from the presence of absorbing boundaries. In order to alleviate this issue, we set out to study and implement new propagators that improved the performance of the RK method – a project discussed in Chapter 5.

Chapter 5

Numerical Propagators

In Chapter 4 we managed to optimize laser pulses to induce the Coulomb explosion of small sodium clusters, and we found that, even for short pulses with a duration of a few tens of femtoseconds, the effect of the nuclei dynamics cannot be neglected. In order to compute the gradient of the target functional with respect to the optimization parameters, we need both an accurate forward propagation of the equations of motion and the backpropagation of an auxiliary system (the costate). Even though EMD+TDDFT is a relatively computationally cheap method, these propagations were very time consuming. The numerical difficulties are mostly due to the backwards propagation, and forced us to use the fourth order Runge-Kutta method (RK4), because of its robustness. The size of the systems that we could tackle with our combination of QOCT with EMD+TDDFT was rather limited. This was the motivation that drove us to do research on new methods of propagation for the time-dependent Kohn-Sham (TDKS) equations and for the EMD+TDDFT equations. This is the theme of this chapter.

In Section 5.1 of this chapter we start with a proof of the symplecticity of the TDKS equations. Then, we study the application to the TDKS equations of propagators from four different families that have been scarcely tested in the context of TDDFT: the multistep methods, the Runge-Kutta propagators, the exponential Runge-Kutta integrators and the commutator free Magnus expansion. We will analyze both the accuracy and the cost of each propagator, and compare them with the exponential midpoint rule (EMR), a well established numerical method in the field of electronic structure. In Section 5.1 we will only be concerned with systems where the nuclei are fixed. We will find that the best integrator of all the ones that were tried is the order four commutator free Magnus expansion. The research presented in this section was published in Ref. [75].

In Section 5.2 we will adapt the commutator free Magnus schemes to a model that takes the dynamics of the nuclei into account, such as the EMD that we used in Chapter 4. In

order to do so, we will rewrite the EMD+TDDFT equations of movement (Eqs. 2.66) in a way that allows us to treat the hybrid quantum-classical system as a nonlinear Schrödinger equation, and then we will implement and test the integrators just like in the first section. The methodology and results presented in this section were published in Ref. [69].

5.1 Propagators for the Kohn-Sham Time-Dependent Equations

As we have already discussed, TDDFT is a widely spread approach for the simulation of many electron systems. It changes the real, interacting problem with an equivalent one where the electrons do not interact with each other, but are subjected to the one-electron Kohn-Sham potential. The equations of motion for these non interacting electrons are the TDKS equations (Eq. 2.57), which gives us the evolution of the Kohn-Sham orbitals $\{\varphi_i\}$ in terms of the Kohn-Sham Hamiltonian $\hat{H}_{\mathrm{KS}}[n](t)$. This Hamiltonian is a linear Hermitian operator with a possible explicit dependence on time (e.g., due to the presence of a laser pulse) and an implicit one through the dependence on the electronic density n. Theoretically, it depends on the full history of the density, and not only on the density at the present time t. Unfortunately, there are currently no accurate exchange and correlation (XC) functionals that include those memory effects. In practice, almost every TDDFT implementation uses the adiabatic approximation: one assumes that the Hamiltonian at time t only depends on the density at that moment, $n(t)$.

After discretization of the Hilbert space, TDKS equations take the form of first order ordinary differential equations (ODEs) in this adiabatic approximation – after discretization of the Hilbert space (otherwise, they would belong to the larger class of the so-called *delay differential equations*). A general introduction to the methodology to solve ODEs was presented in section 2.4 of chapter 2. The field of numerical ODE integration is a well established one, with its origins going all the way back to the time of the creation of calculus in the XVII century. These many years of research have produced a plethora of methods for the propagation of ODEs [80, 81, 79], all of them theoretically applicable to the TDKS equations. We set out to implement and analyze schemes from four families that have been scarcely – if at all – tested in the area of electronic structure: multistep methods, the Runge-Kutta propagators, the exponential Runge-Kutta integrators and the commutator free Magnus expansion.

As we already pointed in section 2.4, we can divide the propagators depending on how many previous steps they require (one-step, or multistep). Also, we can divide them on

whether an algebraic system of equations has to be solved on each iteration of the propagation (implicit versus explicit). We also discussed how some integrators preserve the possible geometrical structure of the equations that are to be solved. For example, the symplecticity that is present in classical Hamiltonian systems and, as we saw, also holds for Schrödinger's equation. The question arises now: are the TDKS equations also symplectic? As we will prove below, this is indeed the case in the adiabatic approximation. Note that the implicit schemes are generally better than the explicit ones for the conservation of the geometrical structure of the system when we deal with long propagations.

We can also divide the Kohn-Sham Hamiltonian into a linear (the kinetic term) and non linear (the Hartree, XC and external potentials) parts. This is specially relevant when we deal with "stiff problems", as the kinetic term is responsible for the possible stiffness of the TDKS equations. There is no clear consensus about the definition of stiffness, but a practical, generally accepted one is: a stiff problem is one where the implicit methods of propagation perform significantly better than the explicit ones. The exponential Runge-Kutta propagators were developed to deal with this specific problem, and were tested for TDDFT recently [104].

In the rest of the section we will first discuss the symplecticity of the TDKS equations (subsection 5.1.1). Then, we will show the results of the analysis of the propagators implemented (subsection 5.1.2). This section is based on Ref. [70].

5.1.1 Symplecticity of the Kohn-Sham equations

The symplecticity of a dynamical system is proven if one is able to rewrite it as a "classical" Hamiltonian system. This is what we show here for the case of the TDKS equations.

Let us write the Kohn-Sham Hamiltonian as

$$\hat{H}[n(t)] = \hat{T} + \hat{V} + \hat{V}_{\mathrm{HXC}}[n(t)]\,, \tag{5.1}$$

where $\hat{T}$ is the kinetic operator, $\hat{V}$ is the external potential operator and $\hat{V}_{\mathrm{HXC}}[n(t)]$ is the Hartree, exchange and correlation term. Using the coordinate representation, and using φ_m to denote the Kohn-Sham orbitals:

$$\langle \mathbf{r}\sigma|\hat{H}[n(t)]|\varphi_m(t)\rangle = -\tfrac{1}{2}\nabla^2\varphi_m(\mathbf{r}\sigma,t) + v(\mathbf{r})\varphi_m(\mathbf{r}\sigma,t) + v_{\mathrm{Hxc}}[n(t)](\mathbf{r})\varphi_m(\mathbf{r}\sigma,t)\,, \tag{5.2}$$

Expanding the Kohn-Sham orbitals in a one-electron basis $\{|\phi_i\rangle\}$

$$|\varphi_m\rangle = \sum_i c_{mi}|\phi_i\rangle\,, \tag{5.3}$$

the TDKS equations can be written as

$$\dot{c}_m = -iH[c]c_m\,, \tag{5.4a}$$

$$c_{mi}(0) = \langle \phi_i | \varphi_m^0 \rangle\,, \tag{5.4b}$$

where the matrix $H[c]$ is given by

$$H[c]_{ij} = \langle \phi_i | \hat{H}[c] | \phi_j \rangle\,. \tag{5.5}$$

We have rewritten the dependence of the Hamiltonian on the (instantaneous) density as a dependence on the set of coefficients c, which we will split into its real and imaginary part:

$$c_{mi} = \tfrac{1}{\sqrt{2}}(q_{mi} + ip_{mi})\,. \tag{5.6}$$

Now Eq. 5.4a takes the form

$$\dot{q}_m + i\dot{p}_m = -i(\Re H[q,p] + \Im H[q,p])(q_m + ip_m)\,, \tag{5.7}$$

or separating into real and imaginary parts

$$\dot{q}_m = \quad \Im H[q,p]q_m + \Re H[q,p]p_m\,, \tag{5.8a}$$

$$\dot{p}_m = -\Re H[q,p]q_m + \Im H[q,p]p_m\,. \tag{5.8b}$$

Now we have to find the Hamiltonian function $H(q,p)$ that would allow us to write the TDKS system as a classical Hamiltonian system, i.e. as in Eqs. 2.78.

While the straightforward choice of the Kohn-Sham noninteracting energy does not work for this purpose, we can use the ground state functional:

$$E[n] = T_{\mathrm{S}}[n] + V[n] + E_{\mathrm{Hxc}}[n]\,. \tag{5.9}$$

Here n represents the instantaneous time-dependent density, so we are evaluating this energy functional adiabatically. As the density is a function of the Kohn-Sham orbitals, the energy is a functional of $\{\varphi\}$. If we use the new variables (q,p) to represent them we can define the Hamiltonian function

$$H(q,p) = T_{\mathrm{S}}(q,p) + V(q,p) + E_{\mathrm{Hxc}}(q,p)\,. \tag{5.10}$$

The non interacting kinetic energy T_S takes the form

$$T_S(q,p) = \tfrac{1}{2}\sum_m q_m \Re T q_m + \tfrac{1}{2}\sum_m p_m \Re T p_m + \sum_m p_m \Im T q_m \,, \tag{5.11}$$

and the external potential is

$$V(q,p) = \tfrac{1}{2}\sum_m q_m \Re V q_m + \tfrac{1}{2}\sum_m p_m \Re V p_m + \sum_m p_m \Im V q_m \,. \tag{5.12}$$

We can see that both T_S and V fulfill the conditions for a Hamiltonian system (Eqs. 2.78) calculating their partial derivatives

$$\frac{\partial T_S(q,p)}{\partial q_{mi}} = \sum_j \left(\Re T_{ij} q_{mj} - \Im T_{ij} p_{mj}\right) , \tag{5.13a}$$

$$\frac{\partial T_S(q,p)}{\partial p_{mi}} = \sum_j \left(\Re T_{ij} p_{mj} + \Im T_{ij} q_{mi}\right) , \tag{5.13b}$$

$$\frac{\partial V(q,p)}{\partial q_{mi}} = \sum_j \left(\Re V_{ij} q_{mj} - \Im V_{ij} p_{mj}\right) , \tag{5.13c}$$

$$\frac{\partial V(q,p)}{\partial p_{mi}} = \sum_j \left(\Re V_{ij} p_{mj} + \Im V_{ij} q_{mi}\right) , \tag{5.13d}$$

and comparing them with Eqs. 5.8.

The Hartree, exchange and correlation term requires a bit more work. Using the chain rule, we compute its partial derivatives:

$$\frac{\partial E_{\mathrm{Hxc}}(p,q)}{\partial q_{mi}} = \int \mathrm{d}\mathbf{r}\, \frac{\delta E_{\mathrm{Hxc}}}{\delta n(q,p;\mathbf{r})} \frac{\partial n(q,p;\mathbf{r})}{\partial q_{mi}} , \tag{5.14a}$$

$$\frac{\partial E_{\mathrm{Hxc}}(p,q)}{\partial p_{mi}} = \int \mathrm{d}\mathbf{r}\, \frac{\delta E_{\mathrm{Hxc}}}{\delta n(q,p;\mathbf{r})} \frac{\partial n(q,p;\mathbf{r})}{\partial p_{mi}} , \tag{5.14b}$$

where $n(q,p)$ is the density obtained from the orbitals $\varphi_i(q,p)$. We know that the functional derivative of E_{Hxc} with respect to the density is the Hartree, exchange and correlation potential v_{Hxc}

$$\frac{\delta E_{\mathrm{Hxc}}(q,p)}{\delta n(q,p;\mathbf{r})} = v_{\mathrm{Hxc}}(q,p;\mathbf{r}) \,. \tag{5.15}$$

Now we have to write the density as a function of the (q,p) variables to compute its partial derivatives, so we rewrite it as

$$n(q,p;\mathbf{r}) = \tfrac{1}{2}\sum_{\substack{\sigma,m\\ij}}(q_{mi}-ip_{mi})(q_{mj}+ip_{mj})\phi_i^*(\mathbf{r}\sigma)\phi_j(\mathbf{r}\sigma)\,, \tag{5.16}$$

which gives us

$$\frac{\partial n(q,p;\mathbf{r})}{\partial q_{mi}} = \sum_j q_{mj}\Re\sum_\sigma \phi_i^*(\mathbf{r}\sigma)\phi_j(\mathbf{r}\sigma) - \sum_j p_{mj}\Im\sum_\sigma \phi_i^*(\mathbf{r}\sigma)\phi_j(\mathbf{r}\sigma)\,, \tag{5.17a}$$

$$\frac{\partial n(q,p;\mathbf{r})}{\partial p_{mi}} = \sum_j q_{mj}\Im\sum_\sigma \phi_i^*(\mathbf{r}\sigma)\phi_j(\mathbf{r}\sigma) + \sum_j p_{mj}\Re\sum_\sigma \phi_i^*(\mathbf{r}\sigma)\phi_j(\mathbf{r}\sigma)\,. \tag{5.17b}$$

Finally, substituting these results into Eqs. 5.14 we find

$$\begin{aligned}\frac{\partial E_{\mathrm{Hxc}}(p,q)}{\partial q_{mi}} &= \sum_j \left(\Re V^{\mathrm{Hxc}}[q,p]_{ij}q_{mj} - \Im V^{\mathrm{Hxc}}[q,p]_{ij}p_{mj}\right)\,,\\ \frac{\partial E_{\mathrm{Hxc}}(p,q)}{\partial p_{mi}} &= \sum_j \left(\Im V^{\mathrm{Hxc}}[q,p]_{i,j}q_{mj} + \Re V^{\mathrm{Hxc}}[q,p]_{ij}p_{mj}\right)\,,\end{aligned} \tag{5.18a}$$

where $V^{\mathrm{Hxc}}[q,p]$ is a matrix whose elements are

$$V^{\mathrm{Hxc}}[q,p]_{ij} = \langle\phi_i|\hat{V}_{\mathrm{Hxc}}[q,p]|\phi_j\rangle\,. \tag{5.19}$$

Once again, by comparing with Eqs. 5.8, one can see that the partial derivatives of E_{Hxc} present the right structure, and thus it completes the proof that the TDKS equations form a Hamiltonian system.

5.1.2 Results

In the following, we will use this notation: φ_i are the time-dependent Kohn-Sham orbitals, that we will collectively group as $\boldsymbol{\varphi}$. The TDKS equations, as an ODE system, can then be written as:

$$\dot{\boldsymbol{\varphi}}(t) = f(\boldsymbol{\varphi}(t),t)\,, \tag{5.20}$$

where the dynamical function is defined as $f(\boldsymbol{\varphi}(t),t) = -iH_{\mathrm{KS}}[\boldsymbol{\varphi}(t),t]\boldsymbol{\varphi}(t)$. Furthermore, we will also simplify $H_{\mathrm{KS}}[\boldsymbol{\varphi}(t),t]$ as $H_{(t)}$.

For the study of the accuracy and computational cost of the propagation methods, we used a system consisting of a benzene molecule subject to an instantaneous perturbation at

the beginning of the simulation in the form of an electric field along the z axis

$$\varphi_i^0(t=0^+) = e^{ikz}\varphi_i^0\,, \tag{5.21}$$

where $\{\varphi_i^0\}$ are the ground-state Kohn-Sham orbitals, and $k = 0.1$ a.u. Then we let it evolve freely for a time $T = 2\pi$. We put the molecule in a spherical box of radius $r = 12$ a.u., with a grid spacing of $a = 0.4$ a.u.

We compared the results obtained for the wave function and the energy at the end of the propagation with an "exact" reference calculation, obtained with the RK4 formula using a very small time step. We define the error in the wave function as:

$$E_{\mathrm{wf}}(T,\Delta t) = \sqrt{\sum_i ||\varphi_i(T) - \varphi_i^{\mathrm{exact}}(T)||^2}\,. \tag{5.22}$$

For the error in the energy, we have used:

$$E_{\mathrm{energy}}(T,\Delta t) = |E(T) - E^{\mathrm{exact}}(T)|^2\,. \tag{5.23}$$

Here $\varphi_i^{\mathrm{exact}}$ and E^{exact} are the Kohn-Sham orbitals and energy obtained from the "exact" calculation.

Commutator Free Magnus Expansion

In section 2.4.4 we presented the general Magnus expansion family of propagators for linear systems. We presented as an example the simplest of them all, the exponential midpoint rule (EMR). As we discussed, it can be extended to deal with a nonlinear set of equations such as the TDKS ones, by predicting future Hamiltonians via extrapolation of previous time steps.

We also showed in section 2.4.4 some variations of it that had been used in the past to somehow improve its behavior:

1. The enforced time reversal symmetry (ETRS)

$$\varphi(t) = e^{-i\frac{\Delta t}{2}\hat{H}_{(t)}} e^{-i\frac{\Delta t}{2}\hat{H}_{(t-\Delta t)}} \varphi(t-\Delta t)\,, \tag{5.24}$$

   that is an implicit scheme, as $H_{(t)}$ on the right hand side depends on the unknown $\varphi(t)$.

2. The approximated enforced time reversal symmetry (AETRS), which is the ETRS, but one uses an extrapolated Hamiltonian $H_{(t)}^{\mathrm{extr}}$ instead of $H_{(t)}$ to turn the method into an explicit formula.

Another way to attempt to improve over the EMR is to use higher-order Magnus expansions. This route finds the difficulty, however, that the formulas that define them present commutators of the Hamiltonian at different times that are difficult to compute (see Eqs. 2.120). The commutator free Magnus (CFM) expansions were proposed by Blanes et al. [15] as an alternative to the classical Magnus expansions that gets rid of those commutators. Their validity can also be extended to the nonlinear case by making use of the extrapolation method.

We have implemented several of these methods. They are essentially products of exponentials of operators; a general formula for them all is:

$$\hat{U}^{q,m}(t,t-\Delta t) = \prod_{i=1}^{m} e^{\hat{D}_i}\,, \tag{5.25}$$

with m being the number of exponentials, q is the order of the resulting propagator, and $\hat{D}_i$ are linear operators carefully chosen to ensure the order of the method.

For example, we have tested an order four method presented in Eq. 43 from Ref. [15], which we will call CFM4. It is defined as:

$$\varphi(t) = e^{-i\Delta t\alpha_1\hat{H}_{(t_1)} - i\Delta t\alpha_2\hat{H}_{(t_2)}} e^{-i\Delta t\alpha_2\hat{H}_{(t_1)} - i\Delta t\alpha_1\hat{H}_{(t_2)}} \varphi(t-\Delta t)\,. \tag{5.26}$$

where $\alpha_1 = \frac{3+2\sqrt{3}}{12}$, $\alpha_2 = \frac{3-2\sqrt{3}}{12}$, $t_1 = t - \Delta t + \left(\frac{1}{2} - \frac{\sqrt{3}}{12}\right)\Delta t$ and $t_2 = t - \Delta t + \left(\frac{1}{2} + \frac{\sqrt{3}}{12}\right)$. The computation of the Hamiltonians at the intermediate times t_1 and t_2 imply the solution of a non linear algebraic system, i.e., we would have an implicit propagation method. To turn CFM4 into an explicit propagator, in our implementation we use extrapolation to compute the Hamiltonians at these times. If the extrapolation is done at order four the order of the method is conserved – a fact that we have also checked numerically.

The top and the bottom panels of Fig. 5.1 show, respectively, the error in the energy and the in the wave function, as a function of the time step for the EMR, ETRS, AETRS and CFM4 propagators. The data has been plotted using logarithmic scales in both axes. In this way, the curves become straight lines in the small Δt limit, its slope measuring the order of the integrator (in the case of the wave function). The EMR, ETRS and AETRS are propagators of order two, although notice that for larger values of Δt they behave as if their order was four, as one can see in the figure. For values of the time step up to 10^{-2} a.u., all the methods present similar accuracy except for the EMR, which becomes unstable (as we can see from the fact that there is no point for the larger value of the time step in Fig. 5.1). For smaller values of Δt, only the CFM4 really behaves as a true fourth order method. It is the most precise among these methods in this range of the time step.

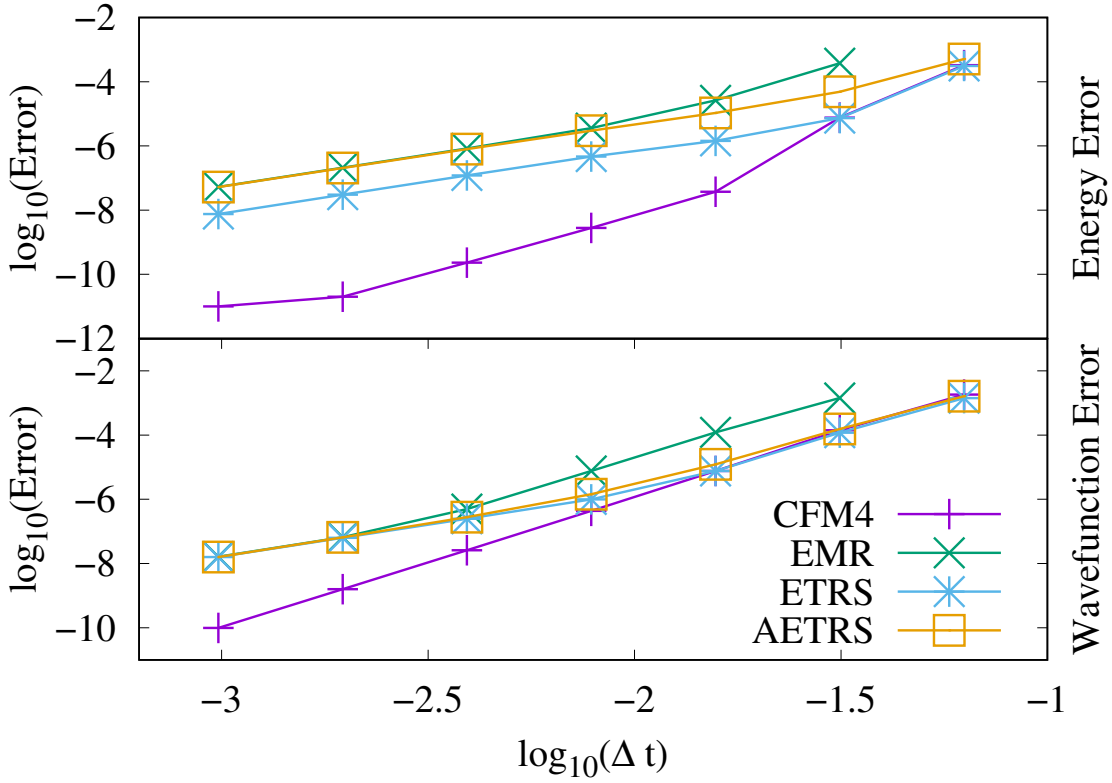

Fig. 5.1 Error in the total energy (top panel) and in the wave function (bottom panel), as a function of the time-step, for the various reference propagators (ETRS, AETRS and EMR) and for the CFM4 propagator.

Fig. 5.2 shows the cost in seconds of the propagators as a function of the error in the wave function, again using logarithmic scales for the axes. This kind of plot is useful because it makes easy to identify the best method for a given precision. The required precision is to be chosen by the user and is problem dependent. As we can see from the figure, for values of the error up to 10^{-6} all the methods have a similar computational cost, but for smaller values of the error the CFM4 is notably faster, which makes it the most efficient method overall.

Multistep Methods

As discussed in section 2.4.3, the multistep methods are the ones that use a number $s > 1$ of previous steps in the formula to compute the following one. To calculate the first s steps in a propagation, one obviously needs a different method, and in our case we used a single-step method, the explicit fourth order Runge-Kutta propagator (its Butcher's tableau is Eq. 2.95).

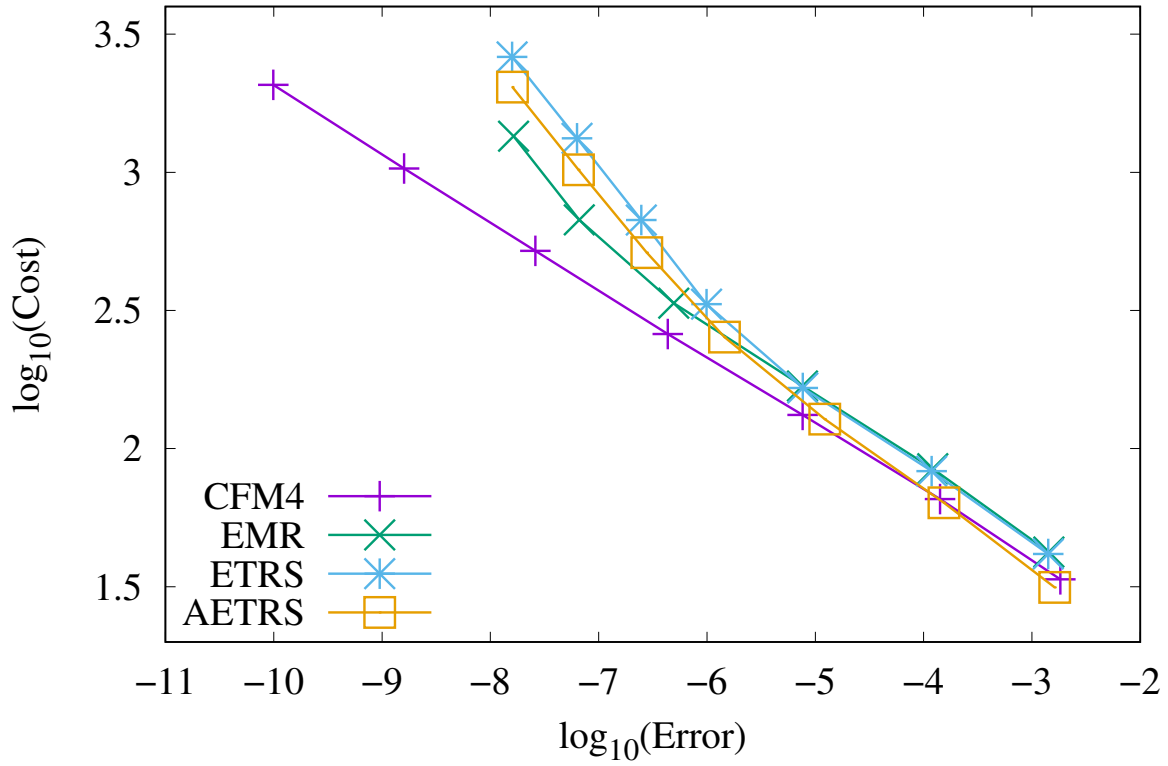

Fig. 5.2 Cost of the method, as a function of the error obtained (in the wave function), for the various reference propagators (ETRS, AETRS and EMR) and for the CFM4 propagator.

We analyzed and implemented various linear multistep integrators, which in general we can write as

$$\varphi(t) + \sum_{j=1}^{s} a_{s-j}\varphi(t - j\Delta t) = \Delta t \sum_{j=0}^{s} b_{s-j} f(t - j\Delta t, \varphi(t - j\Delta t)), \tag{5.27}$$

where the $\{a_j\}_{j=0}^{s-1}$ and $\{b_j\}_{j=0}^{s}$ coefficients characterize the method. For $b_s = 0$ we have explicit multistep integration methods like the Adams-Bashforth (AB) method, while for $b_s \neq 0$ we will have implicit ones like the Adams-Moulton (AM) formulas and the Backward Differentiation formula (BDF). For a detailed explanation about these propagators check section 2.4.3. In short, we have implemented and tested the following:

1. The AB formulas, given by:

$$\varphi(t) = \varphi(t - \Delta t) - \sum_{j=1}^{s} b_{s-j}^{\mathrm{AB}} i\Delta t \varphi^{(j)}, \tag{5.28}$$

   where $\varphi^{(j)} = H_{(t-j\Delta t)}\varphi(t - j\Delta t)$.

2. The AM formulas, given by:

$$(I + b_s^{\mathrm{AM}} i\Delta t H_{(t)})\varphi(t) = \varphi(t - \Delta t) - \sum_{j=1}^{s} b_{s-j}^{\mathrm{AM}} i\Delta t \varphi^{(j)}. \tag{5.29}$$

   These are implicit methods, whose solution we obtained using a simple iterative procedure.

3. The predictor-corrector scheme to approximate the AM formulas with an explicit scheme. We use AB to find an approximate solution $\tilde{\varphi}(t)$ (predictor), and then we use it to find the Hamiltonian of Eq. 5.29. We labeled this method ABM.

4. We also linearized the AM methods using extrapolation to approach the Hamiltonian, turning Eq. 5.29 into a linear equation. We called this scheme lAM.

5. The backwards differentiation formula (BDF):

$$(I + b_s^{\mathrm{BDF}} i\Delta t H_{(t)})\varphi(t) = -\sum_{j=1}^{s} a_{s-j}^{\mathrm{BDF}} \varphi(t - j\Delta t). \tag{5.30}$$

   This particular family of propagators is proficient in the integration of stiff equations. The reason behind its success lies in the extent of its stability region, as it includes the

negative real axis, which is where the real part of the eigenvalues of stiff problems lie (check section V.1 from Ref. [81] for a more careful discussion).

We tested these methods for $s = 1, ..., 5$ and compared them with the EMR. The results of the best performer from each family are plotted in Figs. 5.3 and 5.4, except for the BDF due to its poor performance. The number next to the label of the propagators indicates the number of previous steps required (s). We found out that the EMR is more stable than all the multistep methods for large time steps, but the multistep propagators beat it in accuracy. This is what we would expect, as the EMR is an order two propagator and AB4 and ABM4 are order four propagators, AM4 has fifth order and lAM5 is of order six. As we can see, the most precise one is lAM4 which reaches the numerical precision of our machines for the smaller values of Δt.

Fig. 5.4 shows the cost of the integrators as a function of the error in the wave function. The best choice for error values above 10^{-7} is the EMR, being overtaken by ABM4 and lAM5 when we desire a higher precision. From the figure we can see that the linearization improves notably the performance of the AM methods, making the linearized version the optimal choice for an error smaller than 10^{-7}.

To finish this section, we show the results of the BDF propagators for all the values of s considered in Fig. 5.5. In the left panel we can see that increasing the number of previous steps does not increase the computational cost of the multistep method. At the same time, the right panel shows how each time that we add an additional step the order of the propagator also increases by one. Sadly, adding previous steps to the propagators makes them increasingly unstable, as we can see from the fact that both BDF1 and BDF2 have better stability properties than EMR, but as soon as $s \geq 3$ this is no longer true. Actually, there is solid mathematical proof [79] stating that the BDF methods are unstable for $s \leq 7$.

Runge-Kutta Methods

We will now focus on the Runge-Kutta (RK) schemes presented in section 2.4.2. We recall that the "standard" RK propagators can be written as

$$\varphi(t) = \varphi(t - \Delta t) + \Delta t \sum_{i=1}^{s} b_i Y_i \,, \tag{5.31}$$

$$Y_i = f(\varphi(t - \Delta t) + \Delta t \sum_{j=1}^{s} a_{ij} Y_j, t_i) \,, \tag{5.32}$$

where f is the dynamical function of the ODE system, and the time-steps are $t_i = t - \Delta t + c_i \Delta t$. Each method is characterized by the choice of s, and by the constants a_{ij}, b_i, and c_i. If the

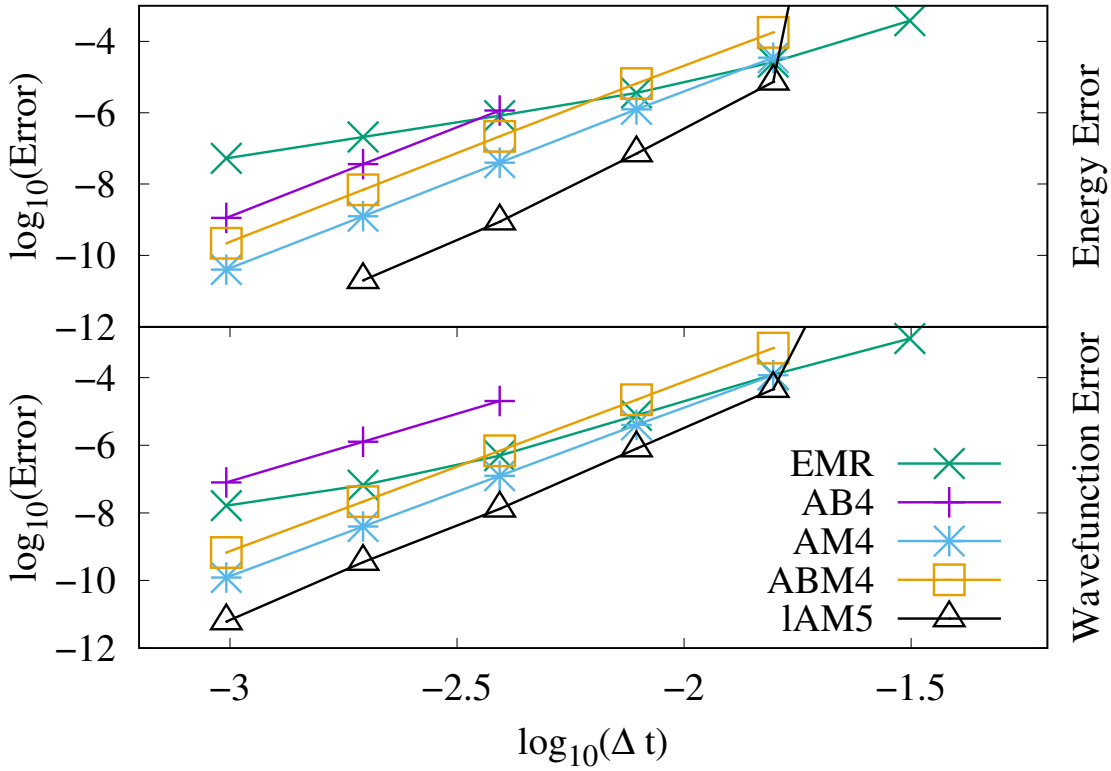

Fig. 5.3 Error in the total energy (top panel) and in the wave function (bottom panel), as a function of the time-step, for the various multistep methods (AB, AM, ABM and linearized AM) and for the EMR propagator.

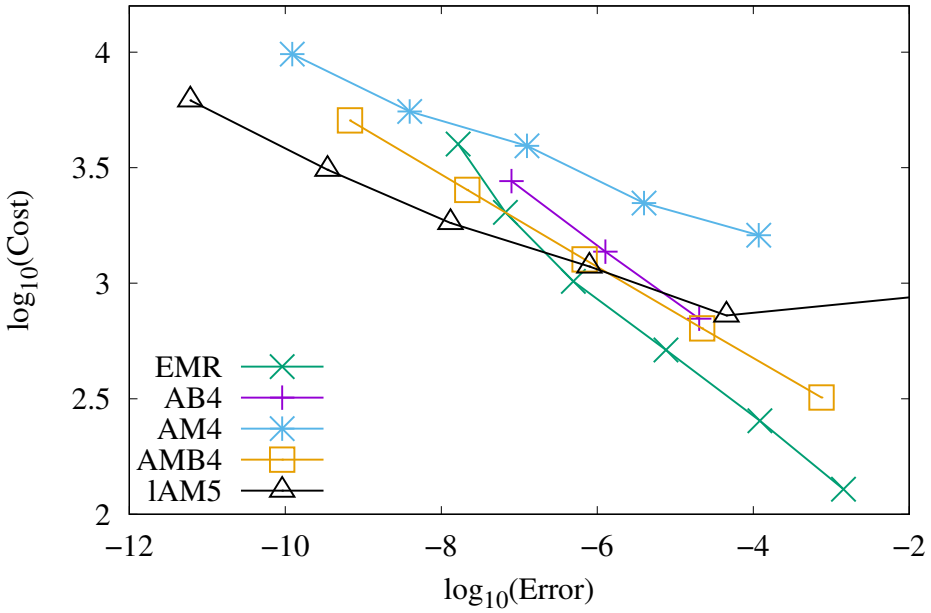

Fig. 5.4 Cost of the method, as a function of the error obtained (in the wave function), for the various multistep methods (AB, AM, ABM and linearized AM) and for the EMR propagator.

coefficients $a_{ij} = 0$ for $i \leq j$, the methods are explicit; otherwise they involve implicit formulas. The explicit RK methods perform poorly when dealing with stiff problems, which was the motivation for the development of the implicit versions. The implicit propagators imply the solution of an algebraic system whose dimension grows as $m \times s$, where m is the dimension of the original system and s is the number of stages of the method. This algebraic system is significantly larger than the one that appears for the implicit multistep methods, whose algebraic systems only grows with m.

A way to ensure that the implicit RK (imRK) propagators have good stability and conservation properties is to demand that they are symplectic. One can do this [182] if the $s \times s$ matrix M defined as

$$m_{ij} = b_i a_{ij} + b_j a_{ji} - b_i b_j \,, \tag{5.33}$$

satisfies $M = 0$. From this equation we can further deduce that no explicit RK propagator can be symplectic.

We have implemented explicit RK integrators up to order four. The reason behind this choice resides in the fact that for higher orders, the number of stages s required to guarantee a given order p is strictly larger than p [27, 25, 79]. Since the cost of the method grows with s, it is not convenient going beyond that number. For this reason, the only explicit method whose results we present in this work is the popular fourth order RK scheme, labeled RK4,

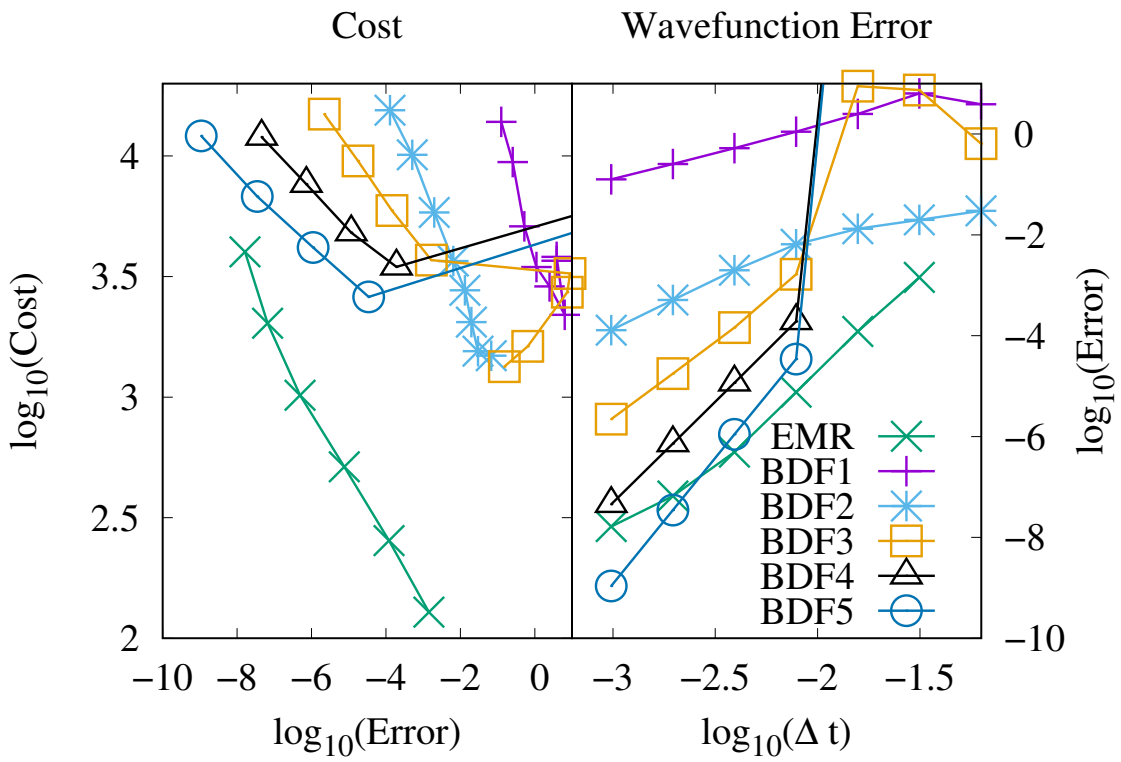

Fig. 5.5 Left: Cost as a function of the error for the BDF methods (going from $s = 1$ to 5) and for the EMR propagator. Right: Error in the propagated wave function, as a function of the time-step, for the BDF methods (going from 1 to 5 previous steps) and for the EMR propagator.

and characterized by the following Butcher's tableau:

$$\begin{array}{c|cccc} 0 & & & & \\ \frac{1}{2} & \frac{1}{2} & & & \\ \frac{1}{2} & 0 & \frac{1}{2} & & \\ 1 & 0 & 0 & 1 & \\ \hline & \frac{1}{6} & \frac{1}{3} & \frac{1}{3} & \frac{1}{6} \end{array} \tag{5.34}$$

Among the implicit RK methods, the Gauss-Legendre collocation schemes are the most popular, and relevant for this work as they are both symplectic and symmetric. A Gauss-Legendre formula with s stages is of order $2s$. We tested the implicit midpoint rule, which is the order two method ($s = 1$; imRK2)

$$\begin{array}{c|c} \frac{1}{2} & \frac{1}{2} \\ \hline & 1 \end{array} \tag{5.35}$$

It may be written down in terms of a single nonlinear equation for $\varphi(t)$:

$$\left(I + \frac{i}{2}\Delta t H\left[\overline{\varphi}, t - \tfrac{1}{2}\Delta t\right]\right)\varphi(t) = \left(I - \frac{i}{2}\Delta t H\left[\overline{\varphi}, t - \tfrac{1}{2}\Delta t\right]\right)\varphi(t - \Delta t)\,, \tag{5.36}$$

where $\overline{\varphi} = \frac{1}{2}[\varphi(t) + \varphi(t - \Delta t)]$. This method is the "conjugate" of the trapezoidal or Crank-Nicolson rule [80]. For this reason, there is some confusion in the literature, and both of them are sometimes referred simply as Crank-Nicolson.

We also studied the following order four implicit RK method ($s = 2$;imRK4):

$$\begin{array}{c|cc} \frac{1}{2}-\frac{\sqrt{3}}{6} & \frac{1}{4} & \frac{1}{4}-\frac{\sqrt{3}}{6} \\ \frac{1}{2}+\frac{\sqrt{3}}{6} & \frac{1}{4}+\frac{\sqrt{3}}{6} & \frac{1}{4} \\ \hline & \frac{1}{2} & \frac{1}{2} \end{array} \tag{5.37}$$

To solve the non linear equations that appear for these methods, we use a simple self consistent iterative method just as for the AM propagators: each iteration implies the solution of a linear system, whose solution is used to create the problem linear system for the following iteration. This idea allows us to define linearized versions of the Gauss-Legendre collocation methods – just like we did with AM –, where we stop the self consistent cycle in the first step, that is solved using an extrapolated Hamiltonian as input.

In Fig. 5.6 we show the errors obtained with this method for the propagation of our benchmark system, as a function of the time step. The energy obtained from both imRK4 and

lRK4 is so accurate that for values of the time step smaller than $10^{-1.8}$ we already reach the numerical precision of our machines, which is the reason behind the disappearance of those points. From the wave function error we can see that, in terms of accuracy, the EMR beats the order two RK methods by a large margin, and it is competitive with the order four methods up to $\Delta t \approx 10^{-2.5}$. On the other hand, the EMR cannot deal with the larger values of the time step, unlike the rest of the implicit RK propagators, and is beaten by every other method when we look at the conservation of the energy. The explicit RK4 method is worse than the implicit ones if we only look at the accuracy in the wave function or the energy. From this figure, we can also see that the linearized methods present almost the same behavior as the "complete" ones when we look at the error in the wave function. However, regarding the conservation of the energy, we find sensible differences between the order two propagators.

Fig. 5.7 shows the cost of the integrators as a function of the error in the wave function, i.e. their error-dependent efficiency. The explicit methods have a better performance than the implicit ones: both EMR and RK4 outclass the other propagators. The EMR is the most efficient one up to errors of 10^{-8}, where RK4 overtakes it. Comparing the linearized methods with their regular counterparts, lRK2 is faster than imRK2, but in the case of the order four propagators both of them have the same cost. The meaning of this fact is that the self consistent cycle actually converges in one iteration, and thus there is no real difference between them. To finish the study of the standard RK methods, let us remark that the performance of the implicit methods is highly dependent of the quality of the solver for the linear systems: for example, the use of a good preconditioner is known to strongly accelerate the solution.

Exponential Runge-Kutta Methods

The last family of propagators that we tested is the one of the recently proposed exponential Runge-Kutta (ERK) methods [88, 144, 147]. These schemes were developed to deal with those stiff problems for which one can identify the piece of the Hamiltonian that is responsible for the stiffness. The idea is then solving the stiff part of the system exactly, and then approximating the rest of the problem using a quadrature formula.

This could be the case for the TDKS equations, that can be divided as:

$$\dot{\varphi}(t) = -iT\varphi(t) - iV[\varphi(t),t]\varphi(t)\,, \tag{5.38}$$

where the kinetic operator T is supposed to be the stiff part of the equation, and V is the Kohn-Sham potential (that contains the nonlinearity).

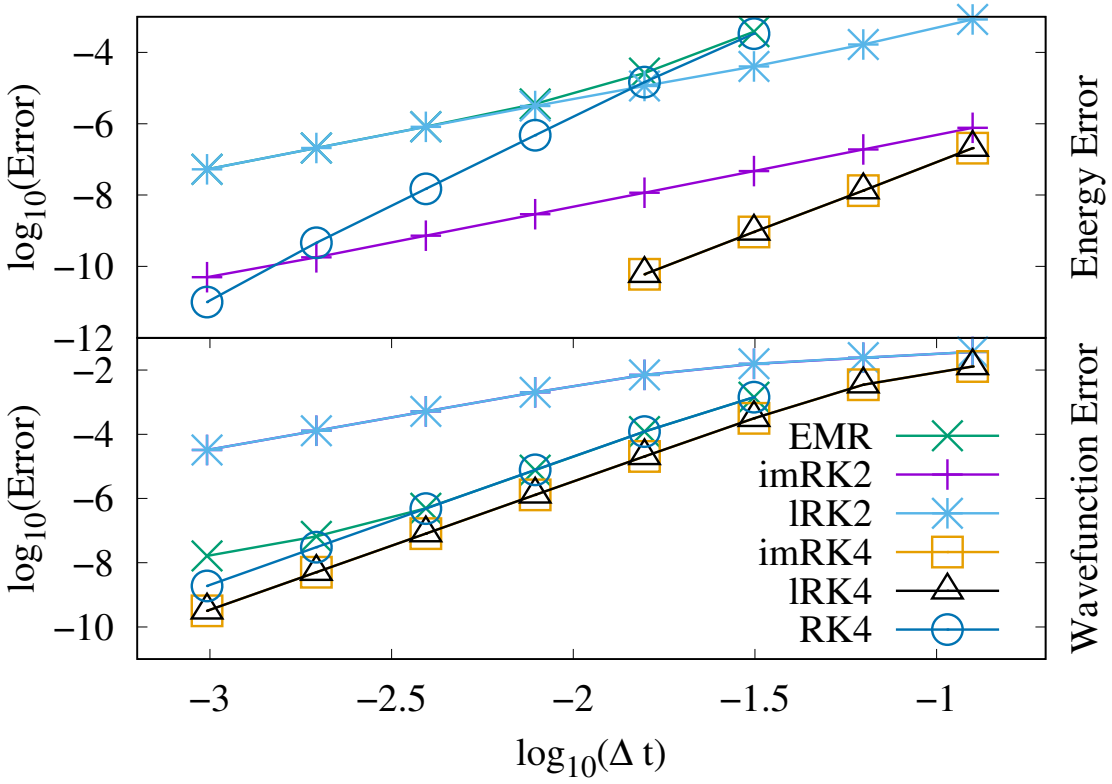

Fig. 5.6 Error in the total energy (top panel) and in the wave function (bottom panel), as a function of the time-step, for the various RK methods (implicit and linearized RK2 and RK4 and explicit RK4) and for the EMR propagator.

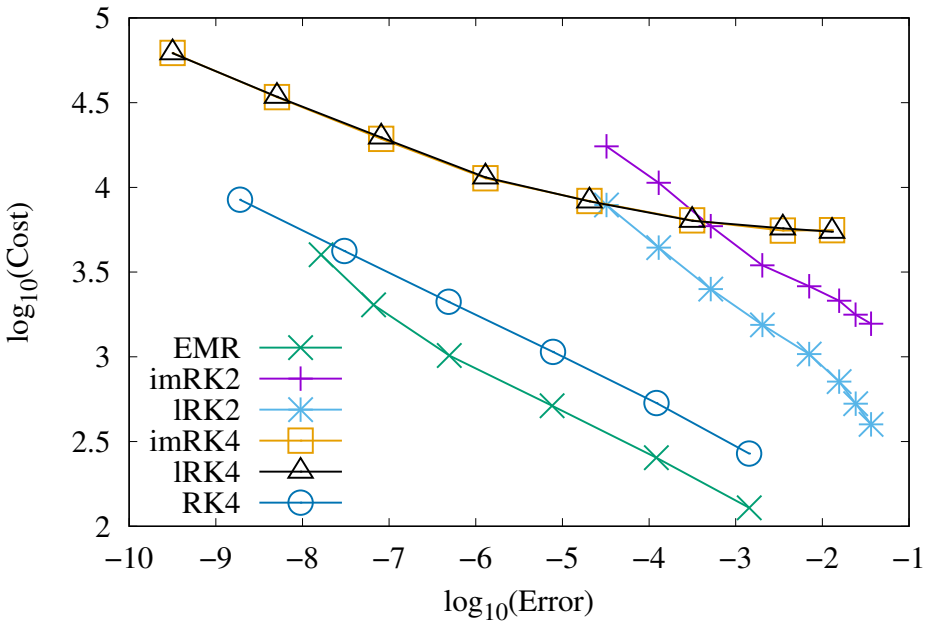

Fig. 5.7 Cost of the method, as a function of the error obtained (in the wave function), for the various RK methods (implicit and linearized RK2 and RK4 and explicit RK4) and for the EMR propagator.

Using this notation, the general form of the ERK propagators is:

$$\varphi(t) = e^{-i\Delta t T}\varphi(t-\Delta t) - i\Delta t \sum_{i=1}^{s} \bar{b}_i(-i\Delta t T)V[Y_i,t_i]Y_i\,, \tag{5.39}$$

where:

$$Y_i = e^{-ic_i\Delta t T}\varphi(t-\Delta t) - i\Delta t \sum_{j=1}^{s} \bar{a}_{ij}(-i\Delta t T)V[Y_j,t_j]Y_j\,. \tag{5.40}$$

The "Runge-Kutta" in the name of the ERK methods stems from the fact that the quadrature formulas used to integrate the potential part of the Hamiltonian are the same than the ones used to define the standard RK methods. As a consequence, the operator functions $\bar{a}_{ij}$ and $\bar{b}_i$, for $T = 0$, actually become the constants a_{ij} and b_i that define the RK propagators. Together with the c_i coefficients they define the ERK methods, which can be either explicit or implicit like the regular RK integrators.

The explicit ERK methods require the computation of some auxiliary functions $Y_i(Y_j,t_i)$ for $j < i$ and $i = 1,\ldots,s$, where s is the number of stages. The coefficients $\bar{a}_{ij}$ and $\bar{b}_i$ are linear

combinations of the ϕ_i functions, defined as:

$$\phi_i(z) = \sum_{j=0}^{\infty} \frac{z^j}{(i+j)!}\,. \tag{5.41}$$

Notice that this Taylor expansion definition of the functions is very similar to the definition of the exponential; this fact simplifies the implementation of the ERK methods: one can use a single subroutine to compute both the linear combinations of the ϕ_i functions and the regular exponentials.

As an example, the first propagator of the ERK family is the exponential version of the Euler method, which we call ERK1, and is given by

$$\varphi(t) = \varphi(t-\Delta t) + \Delta t\,\phi_1(\Delta t T) V[\varphi(t-\Delta t), t-\Delta t]\varphi(t-\Delta t)\,. \tag{5.42}$$

We implemented a general algorithm for a wide array of ERK schemes, described in Ref. [89]. We found that the best performing schemes from that work are: method 5.4 for order 2 (ERK2), method 5.8 for order 3 (ERK3), and method 5.17 for order 4 (ERK4).One can write the Butcher tableau for the ERK methods just like for the standard RK methods, where the coefficients a_{ij} and b_i are substituted by linear combinations of the ϕ_i functions. As an example, let us present here the Butcher tableau corresponding to the ERK2 method:

$$\begin{array}{c|cc} 0 & & \\ \frac{1}{2} & \frac{1}{2}\phi_1 & \\ \hline & 0 & \phi_1 \end{array} \tag{5.43}$$

The tableaux corresponding to the methods we have tested can be found in Ref. [89].

As it happens for the regular RK methods, none of the explicit variants as the ones we just mentioned can be symplectic. However, the the implicit ones can be: For one ERK formula to be symplectic, it requires that the RK method upon which it is based be symplectic, and additionally, the functions $\bar{a}_{ij}$ and $\bar{b}_i$ must fulfill [147]:

$$\bar{a}_{ij}(-i\Delta t T) = a_{ij} e^{-i\Delta t (c_i - c_j) T}\,, \tag{5.44a}$$

$$\bar{b}_i(-i\Delta t T) = b_i e^{-i(1-c_i)\Delta t T}\,. \tag{5.44b}$$

We have tried one of these: the exponential version (imERK2) of the imRK2 propagator. It is defined as:

$$\varphi(t) = e^{-i\Delta t T}\varphi(t-\Delta t) - i\Delta t\, e^{-i\frac{1}{2}\Delta t T} V\left[Y, t - \frac{\Delta t}{2}\right] Y\,, \tag{5.45}$$

with

$$Y = e^{-i\frac{\Delta t}{2}T}\varphi(t-\Delta t) - i\frac{\Delta t}{2}V\left[Y, t-\frac{\Delta t}{2}\right]Y\,. \tag{5.46}$$

The error in the wave function and the energy as a function of the time step, for all these ERK propagators, is displayed in Fig. 5.8. All of them show their expected order for the whole range of time steps that was explored. The implicit propagator imERK2 has a wider range of stability than the explicit ERK integrators, as expected. imERK2 predicts the energy more accurately than its explicit counterpart up to $\Delta t \approx 10^{-2.7}$. ERK4 is the best propagator as far as energy conservation is concerned, and all the ERK methods are better than the EMR in this regard. Conversely, when we look at the error in the wave function, the EMR has a similar behavior as the ERK4 up to $\Delta t \approx 10^{-2.5}$. ERK4 is more precise for smaller values. imERK2 is slightly more accurate than ERK2 for the wave function, while ERK2 is better for the energy when the time step is smaller than $10^{-2.5}$.

About the performance of these methods, Fig. 5.9 shows the cost vs. accuracy plot that really tells which is the most efficient method. And we see that in fact none of them come close to the EMR, as they are computationally expensive. Nevertheless, among them, the most efficient one is the ERK4, as it outclasses all the other methods for values of the error in the wave function below $10^{-2.2}$.

5.2 Propagators for Hybrid Quantum-Classical Systems

In the previous section we proved the symplecticity of the TDKS equations in the adiabatic approximation and studied the performance of different numerical integrators for systems for which the electrons are treated using TDDFT, and the nuclei are kept fixed. From that analysis we found out that the CFM methods beat all the other propagators in terms of cost/accuracy. The next logical step is to adapt this family of propagators to a model that takes the dynamics of the nuclei into account. In particular, we focus on the EMD+TDDFT model, since it is the one that we used in Chapter 4.

Usually, the way to approach the propagation of hybrid systems consists on using two different methods for the classical and quantum equations. The experience shows that the error associated to this combination of methods is typically not large. Normally, a more accurate and expensive propagator is used for the electronic equations, and a faster and cheaper method for the classical system. As the movement of the nuclei is, in the most common situations, orders of magnitude slower than the electronic one, the chosen algorithms for the nuclear propagation are usually robust and cheap. For example, the Verlet propagator [215] is a popular election. On the other hand, the quantum equations of motion

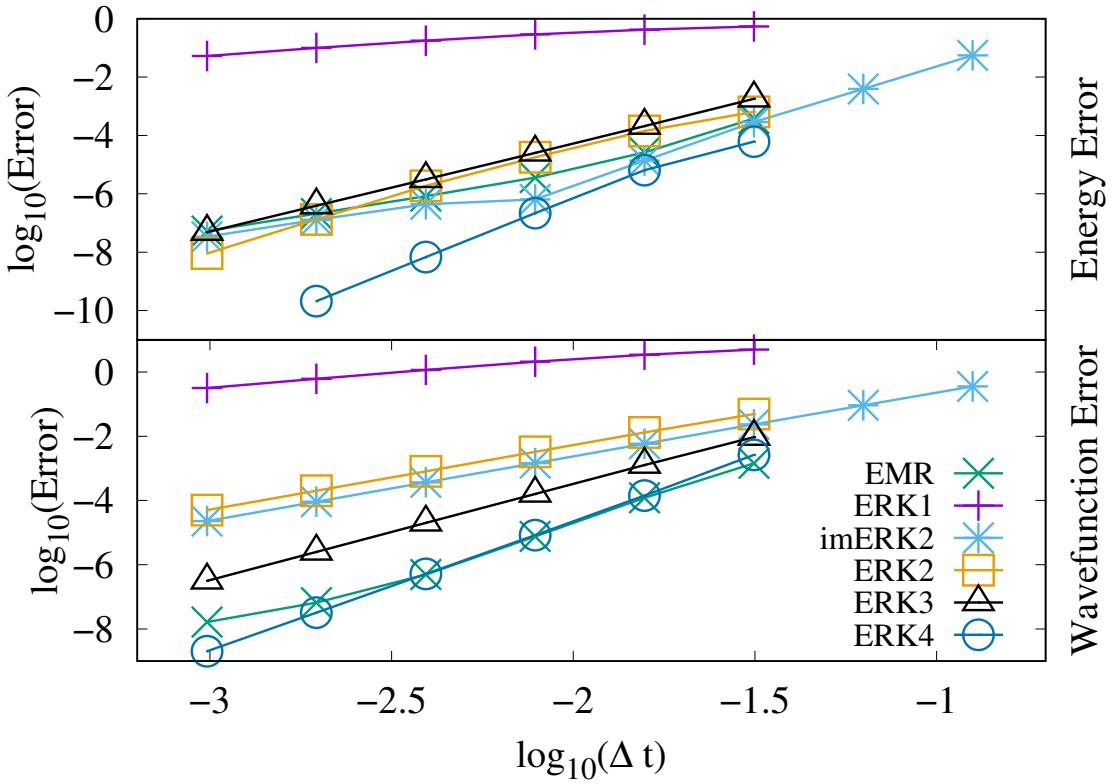

Fig. 5.8 Error in the total energy (top panel) and in the wave function (bottom panel), as a function of the time-step, for the various exponential RK methods (exponential Euler method, implicit RK2 and explicit RK2, RK3 and RK4) and for the EMR propagator.

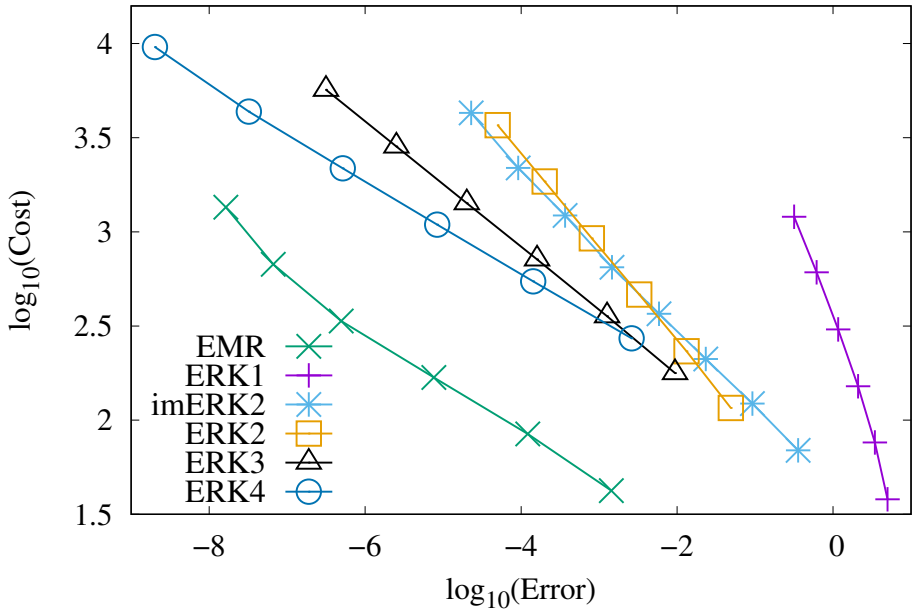

Fig. 5.9 Cost of the method, as a function of the error obtained (in the wave function), for the various exponential RK methods (exponential Euler method, implicit RK2 and explicit RK2, RK3 and RK4) and for the EMR propagator.

are typically much more computationally expensive. As we have mentioned before, after the discretization of the spatial variables, the quantum equations transform into a system of ODEs, for which hundreds or even thousands of integration techniques exist [80, 81, 79].

Unfortunately, approaching the problem in this way – by using different propagators for the classical and quantum subsystems – can spoil some of the properties of the propagators, such as the symplecticity or the accuracy order of the method. If one designs from the start a single propagator for the whole system, it is possible to do it correctly in order to ensure the conservation of those properties. Nonetheless, the development of schemes adapted to hybrid models seems to be a small part of the numerical integration field, and few authors have worked on them [152, 86, 87, 153, 154, 174, 98, 76]. In this section, we describe an alternative to these schemes, based on extending the previous work on CFM expansions for the TDKS equations.

The EMD+TDDFT model used in Chapter 4 is a non-adiabatic, classical-quantum hybrid scheme where the electronic part is computed with TDDFT. We rewrite Newton's equations of movement for the nuclei in a nonlinear Schrödinger-like form, allowing us to implement a single propagator that takes care of both the classical and quantum parts of the system. As we have detailed in the previous section (and published in Ref. [70]), the CFM expansions [15, 9] showed a remarkable success in the propagation of the TDKS equations when compared with

other families of integrators, like the well known EMR or the classical RK4. For this reason we chose to implement different CFM schemes for the propagation of the EMD+TDDFT model, and also extended the previous study by analyzing higher order CFM expansions.

Initially, these methods were developed for linear systems. However, both the TDKS equations for the electrons and the Newton's equations for the nuclei are generally nonlinear. Therefore, the equations of motion of the EMD+TDDFT model take the form of a nonlinear Schrödinger equation. The CFM propagators require the application of the Hamiltonian at intermediate points of the propagation interval. However, when the problem is nonlinear we do not know the Hamiltonian at these points, since it depends on the state of the system. Although there are proposals for the generalization of the CFM schemes to the nonlinear case [15], we have opted for a simpler linearization method: using extrapolation, we approximate the Hamiltonian from previous propagating steps to the intermediate points of the propagation interval that the integrator needs. In this way we are turning the CFM expansions into some kind of multistep explicit propagators, which implies the need to save a certain number of previous positions, velocities and Hamiltonians of the system.

We start with a brief description of the EMD+TDDFT model and the method to rewrite Newton's equation as a Schrödinger one for hybrid systems in subsection 5.2.1, then we will talk about the CFM propagators and its implementation in subsection 5.2.2. Finally, we present the results in subsection 5.2.3. This section is based on Ref. [69].

5.2.1 Classical-Quantum Systems as a Schrödinger-like Equation

The combination of the EMD with TDDFT has proven to be a good way to deal with Molecular Dynamics problems where the classical adiabatic approach fails, such as situations that involve high intensity, short duration laser pulses like those discussed in Chapter 4. The equations of movement for this model are:

$$i\frac{\mathrm{d}}{\mathrm{dt}}|\varphi_i\rangle = \hat{H}_{\mathrm{KS}}(q,\varphi)|\varphi_i\rangle\,, \tag{5.47a}$$

$$\dot{q}_\alpha = \frac{1}{m_\alpha}p_\alpha\,, \tag{5.47b}$$

$$\dot{p}_\alpha = F_\alpha[q(t),\varphi(t),t]\,. \tag{5.47c}$$

where the latin index i runs over the N electrons of the system, the greek index α runs over the classical coordinates q_α and p_α, m_α are the nuclear masses, F_α is the force associated to each classical degree of freedom and $\hat{H}_{\mathrm{KS}}(q,\varphi)$ is the Kohn-Sham Hamiltonian (that typically depends on the position, but not the momenta, of the nuclei, and which depends also on the Kohn-Sham orbitals φ through their density). For a more detailed explanation of

the model, check Chapter 2, section 2.3. Here we use the following expression for the force exerted over the nucleus α:

$$F_\alpha[q(t),\varphi(t),t] = -\sum_i \langle\varphi_i(t)|\frac{\partial \hat{H}_{\mathrm{KS}}}{\partial q_\alpha}|\varphi_i(t)\rangle - \frac{\partial}{\partial q_\alpha}W(q(t)) + F_\alpha^{\mathrm{ext}}(t)\,, \tag{5.48}$$

where W is the nucleus-nucleus interaction and F_α^{ext} takes account of the external forces on the nucleus.

The inclusion of TDDFT in the EMD model brings the nonlinearity of the TDKS equations with it, because as we know the Kohn-Sham Hamiltonian depends on the density, which in turn depends on the Kohn-Sham orbitals. Anyway, even if our description of the electrons were carried out by a set of linear equations, Eqs. 5.47 ends up as a nonlinear set of equations due to the coupling to the classical subsystem. As we mentioned above, the usual approach to the propagation of hybrid systems is to use an integrator for the classical part (e.g. the Verlet integrator) and another one for the quantum one. While this approach might work, we risk ruining some properties of the propagators, like the order of accuracy with respect to the time step or its symplecticity.

The first step for developing a hybrid propagator that treats consistently both subsystems on the same footing should consist on looking for a way to consider both sets of equations as members of the same family, in order to be able to apply the same method to them. One possible way to do this is to consider the hybrid model as one symplectic (Hamiltonian) system. We know that both the classical equations as well as the quantum ones are symplectic, so combining them also results in a Hamiltonian system [18, 1]. This means that we can build a Hamiltonian function (using the position and momentum variables and following the same approach from the previous section for the quantum wave function), and a hybrid bracket, from which to derive the dynamics. Then we could apply any propagator suitable for this kind of systems. The problem with this scheme is that a series of nested Poisson brackets appear when we attempt to develop formulas that are accurate to high order, and those nested brackets imply the need for higher order derivatives which is a very computationally expensive procedure.

Because of this reason, we have not followed that approach based on using hybrid Poisson brackets. In our approach, we simply regard the full system as a nonlinear Schrödinger equation:

$$\dot{y}(t) = -iH(y(t),t)y(t)\,, \tag{5.49a}$$

$$y(0) = y_0\,. \tag{5.49b}$$

The state vector y includes both the classical and quantum degrees of freedom:

$$y = \begin{bmatrix} q \\ v \\ \varphi \end{bmatrix}, \tag{5.50}$$

where q represents all the nuclear positions, v all the velocities and φ all the Kohn-Sham orbitals in some basis. Now the nonlinear Schrödinger equation takes the form:

$$\begin{pmatrix} \dot{q}(t) \\ \dot{v}(t) \\ \dot{\varphi}(t) \end{pmatrix} = -i \begin{pmatrix} H_C(q(t),\varphi(t),t) & 0 \\ 0 & H_{\mathrm{KS}}(q(t),\varphi(t),t) \end{pmatrix} \begin{pmatrix} q(t) \\ v(t) \\ \varphi(t) \end{pmatrix}, \tag{5.51}$$

where H_{KS} is the matrix representation of the Kohn-Sham Hamiltonian and the "classical" Hamiltonian H_C is defined as:

$$H_C(q(t),\varphi(t),t) = i \begin{pmatrix} 0 & 1 \\ \frac{F(q(t),\varphi(t),t)}{mq(t)} & 0 \end{pmatrix}. \tag{5.52}$$

As we can see from Eq. 5.52, in order to turn Newton's equations into a Schrödinger-like form we had to divide by the positions $q(t)$ in the definition of the matrix – a division that is canceled later by the matrix vector multiplication. Also, it is remarkable that Eq. 5.51 is block diagonal, which implies that the classical and quantum particles only interact through the definition of their Hamiltonians.

It remains to see how we have dealt with the nonlinearity. We can rewrite the system of equations in the extended variables

$$\dot{u}(t) = -iH(v(t),t)u(t), \qquad u(0) = y_0 \tag{5.53a}$$

$$\dot{v}(t) = -iH(u(t),t)v(t), \qquad v(0) = y_0, \tag{5.53b}$$

which has the unique solution $u(t) = v(t) = y(t)$. Now we take $v(t)$ as the approximation to $y(t)$ and $u(t)$ as a time-dependent function in the equation of $v(t)$. If we want to preserve the properties of the propagator, we have to find approximations to $u(t)$ such that the approximations to $H(u(t),t)$ at the instants required by the method correspond to Hermitian operators. As the Hamiltonian is multiplied by a factor Δt, if we compute $v(t)$ with a method of order s we only need for $u(t)$ to have an accuracy up to order $s-1$. We can obtain those approximations with extrapolations of the results obtained in the $s-1$ previous steps of

the propagation. However, as we will see in the following section, using a higher order extrapolation can result in higher accuracies for the method.

5.2.2 Implementation

Now that we have a way to write the equations of motion of a hybrid system as a nonlinear Schrödinger-like equation, we will now describe the implementation of the CFM methods that we have used and tested.

First of all, let us change the notation for the CFM integrators from the previous section, as we will now use different propagators with the same order:

$$y(t+\Delta t) = \Gamma_M^{[S]}(H) y(t)\,, \tag{5.54a}$$

$$\Gamma_M^{[S]}(H) = \prod_{k=1}^{M} \exp\left[-i\Delta t \sum_{\mu}^{K} \alpha_{k\mu} H(t_\mu)\right], \tag{5.54b}$$

where M is the number of exponentials of the method and S is the accuracy order of the resulting method. As we commented in the previous section, one needs a number K of Hamiltonians at intermediate times t_μ within the propagation interval $[t, t+\Delta t]$, and this leads to the need of either solving a nonlinear algebraic system to find these values or to approximate the Hamiltonian at these times with extrapolation. Once again we chose to use extrapolation to find those Hamiltonians; we will use the notation $H[t_\mu]$ for the approximated extrapolated Hamiltonians. To perform the extrapolation we have to store a number of previous states $y(t-\Delta t), \ldots, y(t-s\Delta t)$ (or the corresponding Hamiltonians, whatever it is more convenient). If the order of the propagation is s, we also need to perform our extrapolation with order s to preserve the accuracy of the integrator.

We can rewrite Eq. 5.51 as two subsystems, thanks to its block-diagonal structure:

$$\begin{pmatrix} q(t+\Delta t) \\ v(t+\Delta t) \end{pmatrix} = \Gamma_M^{[S]}(H_C) \begin{pmatrix} q(t) \\ v(t) \end{pmatrix}, \tag{5.55}$$

$$\varphi(t+\Delta t) = \Gamma_M^{[S]}(H_{\mathrm{KS}})\varphi(t)\,. \tag{5.56}$$

Now for the implementations of the CFM schemes we used the following algorithm:

1. Compute $\{q[t_\mu]\}$ extrapolating from $q(t), q(t-\Delta t), \ldots, q(t-s\Delta t)$.
2. Compute $\{F[t_\mu]\}$ extrapolating from $F(t), F(t-\Delta t), \ldots, F(t-s\Delta t)$.
3. Compute $\{H_{\mathrm{KS}}[t_\mu]\}$, extrapolating from $H_{\mathrm{KS}}(t), H_{\mathrm{KS}}(t-\Delta t), \ldots, H_{\mathrm{KS}}(t-s\Delta t)$.

4. $H_C[t_\mu] = i \begin{pmatrix} 0 & 1 \\ \frac{1}{m}\frac{F[t_\mu]}{q[t_\mu]} & 0 \end{pmatrix}$
5. $\begin{pmatrix} q(t+\Delta t) \\ v(t+\Delta t) \end{pmatrix} = \Gamma_M^{[S]}(H_C) \begin{pmatrix} q(t) \\ v(t) \end{pmatrix}$
6. $\varphi(t+\Delta t) = \Gamma_M^{[S]}(H_{\mathrm{KS}})\varphi(t)$
7. Compute $F(t+\Delta t)$ and $H_{\mathrm{KS}}(t+\Delta t)$, necessary inputs for the next iteration.

We implemented four CFM schemes, two with order four and two with order six. The first fourth order method is the one that we already tested in the previous section [15, 6], composed by two exponentials:

$$\Gamma_2^{[4]}(H) = e^{-i\Delta t(\alpha_1 H[t_1]+\alpha_2 H[t_2])} e^{-i\Delta t(\alpha_2 H[t_1]+\alpha_1 H[t_2])}, \tag{5.57}$$

where the constants α_i and t_i are given by:

$$\begin{cases} \alpha_1 = & \frac{3-2\sqrt{3}}{12}, & \alpha_2 = & \frac{3+2\sqrt{3}}{12}, \\ c_1 = & \frac{1}{2}-\frac{\sqrt{3}}{6}, & c_2 = & \frac{1}{2}+\frac{\sqrt{3}}{6}, \\ t_1 = & t+c_1\Delta t, & t_2 = & t+c_2\Delta t. \end{cases} \tag{5.58}$$

The other order four method that we have tested, $\Gamma_4^{[4]}$ [9], is designed for Hamiltonian functions that can be decomposed in two parts

$$H(y(t),t) = T + V(y(t),t), \tag{5.59}$$

where T is the kinetic term (linear and time-independent) and $V(y(t),t)$ is the (nonlinear and time-dependent) potential, whose exponential is easy to calculate (because is either diagonal or can be brought to diagonal form without significant cost, for example). The propagator is defined as

$$\Gamma_4^{[4]} = e^{-i\Delta t\tilde{V}_4} e^{-i\frac{\Delta t}{2}(T+\tilde{V}_3)} e^{-i\frac{\Delta t}{2}(T+\tilde{V}_2)} e^{-i\Delta t\tilde{V}_1},$$

where:

$$\begin{cases} \tilde{V}_1 = & a_{11}V_1 + a_{12}V_2 + a_{13}V_3\,, \\ \tilde{V}_2 = & a_{21}V_1 + a_{22}V_2 + a_{23}V_3\,, \\ \tilde{V}_3 = & a_{23}V_1 + a_{22}V_2 + a_{21}V_3\,, \\ \tilde{V}_4 = & a_{13}V_1 + a_{12}V_2 + a_{11}V_3\,, \end{cases} \tag{5.60}$$

and

$$V_1 = V[t + c_1\Delta t]\,, \qquad V_2 = V[t + c_2\Delta t]\,, \qquad V_3 = V[t + c_3\Delta t]\,, \tag{5.61}$$

are extrapolated potentials. Theoretically, as we can do a fast evaluation of $e^{-i\Delta t\tilde{V}_1}$ and $e^{-i\Delta t\tilde{V}_4}$, the cost of this method is similar to one with only two exponentials. The $\{a_{ij}\}$ and $\{c_i\}$constants that appear in these equations are

$$\begin{cases} a_{11} = & \dfrac{10+\sqrt{15}}{180}\,, & a_{12} = & -\dfrac{1}{9}\,, & a_{13} = & \dfrac{10-\sqrt{15}}{180}\,, \\ a_{21} = & \dfrac{10+8\sqrt{15}}{180}\,, & a_{22} = & \dfrac{2}{3}\,, & a_{23} = & \dfrac{10+8\sqrt{15}}{180}\,, \\ c_1 = & \dfrac{1}{2} - \dfrac{\sqrt{15}}{10}\,, & c_2 = & \dfrac{1}{2}\,, & c_3 = & \dfrac{1}{2} + \dfrac{\sqrt{15}}{10}\,. \end{cases} \tag{5.62}$$

For this method to work, the generators α_i defined as

$$\alpha_1 = -i\Delta t(T + V_2)\,, \tag{5.63a}$$

$$\alpha_2 = -i\Delta t\frac{\sqrt{15}}{3}(V_3 - V_1)\,, \tag{5.63b}$$

$$\alpha_3 = -i\Delta t\frac{10}{3}(V_3 - 2V_2 + V_1)\,, \tag{5.63c}$$

must fulfill the condition $[\alpha_2, \alpha_3] = 0$.

In our case, we have two separate subsystems, and therefore we have to separate both the classical and the quantum Hamiltonians in a suitable way that respects that condition.

$$\begin{aligned} H(y(t),t) &= \begin{pmatrix} H_C(q(t),\varphi(t),t) & 0 \\ 0 & H_{\mathrm{KS}}(q(t),\varphi(t),t) \end{pmatrix} \\ &= \begin{pmatrix} T_C + V_C(q(t),\varphi(t),t) & 0 \\ 0 & T_Q + V_Q(q(t),\varphi(t),t) \end{pmatrix}. \end{aligned} \tag{5.64}$$

This division for both subsystems entails the definition of both classical and quantum generators α_{Ci} and α_{Qi}. The two sets have to verify the commutation rule written above. The

division of the quantum part is trivial, as we already have kinetic and potential terms and the commutator $[\alpha_{Q2}, \alpha_{Q3}] = 0$ is fulfilled (the potential terms are diagonal in real space). For the classical Hamiltonian we have found out that making $T_C = 0$ and $V_C(q(t), \varphi(t), t) = H_C(q(t), \varphi(t), t)$ is a valid choice and $[\alpha_{C2}, \alpha_{C3}] = 0$.

This division of the Hamiltonian into a kinetic and a potential term is also used in the first order six method that we implemented, $\Gamma_5^{[6]}$. This method consists of five exponentials, but only three are computationally expensive:

$$\Gamma_5^{[6]} = e^{-i\Delta t\tilde{V}_5} e^{-i\Delta t(b_1 T + \tilde{V}_4)} e^{-i\Delta t(b_2 T + \tilde{V}_3)} e^{-i\Delta t(b_1 T + \tilde{V}_2)} e^{-i\Delta t\tilde{V}_1} .$$

The linear combinations of V_1, V_2 and V_3 that conform the $\tilde{V}_i$ are the same as in Eq. 5.61, and the quadrature points c_i are those from Eq. 5.62.

Finally, we implemented another order six propagator, $\Gamma_4^{[6]}$. It consists of four exponentials, but only two of them involve the costly kinetic term:

$$\Gamma_4^{[6]} = e^{-i\Delta t(\tilde{V}_4 + \Delta t^2 \tilde{V})} e^{-i\frac{\Delta t}{2}(T + \tilde{V}_3)} e^{-i\frac{\Delta t}{2}(T + \tilde{V}_2)} e^{-i\Delta t(\tilde{V}_1 + \Delta t^2 \tilde{V})} .$$

This method shares the same potential terms $\tilde{V}_i$ as the previous propagator $\Gamma_5^{[6]}$, but a new $\tilde{V}$ appears, defined by

$$\tilde{V} = i\frac{y}{\Delta t^3} [\alpha_2, [\alpha_1, \alpha_2]] , \tag{5.65}$$

where $y = 1/43200$, and α_i are the generators defined in Eqs. 5.63.

Although the inclusion of this last commutator apparently contradicts the "commutator free" concept that characterize these methods, in some circumstances it might be advantageous to include some easy to compute commutators. For the quantum part, if we assume that the potential term is a local function in real space, Eq. 5.65 can be reduced to

$$\tilde{V}_Q = i\frac{y}{\Delta t^3} [\alpha_{Q2}, [\alpha_{Q1}, \alpha_{Q2}]] . \tag{5.66}$$

This term has to be easy to compute, or small enough to neglect, or otherwise the performance of the method will be affected significantly.

For the nuclear case, we have

$$\begin{pmatrix} q(t+\Delta t) \\ v(t+\Delta t) \end{pmatrix} = e^{-i\Delta t(\tilde{H}_{C4} + \Delta t^2 \tilde{H}_C)} e^{-i\frac{\Delta t}{2}\tilde{H}_{C3}} e^{-i\frac{\Delta t}{2}\tilde{H}_{C2}} e^{-i\Delta t(\tilde{H}_{C1} + \Delta t^2 \tilde{H}_C)} \begin{pmatrix} q(t) \\ v(t) \end{pmatrix} ,$$

where we have defined the $\tilde{H}_{Ci}$ matrices as

$$H_{Cj} = H_C[t_j] = i \begin{pmatrix} 0 & \delta_{j2} + \delta_{j3} \\ \lambda_j & 0 \end{pmatrix}, \tag{5.67}$$

with $\lambda_j = \left(\frac{1}{m}\right) F[t_j]/q[t_j]$. Now Eq. 5.65 takes the form

$$\tilde{H}_C = i\frac{y}{\Delta t^3}\left[\alpha_{C2}, [\alpha_{C1}, \alpha_{C2}]\right] = \frac{i}{51840} \begin{pmatrix} 0 & 0 \\ (\lambda_3 - \lambda_1)^2 & 0 \end{pmatrix}. \tag{5.68}$$

5.2.3 Results

We have studied the CFM propagators for the EMD+TDDFT model using the same methodology as in subsection 5.1.2, but in this case we have used an Hydrogen molecule in the presence of a laser field $\varepsilon(t)$ with the shape

$$\varepsilon(t) = A\sin(\omega t), \tag{5.69}$$

where the amplitude is $A = 0.1$ a.u. and the frequency is $\omega = 10$. The molecule was placed in a spherical simulation box with radius $R = 10$ a.u., with a grid spacing $h = 0.4$ a.u. and the total simulation time was set up to $T = 20\pi$.

For the analysis of the accuracy and cost of the propagators, in this case we only look at the error in the wave function (defined in Eq. 5.22), as the energy is not conserved due to the effect of the laser pulse. In order to get the exact reference values of the Kohn-Sham orbitals, we have used once again the RK4 method with a very small time step. About the cost of the propagator, we have considered both the time in seconds and the number of applications of the Hamiltonian that each method required, and we plotted them as a function of the wave function error. The results obtained from the CFM schemes have been compared with the EMR integrator.

Fig. 5.10 shows the error of the wave function as a function of the time step, using logarithmic scales in both axes. As we can see, the CFM methods are notably more precise than the EMR. We cannot distinguish the CFM methods of the same order in this figure, as they produce results with almost the same accuracy. This is caused because the dominant error is the one from the extrapolation, which is the same for methods with the same order.

In Fig. 5.11 the cost (in seconds) of the propagation is plotted as a function of the attained error in the wave function. The axes are also in logarithmic scale. From the figure, we can see that the order 6 CFMs are more efficient than their order 4 counterparts if one needs errors below $\approx 10^{-4.5}$. $\Gamma_4^{[6]}$ is the best propagator for this range of errors. On the other hand,

for errors above $\approx 10^{-4.5}$, $\Gamma_2^{[4]}$ beats the order 6 formulas by a small margin. In any case, the EMR is completely outclassed by the CFM schemes.

The previous figures were obtained with calculations in which the extrapolation that deals with the nonlinearity were perfomed with accuracy order equal to the order of the underlying method (4 or 6). In contrast, the following two figures, Figs. 5.12 and 5.13 show the same calculations but with extrapolations done at order 12. There is a sensible increase in the accuracy of the CFM methods, which are now at least four orders of magnitude more accurate than the EMR. This increase in the precision confirms the fact that the extrapolation error dominates the propagation in the case of the CFM methods. However, this increase in accuracy also entails a reduction of the stability region for the CFM propagators. This is reflected by the first point (on the right) of the figures: while the EMR method remains functional, the error of the CFM integrators is very large (it starts diverging). While $\Gamma_2^{[4]}$ presents an order four behavior, matching the theoretical prediction, $\Gamma_4^{[4]}$ is slightly more precise, and shows an order higher than 4. Both order 6 methods show a similar behavior, reaching numerical accuracy ($\approx 10^{-12}$) for time steps as large as $\Delta t \approx 10^{-2.4}$. From the cost/accuracy plot of Fig. 5.13, once again it is shown that the best choice of propagator depends on the accuracy desired for the problem at hand. The order 6 CFM methods are suitable if the precision required is very high; however, if lower accuracies suffice, the EMR would be a better option. For the intermediate range of accuracy the order 4 methods are the best choices.

5.3 Conclusions

Motivated by the need of fast and accurate methods of numerical integration of the TDKS equations, we set out to test and implement in Octopus propagators from four different families that had not been previously analyzed in the context of TDDFT: Runge-Kutta, exponential Runge-Kutta, multistep methods, and commutator-free Magnus expansions. We implemented these methods in the Octopus code, and ran benchmarking tests using a simple molecular system subject to a laser field. For each method, we measured the error in the wave function and energy as a function of the time-step, and the computational cost in seconds as a function of the error. We compared them with the well-known exponential midpoint rule, that we used as a reference method. The main overall conclusion of this comparison: we found out that the fourth order commutator-free Magnus expansion beats every other method both in terms of accuracy and computational cost.

Regarding the multistep schemes, their main feature is that they maintain a constant cost independently of the number of previous steps considered. Since the accuracy improves with

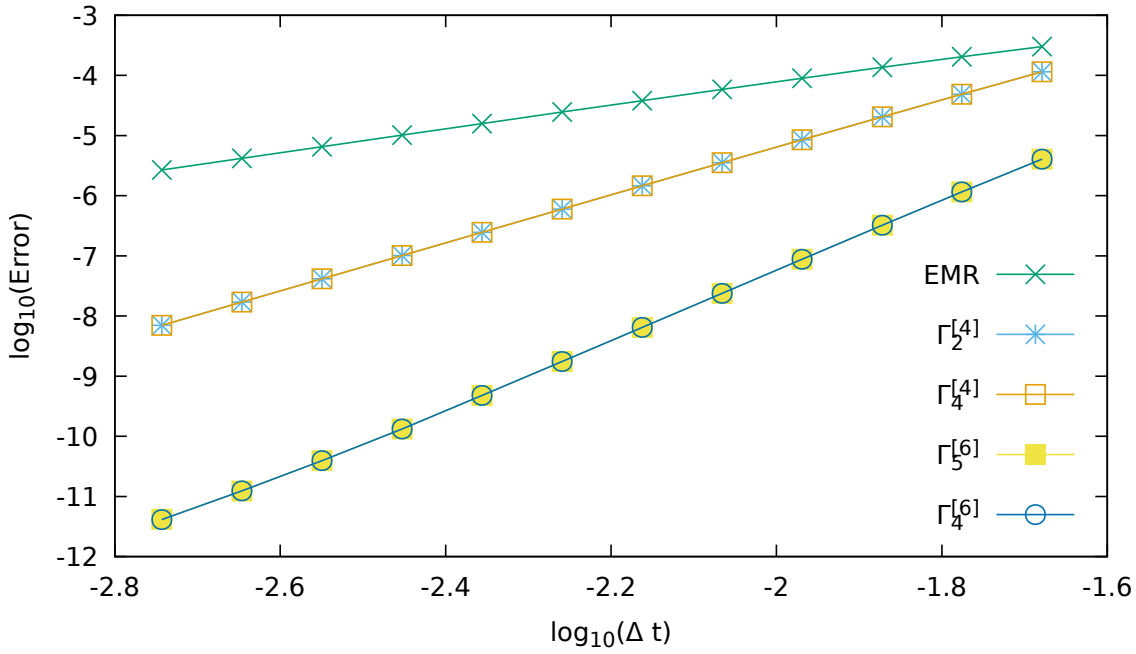

Fig. 5.10 Error in the propagation, measured as the difference of the propagated Kohn-Sham orbitals with respect to the quasi-exact ones (computed with a tiny time step), as a function of the time step. Both the error and the time step are shown in logarithmic scale. The extrapolation order matches that of the underlying method.

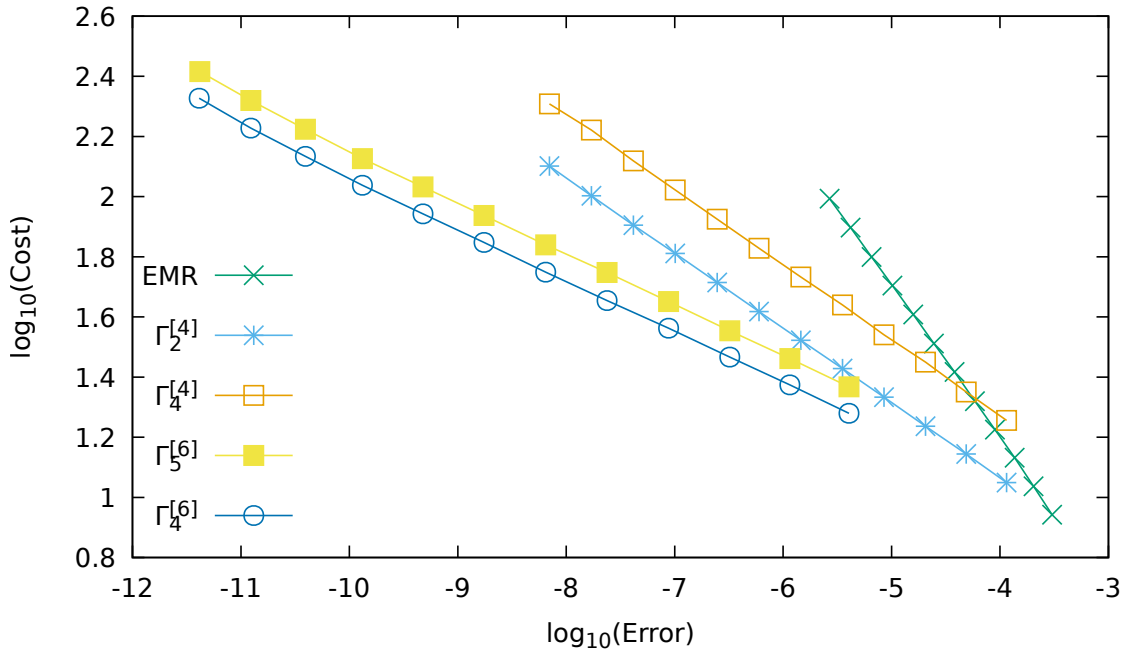

Fig. 5.11 Cost in seconds as a function of the error, both in logarithmic scale. The extrapolation order matches that of the underlying method.

this number, it would seem that by adding a sufficiently large number of steps one would get a very efficient scheme. Unfortunately, the stability region of all multistep methods grows smaller with the number of steps, making them unsuitable. Moreover, the need to store the previous states of the system implies that the available memory is also a limiting factor for this family of integrators.

Among the Runge-Kutta methods, both the regular ones and the exponential ones, the explicit order four Runge-Kutta method is still the best one from this family, in terms of efficiency. The exponential Runge-Kutta and implicit Runge-Kutta methods are at advantage when dealing with stiff problems, however, or if one needs a high degree of conservation of some quantity, i.e., when the symplecticity of the equations of motion is relevant.

Regarding this point, we have also demonstrated the symplecticity of the TDKS equations in the adiabatic approximation. This fact encourages the use symplectic integrators, as they will be generally more successful when dealing with long time propagations.

After this work on the electronic-only problem, we moved on to studying suitable methods for hybrid classical-quantum systems. In particular, we studied and implemented order 4 and order 6 methods from the CFM family, and applied them to the propagation of systems modeled with the EMD+TDDFT combination. We have rewritten the full dynamics of the model as a nonlinear Schrödinger equation. This allows us to apply the same propagator to

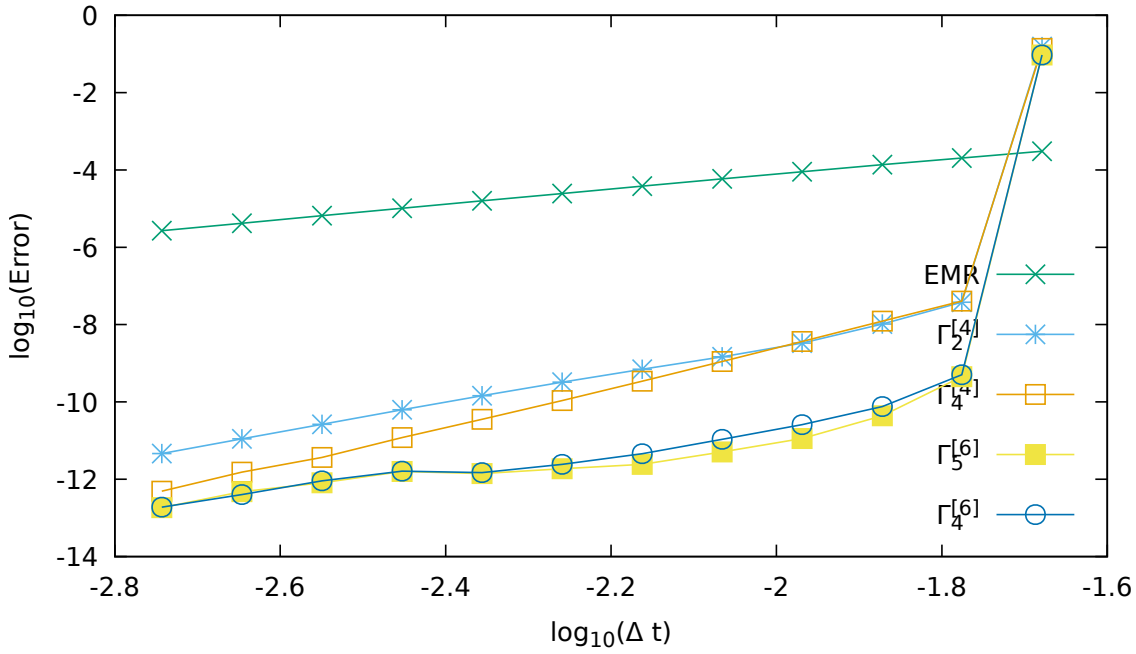

Fig. 5.12 Error in the propagation, measured as the difference of the propagated Kohn-Sham orbitals with respect to the quasi-exact ones (computed with a tiny time step), as a function of the time step, computed using extrapolation of order 12. Both the error and the time step are shown in logarithmic scale.

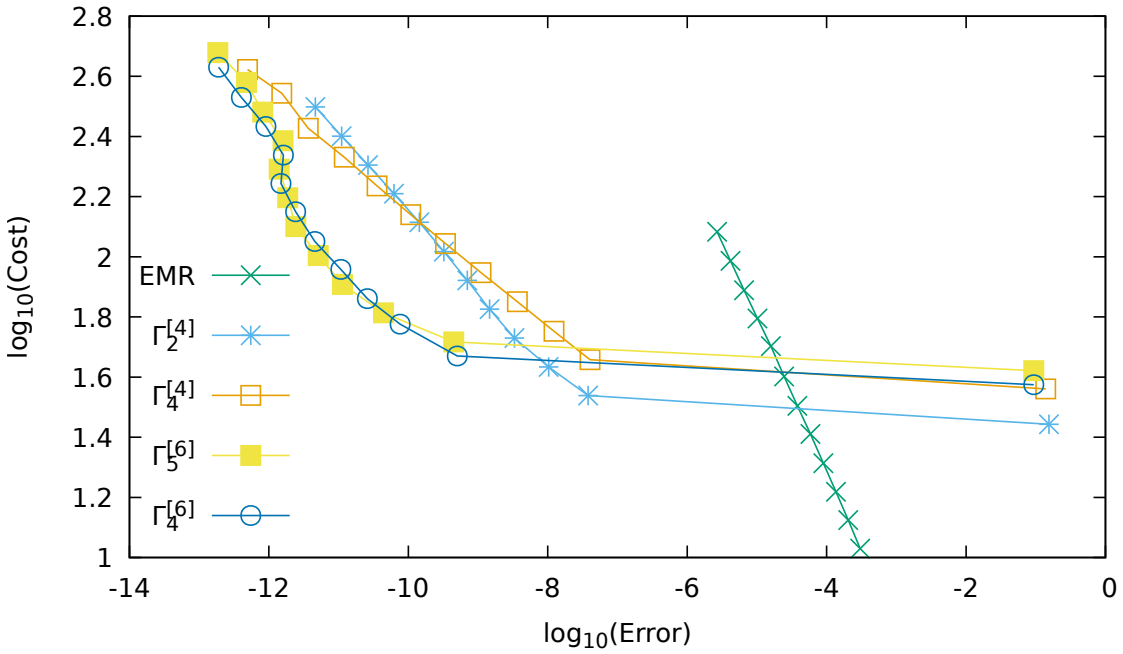

Fig. 5.13 Cost in seconds as a function of the error, both in logarithmic scale, computed using order 12 extrapolation.

the equations of movement of the full system, avoiding the problems derived from using two separate integration methods for the classical and quantum parts. The CFM methods that we implemented were originally devised for linear systems, as the formulas of the propagators require the evaluation of the Hamiltonian at intermediate times of the propagation interval, which is unknown in the case of nonlinear Schrödinger equations. To avoid this problem we have extrapolated the Hamiltonian from previous steps, effectively turning this propagation scheme into a multistep one. The order of the extrapolation must match at least the order of accuracy of the the underlying method for this order to be preserved. We have observed, however, that one can notably increase the accuracy of the methods using higher order extrapolation, at the cost of compromising the stability of the method.

Using an algorithm designed from the start for the combined system ensure its properties (symplecticity, accuracy order with respect to the time step...), while using a different algorithm for each system does not. From the simulations we have found that the proposed schemes are computationally efficient: for the whole range of time steps studied, all the tested variants of the CFM methods improve over the EMR. From the cost vs. accuracy curves, we can then conclude that, if we require highly accurate calculations, the order 6 CFM methods perform better than the order 4 ones. For lower accuracies, the order 4 integrators are however more efficient than their order 6 counterparts.

Chapter 6

Conclusions

In this thesis we have studied different topics in the area of ab initio electronic structure modeling, ranging from the study of the theoretical foundations of DFT to the practical implementation and application, to realistic systems, of the non-adiabatic combination of TDDFT with Ehrenfest dynamics.

More concretely, we have tackled three different problems: (1) We presented a new route to the study of the exchange and correlation functionals (XFCs) in DFT. It may help to improve, systematically, the current approximations. We have tested it on the one-dimensional Hubbard model (1DHM), used as an example: we have optimized the Bethe ansatz local density approximation (BALDA) functional with respect to the in-site interaction parameter of the Hubbard chain; (2) Using the combination of Quantum Optimal Control Theory (QOCT) with TDDFT, together with the non-adiabatic Ehrenfest model of molecular dynamics (EMD), we searched for the shape of (short) laser pulses that better induce the ionization of small sodium clusters leading to their Coulomb explosion; (3) We investigated different families of numerical propagators for the time-dependent Kohn-Sham (TDKS) equations. We measured their accuracy and performance, and compared them with well established methods of propagation within the electronic structure field, like the exponential midpoint rule (EMR) or the explicit order four Runge-Kutta integrator (RK4). Then, we extended the commutator-free Magnus (CFM) methods to the EMD+TDDFT model, developing a methodology to apply the numerical integrator to both parts of a classical-quantum hybrid system by rewriting the equations of motion like a single nonlinear Schroödinger equation.

Regarding the first topic, we researched a new path to the study of XCFs in DFT, that could potentially lead to finding new and better ones. This approach is based on the independence of DFT on the electron-electron interaction function (IF): the theory can be formulated for almost arbitrary shapes of this function, and not only for the real Coulomb one. Based on this idea, we established a numerical procedure to assign to each XCF the IF that better suits it: the exact densities obtained by using this IF are the ones that more closely resemble the ones obtained solving the Kohn-Sham equations with that XCF. Of course, generally, this IF will not be the Coulomb interaction, but we can use this correspondence to improve any parameterized family of XCFs: we optimize the parameters of the XCF with the objective of finding the one whose associated IF is closer to the real one. As a proof of concept, we optimized the BALDA functional, used for the description of the 1DHM, in the context of lattice DFT. First, we explored optimizations with lattice sizes of up to 20 sites. The procedure requires the computation of exact densities, and at this point, the standard diagonalization methods that we were using became too costly in terms of both time and memory. In order to go further, we had to use density matrix renormalization group (DMRG), a theory that is specially well suited for one-dimensional systems. Using DMRG we could expand the BALDA optimization procedure to chains with 40 sites.

We have used the formalism described to find the optimal functional within an existing XCF family – since BALDA is in fact a one-parameter family of functionals –, for one-dimensional model systems. The procedure has proved to be feasible, and returns very precise optimized functionals. The goal now would be to go beyond this simple model, using a similar procedure. The first step is to define the exact, reference IF, which in the normal 3D situation is simply the Coulomb interaction $1/r$ – it is different for the model systems (as for the 1DHM) that we have used up to now. Next, one must choose a parameterized family of XCFs. Then, using the method described above, one finds one corresponding IF for each XCF, and compares it with the reference IF using some appropriate formula for the distance between IFs. Using a minimization algorithm for this distance, one would eventually find the best XCF that, for a given family of external potentials, better reproduce the electronic densities found using the reference IF. Once this procedure has been demonstrated for one dimensional systems, the main obstacle for its extension to two and three dimensional systems is the need to obtain exact reference densities.

Besides the previous work on the theoretical foundations of density-functional based theories, we have also worked on some practical applications of these methods to concrete

problems. In particular, we have applied QOCT to the Ehrenfest model (a classical-quantum hybrid, non-adiabatic form of molecular dynamics) combined with TDDFT for the description of the electrons. The objective was to optimize the shape of short duration laser pulses (a few femtoseconds) to induce the Coulomb explosion of sodium clusters. The pulses were under duration, frequency and fluence constraints, in order to force the final solution to be within the reach of current experimental setups. Also, because a fully unrestricted search would lead to trivial, unphysical solution: obviously, simply raising to infinity the intensity of the pulses one obtains Coulomb explosion. The systems studied were sodium clusters, going one step beyond the previous work done with this methodology, that only treated simple Hydrogen molecules.

We used two optimization targets: the number of escaped electrons at the end of the pulse, and the sum of opposite momenta between pairs of nuclei. Furthermore, the optimizations were carried out in two different manners: either allowing the nuclei to move during the application of the laser (*dynamic optimizations*), or not (*static optimizations*). The goal of making this distinction was to study whether the nuclear movement during the irradiation of these very short pulses was relevant for the ionization. If it is not relevant, the full combination QOCT+EMD+TDDFT is not necessary, and one could perform calculations with QOCT+TDDFT only. We found that the influence of the movement of the nuclei in the case of 16 fs pulses was not relevant, as both the static and dynamic optimizations reached successful solutions. For the 32 fs case, the shape of the pulses obtained with both the static and dynamic optimization schemes started to diverge, although both solutions induced the Coulomb explosion of the cluster. Finally, for the 64 fs pulses the static optimization was unable to produce a satisfactory pulse, making the use of the EMD+TDDFT model necessary.

Another important conclusion of this work is that the *trivial* solutions are not the optimal ones, and therefore one needs the QOCT formalism. By *trivial* solution, we mean for example pulses tuned to the ground state resonance frequency of the cluster. In principle, one would expect that by depositing a lot energy in that excitation, the ionization and Coulomb explosion would follow. However, even for pulses as short as 16 fs, the main peak of the spectra of the optimal laser differs from that resonance frequency of the cluster. The reason must be found in two factors: as electronic charge escape, there is a blueshift in the resonance; and in contrast, as the clusters start to expand, the resonance redshifts. These opposing factors make the optimal solution unpredictable by simple intuitive reasoning, and therefore one must use a method such as QOCT.

As a final conclusion of this work, we found that even when using TDDFT (one of the most computationally cheap first principles approaches to the many electron problem) with Ehrenfest dynamics, the cost of the QOCT calculations was quite high. These calculations

require the propagation of the TDKS equations, and of an auxiliary system called *costate* in the OCT terminology. Those propagations, whose goal is to compute the gradient of the objective functional with respect to the control parameters, must be done with high accuracy. The evolution of this auxiliary system is specially challenging, as it includes non-Hermitian operators. Since we used absorbing boundaries to account for the loss of electrons, the norm of the orbitals vary during the propagation becoming a source of numerical instability. These difficulties were our motivation for the search of faster, more reliable numerical propagators.

Therefore, we started a quest for more efficient propagation methods for the TDKS equations. We studied integrators from four families that have been scarcely (if at all) used by the TDDFT community: commutator-free Magnus expansion, multistep, Runge-Kutta and exponential Runge-Kutta methods. Special attention was put on those propagators that conserve some properties of the equations. We focused on the conservation of the norm and the symplecticity, as we proved that the TDKS equations in the adiabatic approximation form a symplectic system. From the four analyzed families, we found that the best methods, in terms of performance, were the CFM expansions. The multistep methods can be remarkably accurate at a relatively low computational cost if one uses a large number of previous steps. However, when doing that, the memory requirements grow and, more importantly, stability issues appear. These facts make them unsuitable for large or more numerically challenging systems, such as those presenting stiff equations. Among the Runge-Kutta methods, the best one overall is still the standard RK4. The implicit methods only perform better when one has to deal with stiff equations. Finally, the exponential Runge-Kutta integrators, while certainly performing better than the other explicit methods for stiff equations, are expensive to compute, and do not show any improvement in terms of efficiency over the original RK methods.

Given the success of the CFM methods, the next natural step was to implement them for the EMD+TDDFT model that we had used for our previous project. This is a true hybrid classical-quantum model, and probably the propagating method can be extended to other similar classical-quantum approaches. We struggled to use the same propagator for the whole system, in contrast to more usual algorithms, that mix a faster method for the nuclei with a slower, more precise one for the electrons. This mixture can lead to the deterioration of some properties of the propagators. In order to apply the same propagator to the two subsets of equations of motion of the model (Newton's equations for the nuclei and the TDKS

equations for the electrons), we had to rewrite the classical part to present it in a nonlinear Schrödinger-like fashion.

The formulas for the CFM integrators were developed initially for linear systems and require the computation of the Hamiltonian at intermediate times. As the Kohn-Sham Hamiltonian is nonlinear, we dealt with this problem extrapolating the Hamiltonian from the previous steps to these intermediate times, ending with an explicit, multistep method of propagation. While the order of the extrapolation only needs to be the same as the order of the method, we found that going beyond could greatly improve the accuracy of the integrator. We tested two order 4 and two order 6 implementations of the CFM propagators. The four schemes showed better performance than the EMR for all the time steps explored. For low accuracy, the order four methods are a better choice than the order six ones, and also present better stability at larger time-steps. On the other hand, for very high accuracy the order six methods outclass their order four counterparts. This is general conclusion: the more sophisticated formulas become more efficient if high accuracies are required.

With the CFM propagators showing an outstanding performance compared with well established methods like the EMR and RK4, and with an implementation of them that assures us that the properties of the integrator are preserved, the next step would be trying them on bigger, more complex systems. Using the QOCT+EMD+TDDFT formalism, in combination with this family of propagators, one could tackle, for example, the problem of the optimal photo-isomerization of larger molecules, or the problem of inducing a given photo-chemical reaction. Also, one could think of changing the optimization parameters, from those that define an external laser pulse, to internal parameters of the molecule or material. For example, the target could be finding the initial state that has some desired response properties (such as the maximum absorption of light in the visible spectrum, conductivity, etc.)

Chapter 6

Conclusiones

En esta tesis hemos estudiado varios temas en el área del modelado ab initio en estructura electrónica, desde el estudio de los fundamentos teóricos de la DFT, hasta la implementación y aplicación práctica, a sistemas realistas, de la combinación de la TDDFT con la dinámica no adiabática de Ehrenfest.

Más concretamente, hemos abordado tres problemas diferentes: (1) Hemos presentado una nueva ruta para el estudio de funcionales de intercambio y correlación (XCFs) en DFT. Creemos que esta ruta puede ayudar a mejorar, sistemáticamente, las aproximaciones actuales. La hemos probado en el modelo de Hubbard unidimensional (1DHM), usado como ejemplo: hemos optimizado el funcional de la aproximación de densidad local con el ansatz de Bethe (BALDA) con respecto al parámetro de la interacción en el sitio de la cadena de Hubbard; (2) Usando la combinación de la teoría de control óptimo cuántico (QOCT) con TDDFT, junto con el modelo de dinámica molecular no adiabático de Ehrenfest (EMD), hemos buscado la forma de los pulsos láser (cortos) que provocan mejor la ionización de pequeños clusters de sodio llevándolos a su explosión de Coulomb; (3) Hemos investigado diferentes familias de propagadores numéricos para las ecuaciones de Kohn-Sham dependientes del tiempo (TDKS). Hemos medido su precisión y eficiencia, y los hemos comparado con métodos de propagación bien consolidados en el campo de la estructura electrónica, como la regla del punto medio de la exponencial (EMR) o el integrador explícito de cuarto orden de Runge-Kutta (RK4). Después extendimos los métodos libres de conmutadores de Magnus (CFM) al modelo EMD+TDDFT, desarrollando una metodología para aplicar el integrador numérico a ambas partes de un sistema híbrido clásico-cuántico consistente en reescribir las ecuaciones del movimiento como una sola ecuación de Schrödinger no lineal.

Con respecto al primer tema, hemos investigado un nuevo camino para el estudio de XCFs en DFT, que potencialmente podría llevar a encontrar nuevas y mejores aproximaciones. Esta ruta se basa en la independencia de DFT con respecto a la función de interacción electrón-electrón (IF): la teoría puede formularse para formas prácticamente arbitrarias de esta función, y no sólo para la función real de Coulomb. Basándonos en esta idea, hemos establecido un procedimiento numérico para asignar a cada XCF la IF que mejor se le ajusta: las densidades exactas obtenidas usando esta IF son las que más se parecen a las obtenidas resolviendo las ecuaciones de Kohn-Sham con ese XCF. Como prueba de concepto, hemos optimizado el funcional BALDA, usado para la descripción del 1DHM, en el contexto de lattice-DFT. Primero exploramos optimizaciones con un tamaño máximo de la cadena de 20 sitios. Para ir más allá, tuvimos que usar la teoría del grupo de renormalización de la matriz de densidad (DMRG), una teoría que es especialmente adecuada para sistemas unidimensionales. Usando DMRG pudimos expandir la optimización a cadenas de hasta 40 sitios.

Hemos utilizado el formalismo descrito para encontrar el funcional óptimo dentro de una familia existente de XCFs – puesto que BALDA es de hecho una familia uniparamétrica de funcionales –, para sistemas modelo de una dimensión. El objetivo ahora sería ir más allá de este simple modelo, usando un procedimiento similar. El primer paso es definir la IF exacta, usada de referencia, que en una situación normal en 3D es simplemente la interacción de Coulomb $1/r$, pero que para sistemas modelo (como el 1DHM) puede ser diferente. Después se debe elegir una familia parametrizada de XCFs. Entonces, usando el método descrito anteriormente, se busca una IF correspondiente a cada XCF, y se compara con la IF de referencia usando alguna fórmula apropiada para la distancia entre IFs. Usando un algoritmo de minimización sobre esta distancia, puede entonces encontrarse el mejor XCF que, para una familia dada de potenciales externos, mejor reproduce las densidades electrónicas exactas encontradas usando la IF de referencia. Una vez que este procedimiento ha sido demostrado para sistemas unidimensionales, el principal obstáculo para su extensión a sistemas bi y tridimensionales es la necesidad de obtener densidades de referencia exactas.

Además del trabajo previo en los fundamentos teóricos de las teorías basadas en el funcional de la densidad, también hemos trabajado en algunas aplicaciones prácticas de estos métodos a problemas concretos. En particular, hemos aplicado QOCT al modelo de Ehrenfest (un forma híbrida clásico-cuántica de dinámica molecular no adiabática) combinado con TDDFT para la descripción de los electrones. El objetivo era optimizar la forma de pulsos

láser de corta duración (unos pocos femtosegundos) para inducir la explosión de Coulomb de clusters de sodio. La duración, frecuencia y fluencia de los pulsos estaban sujetas a restricciones para asegurar que la solución obtenida estuviera al alcance de los montajes experimentales actuales. Además, una búsqueda sin ninguna restricción daría lugar a una solución trivial y que no se ajusta a la realidad física: obviamente, simplemente aumentando hasta el infinito la intensidad de los pulsos se obtiene la explosión de Coulomb. Los sistemas estudiados fueron clusters de sodio, yendo un paso más allá del trabajo previo hecho con esta metodología, que sólo trataba moléculas simples de hidrógeno.

Utilizamos dos objetivos de optimización distintos: el número de electrones perdidos al finalizar el pulso, y la suma de los momentos opuestos entre parejas de núcleos, también al finalizar el pulso. Además, las optimizaciones se llevaron a cabo de dos maneras diferentes: o bien permitiendo que los núcleos se muevan durante la aplicación del láser (*optimizaciones dinámicas*), o bien con núcleos fijos (*optimizaciones estáticas*). El objetivo de hacer esta distinción era estudiar si el movimiento nuclear durante la irradiación de estos pulsos muy cortos es relevante para la ionización. Si no es relevante, la combinación completa de QOCT+EMD+TDDFT no es necesaria, y los cálculos se podrían realizar utilizando sólo QOCT+TDDFT. Hemos concluido que la influencia del movimiento de los núcleos en el caso de los pulsos de 16 fs no es relevante, ya que tanto las optimizaciones estáticas como las dinámicas alcanzaron soluciones exitosas y parecidas. Para el caso de los pulsos de 32 fs, sin embargo, la forma de los pulsos obtenidos a partir de las optimizaciones estáticas y dinámicas empieza a divergir, aunque ambas soluciones provocan la explosión de Coulomb del cluster. Finalmente, para los pulsos de 64 fs la optimización estática es incapaz de producir un pulso satisfactorio, haciendo necesario el uso del modelo completo QOCT+EMD+TDDFT.

Otra conclusión importante de este trabajo es que las soluciones *triviales* no son las óptimas, y por tanto se necesita el formalismo de QOCT. Por solución *trivial*, nos referimos por ejemplo a pulsos cuya frecuencia se ajusta a la frecuencia de resonancia del estado fundamental del cluster. Sin embargo, incluso para pulsos tan cortos como 16 fs, el pico principal del espectro de los láseres óptimos difiere de la frecuencia de resonancia del cluster. La razón se halla en dos factores: al escaparse la carga electrónica, hay un corrimiento al azul en la resonancia; y en contraste, cuando los clusters empiezan a expandirse, la resonancia experimenta un corrimiento al rojo. Estos factores opuestos hacen que la solución óptima sea impredecible simplemente usando un razonamiento intuitivo, y por tanto se debe utilizar un método como QOCT.

Como una conclusión final de este trabajo, hallamos que incluso cuando se usa TDDFT (uno de los métodos computacionalmente más baratos para lidiar con el problema de muchos electrones) con dinámica de Ehrenfest, el coste de los cálculos de QOCT eran bastante altos.

Estos cálculos requieren la propagación de las ecuaciones TDKS, y de un sistema auxiliar llamado generalmente *coestado* en la terminología de OCT. Estas propagaciones, cuyo objetivo es computar el gradiente del funcional objetivo con respecto a los parámetros de control, deben hacerse con alta precisión. La evolución del sistema auxiliar es especialmente complicada, ya que incluye operadores no hermíticos. Puesto que usamos paredes absorbentes para tener en cuenta la pérdida de electrones, la norma de los orbitales varía durante la propagación convirtiéndose en una fuente de inestabilidad numérica. Estas dificultades fueron nuestra motivación para la búsqueda de propagadores más rápidos y robustos.

Por tanto, empezamos una búsqueda de métodos de propagación más eficientes para las ecuaciones TDKS. Hemos estudiado integradores de cuatro familias que, o bien solo han sido usados esporádicamente, o bien no han sido usados en absoluto por la comunidad que utiliza la TDDFT: la expansión de Magnus sin conmutadores, métodos con varios pasos previos, fórmulas de Runge-Kutta y fórmulas de Runge-Kutta exponencial. Hemos puesto una atención especial en aquellos propagadores que conservan algunas propiedades de las ecuaciones. Nos concentramos en la conservación de la simplecticidad, ya que hemos demostrado que las ecuaciones TDKS, en la aproximación adiabática, forman un sistema simpléctico. De las cuatro familias analizadas, hallamos que los mejores métodos, en términos de eficiencia, son los métodos de Magnus sin conmutadores. Los métodos con varios pasos previos pueden ser notablemente precisos, a un coste computacional relativamente bajo, si se usa un número elevado de pasos previos. Sin embargo, al hacer eso, los requerimientos de memoria crecen y, más importante aún, aparecen problemas de estabilidad. Estos hechos hacen que no sean adecuados para sistemas grandes o numéricamente complejos, tales como aquellos que implican ecuaciones rígidas (*stiff*). Entre los métodos de Runge-Kutta, el mejor de ellos sigue siendo el "estándar" RK4. Los métodos implícitos solo presentan un mejor rendimiento cuando uno tiene que tratar con ecuaciones rígidas. Finalmente, los integradores exponenciales de Runge-Kutta, que ciertamente funcionan mejor que los otros métodos explícitos para ecuaciones rígidas, son caros de computar, y no muestran ninguna mejora en términos de eficiencia con respecto a los métodos RK originales.

Dado el éxito de los métodos CFM, el siguiente paso natural fue implementarlos para el modelo EMD+TDDFT que utilizamos en nuestro proyecto previo. Este es un modelo clásico-cuántico, y probablemente los métodos de propagación que hemos estudiado pueden extenderse a otras aproximaciones clásico-cuánticas similares. Nos hemos esforzado en utilizar el mismo propagador para todo el sistema, en contraste con los algoritmos habituales,

que mezclan un método rápido para los núcleos con uno más lento y preciso para los electrones. Esta mezcla puede dar lugar al deterioro de algunas propiedades de los propagadores. Para aplicar el mismo propagador a los dos subconjuntos de ecuaciones de movimiento (las ecuaciones de Newton para los núcleos y las ecuaciones TDKS para los electrones), tuvimos que reescribir la parte clásica, presentándolo como una ecuación de Schrödinger no lineal – que es la también la forma de las ecuaciones TDKS.

Las fórmulas para los integradores CFM se desarrollaron inicialmente para sistemas lineales y requieren, en cada intervalo de la propagación, del Hamiltoniano a tiempos intermedios. Dado que el Hamiltoniano de Kohn-Sham es no lineal y por lo tanto es desconocido en esos tiempos intermedios, hemos tratado con este problema extrapolando el Hamiltoniano a partir de pasos previos, dando lugar a un método de propagación explícito y dependiente de pasos previos. Aunque el orden de la extrapolación sólo necesita ser del mismo orden que el del método, hallamos que yendo más allá podíamos incrementar cuantiosamente la precisión del integrador. Examinamos dos formulaciones de los propagadores CFM de orden 4 y dos de orden 6. Los cuatro métodos mostraron mejor rendimiento que la EMR para todos los pasos temporales explorados. Para baja precisión, los métodos de orden 4 son una mejor elección que los de orden 6, y también presentan mejor estabilidad para pasos temporales más grandes. Por otro lado, para muy alta precisión los métodos de orden 6 superan a sus equivalentes de orden 4. Esta es una conclusión general: las fórmulas más sofisticadas se vuelven más eficientes si se requieren altas precisiones.

Con los propagadores CFM mostrando un rendimiento sobresaliente comparado con métodos bien consolidados como la EMR o RK4, y con una implementación que nos asegura que las propiedades del integrador se conservan, el siguiente paso sería probarlos para estudiar problemas en sistemas más grandes y complejos. Usando el formalismo QOCT+EMD+TDDFT, combinado con esta familia de propagadores, se podría abordar, por ejemplo, el problema de la fotoisomerización óptima de moléculas grandes, o el problema de inducir una reacción fotoquímica dada. También se podría pensar en cambiar la naturaleza de lo parámetros de optimización: de aquéllos que definen un pulso láser externo, a parámetros internos de la molécula o material. De esta forma, el objetivo podría ser, por ejemplo, encontrar la configuración del estado inicial que posea ciertas propiedades deseadas de respuesta (tales como la máxima absorción de luz en el espectro visible, la conductividad, etc.)

References

[1] Alonso, J. L., Castro, A., Clemente-Gallardo, J., Cuchí, J. C., Echenique, P., and Falceto, F. (2011). Statistics and Nosé formalism for Ehrenfest dynamics. *Journal of Physics A: Mathematical and Theoretical*, 44(39):395004.

[2] Alonso, J. L., Castro, A., Echenique, P., and Rubio, A. (2012). *On the Combination of TDDFT with Molecular Dynamics: New Developments*, pages 301–315. Springer Berlin Heidelberg, Berlin, Heidelberg.

[3] Andrade, X., Strubbe, D., De Giovannini, U., Larsen, A. H., Oliveira, M. J. T., Alberdi-Rodriguez, J., Varas, A., Theophilou, I., Helbig, N., Verstraete, M. J., Stella, L., Nogueira, F., Aspuru-Guzik, A., Castro, A., Marques, M. A. L., and Rubio, A. (2015). Real-space grids and the octopus code as tools for the development of new simulation approaches for electronic systems. *Phys. Chem. Chem. Phys.*, 17:31371–31396.

[4] Assion, A., Baumert, T., Bergt, M., Brixner, T., Kiefer, B., Seyfried, V., Strehle, M., and Gerber, G. (1998). Control of chemical reactions by feedback-optimized phase-shaped femtosecond laser pulses. *Science*, 282(5390):919–922.

[5] Athans, M. and Falb, P. (1966). *Optimal Control: An Introduction to the Theory and Its Applications*. Lincoln Laboratory publications. McGraw-Hill.

[6] Auer, N., Einkemmer, L., Kandolf, P., and Ostermann, A. (2018). Magnus integrators on multicore cpus and gpus. *Comput. Phys. Commun.*

[7] Austin, B. M., Zubarev, D. Y., and Lester, W. A. (2012). Quantum monte carlo and related approaches. *Chemical Reviews*, 112(1):263–288.

[8] Bacca, S. (2016). Structure models: From shell model to ab initio methods. *The European Physical Journal Plus*, 131(4):107.

[9] Bader, P., Blanes, S., and Kopylov, N. (2018). Exponential propagators for the schrödinger equation with a time-dependent potential. *The Journal of Chemical Physics*, 148(24):244109.

[10] Bashforth, F. and Adams, J. C. (1883). *An attempt to test the theories of capillary action by comparing the theoretical and measured forms of drops of fluid.* Cambridge University Press, Cambridge.

[11] Becke, A. D. (2014). Perspective: Fifty years of density-functional theory in chemical physics. *The Journal of Chemical Physics*, 140(18):18A301.

[12] Benettin, G. and Giorgilli, A. (1994). On the hamiltonian interpolation of near-to-the identity symplectic mappings with application to symplectic integration algorithms. *J. Stat. Phys.*, 74(5):1117–1143.

[13] Bethe, H. (1931). Zur theorie der metalle. *Zeitschrift für Physik*, 71(3):205–226.

[14] Blanes, S., Casas, F., Oteo, J., and Ros, J. (2009). The magnus expansion and some of its applications. *Physics Reports*, 470(5):151 – 238.

[15] Blanes, S. and Moan, P. (2006). Fourth- and sixth-order commutator-free magnus integrators for linear and non-linear dynamical systems. *Appl. Numer. Math.*, 56(12):1519 – 1537.

[16] Bloch, F. (1933). Bremsvermögen von atomen mit mehreren elektronen. *Zeitschrift für Physik*, 81(5-6):363–376.

[17] Boltyanskij, V. G., Gamkrelidze, R. V., and Pontryagin, L. S. (1956). On the theory of optimum processes. *Dokl. Akad. Nauk SSSR*, 110:7–10.

[18] Bornemann, F. A., Nettesheim, P., and Schütte, C. (1996). Quantum-classical molecular dynamics as an approximation to full quantum dynamics. *The Journal of Chedoi:10.1021/ed076p171mical Physics*, 105(3):1074–1083.

[19] Botina, J., Rabitz, H., and Rahman, N. (1995). A new approach to molecular classical optimal control: Application to the reaction hcn→hc+n. *The Journal of Chemical Physics*, 102(1):226–236.

[20] Brif, C., Chakrabarti, R., and Rabitz, H. (2010). Control of quantum phenomena: past present and future. *New Journal of Physics*, 12(7):075008.

[21] Brillouin, L. (1926). *Comptes Rendus de l'Academie des Sciences*, 183:24.

[22] Brumer, P. and Shapiro, M. (1986). Control of unimolecular reactions using coherent light. *Chemical Physics Letters*, 126(6):541 – 546.

[23] Buczek, P., Ernst, A., and Sandratskii, L. M. (2011). Different dimensionality trends in the landau damping of magnons in iron, cobalt, and nickel: Time-dependent density functional study. *Phys. Rev. B*, 84:174418.

[24] Burke, K. (2012). Perspective on density functional theory. *The Journal of Chemical Physics*, 136(15):150901.

[25] Butcher, J. (1996). A history of runge-kutta methods. *Appl. Numer. Math.*, 20(3):247 – 260.

[26] Butcher, J. C. (1964). On runge-kutta processes of high order. *Journal of the Australian Mathematical Society*, 4(2):179–194.

[27] Butcher, J. C. (1987). *The Numerical Analysis of Ordinary Differential Equations: Runge-Kutta and General Linear Methods*. Wiley-Interscience, New York, NY, USA.

[28] Caliari, M., Kandolf, P., Ostermann, A., and Rainer, S. (2016). The Leja method revisited: Backward error analysis for the matrix exponential. *SIAM J. Sci. Comput.*, 38(3):A1639–A1661.

[29] Calvayrac, F., Reinhard, P.-G., and Suraud, E. (1998). Coulomb explosion of an cluster in a diabatic electron-ion dynamical picture. *J. Phys. B: At. Mol. Opt. Phys.*, 31(22):5023–5030.

[30] Calvayrac, F., Reinhard, P.-G., Suraud, E., and Ullrich, C. (2000). Nonlinear electron dynamics in metal clusters. *Physics Reports*, 337(6):493–578.

[31] Capelle, K., Lima, N. A., Silva, M. F., and Oliveira, L. N. (2003). Density-functional theory for the hubbard model: Numerical results for the luttinger liquid and the mott insulator. In Gidopoulos, N. I. and Wilson, S., editors, *The Fundamentals of Electron Density, Density Matrix and Density Functional Theory in Atoms, Molecules and the Solid State*, pages 145–168, Dordrecht. Springer Netherlands.

[32] Carrascal, D. J., Ferrer, J., Smith, J. C., and Burke, K. (2015). The hubbard dimer: a density functional case study of a many-body problem. *Journal of Physics: Condensed Matter*, 27(39):393001.

[33] Casida, M. E. (1995). *Time-Dependent Density Functional Response Theory for Molecules*, volume 1, pages 155–192.

[34] Castro, A. (2013). Theoretical Shaping of Femtosecond Laser Pulses for Ultrafast Molecular Photo-Dissociation with Control Techniques Based on Time-Dependent Density Functional Theory. *ChemPhysChem*, 14(7):1488–1495.

[35] Castro, A. (2016). Theoretical shaping of femtosecond laser pulses for molecular photo-dissociation with control techniques based on Ehrenfest's dynamics and time-dependent density-functional theory. *ChemPhysChem*, 17:1601.

[36] Castro, A., Appel, H., Oliveira, M., Rozzi, C. A., Andrade, X., Lorenzen, F., Marques, M. A. L., Gross, E. K. U., and Rubio, A. (2006). octopus: a tool for the application of time-dependent density functional theory. *physica status solidi (b)*, 243(11):2465–2488.

[37] Castro, A. and Gross, E. K. U. (2013). Optimal control theory for quantum-classical systems: Ehrenfest molecular dynamics based on time-dependent density-functional theory. *Journal of Physics A: Mathematical and Theoretical*, 47(2):025204.

[38] Castro, A., Marques, M., and Rubio, A. (2004a). Propagators for the time-dependent Kohn–Sham equations. *J. Chem. Phys.*, 121(8):3425.

[39] Castro, A., Marques, M. A. L., Alonso, J. A., Bertsch, G. F., and Rubio, A. (2004b). Excited states dynamics in time-dependent density functional theory. *The European Physical Journal D - Atomic Molecular and Optical Physics*, 28(2):211–218.

[40] Castro, A., Werschnik, J., and Gross, E. K. U. (2012). Controlling the Dynamics of Many-Electron Systems from First Principles: A Combination of Optimal Control and Time-Dependent Density-Functional Theory. *Phys. Rev. Lett.*, 109(15).

[41] Chan, C. K., Brumer, P., and Shapiro, M. (1991). Coherent radiative control of ibr photodissociation via simultaneous (ω_1, ω_3) excitation. *The Journal of Chemical Physics*, 94(4):2688–2696.

[42] Chan, G. K.-L., Keselman, A., Nakatani, N., Li, Z., and White, S. R. (2016). Matrix product operators, matrix product states, and ab initio density matrix renormalization group algorithms. *The Journal of Chemical Physics*, 145(1):014102.

[43] Chen, C., Yin, Y.-Y., and Elliott, D. S. (1990). Interference between optical transitions. *Phys. Rev. Lett.*, 64:507–510.

[44] Chen, G. P., Voora, V. K., Agee, M. M., Balasubramani, S. G., and Furche, F. (2017). Random-phase approximation methods. *Annual Review of Physical Chemistry*, 68(1):421–445. PMID: 28301757.

[45] Chen, R. and Guo, H. (1999). The chebyshev propagator for quantum systems. *Comput. Phys. Commun.*, 119(1):19 – 31.

[46] Chignola, R., Fabbro, A. D., Pellegrina, C. D., and Milotti, E. (2007). Ab initiophenomenological simulation of the growth of large tumor cell populations. *Physical Biology*, 4(2):114–133.

[47] Cohen, A. J., Mori-Sánchez, P., and Yang, W. (2008). Insights into current limitations of density functional theory. *Science*, 321(5890):792–794.

[48] Cremer, D. (2011). Møller–plesset perturbation theory: from small molecule methods to methods for thousands of atoms. *Wiley Interdisciplinary Reviews: Computational Molecular Science*, 1(4):509–530.

[49] Cremer, D. (2013). From configuration interaction to coupled cluster theory: The quadratic configuration interaction approach. *Wiley Interdisciplinary Reviews: Computational Molecular Science*, 3(5):482–503.

[50] Curtiss, C. F. and Hirschfelder, J. O. (1952). Integration of stiff equations. *Proceedings of the National Academy of Sciences*, 38(3):235–243.

[51] Dion, M., Rydberg, H., Schröder, E., Langreth, D. C., and Lundqvist, B. I. (2004). Van der waals density functional for general geometries. *Phys. Rev. Lett.*, 92:246401.

[52] Dirac, P. A. M. (1930). Note on exchange phenomena in the thomas atom. *Mathematical Proceedings of the Cambridge Philosophical Society*, 26(3):376–385.

[53] Dirac, P. A. M. and Fowler, R. H. (1929). Quantum mechanics of many-electron systems. *Proceedings of the Royal Society of London. Series A, Containing Papers of a Mathematical and Physical Character*, 123(792):714–733.

[54] Dreizler, R. M. and Gross, E. K. U. (1990). *Density Functional Theory: An Approach to the Quantum Many-Body Problem*. Springer-Verlag, Berlin-Heidelberg.

[55] Dyson, F. J. (1949). The radiation theories of tomonaga, schwinger, and feynman. *Phys. Rev.*, 75:486–502.

[56] Eisert, J., Cramer, M., and Plenio, M. B. (2010). Colloquium: Area laws for the entanglement entropy. *Rev. Mod. Phys.*, 82:277–306.

[57] Euler, L. (1768). *Institutionum calculi integralis*. Number v. 1 in Institutionum calculi integralis. imp. Acad. imp. Saènt.

[58] Fatunla, S. O. (1978). An implicit two-point numerical integration formula for linear and nonlinear stiff systems of ordinary differential equations. *Math. Comp.*, 32:1.

[59] Fatunla, S. O. (1980). Numerical integrators for stiff and highly oscillatory differential equations. *Math. Comp.*, 34:373.

[60] Fennel, T., Meiwes-Broer, K.-H., Tiggesbäumker, J., Reinhard, P.-G., Dinh, P. M., and Suraud, E. (2010). Laser-driven nonlinear cluster dynamics. *Reviews of Modern Physics*, 82(2):1793–1842.

[61] Fermi, E. (1927). Un methodo satistico par la determinazione di alcune proprietˆ dell'atome [j]. *Rend Accad Naz del Lincei cl Sci fis Mat e Nat, 1927, 23 (6)*, pages 602–607.

[62] Flocard, H., Koonin, S. E., and Weiss, M. S. (1978). Three-dimensional time-dependent hartree-fock calculations: Application to ^{16}O + ^{16}O collisions. *Phys. Rev. C*, 17:1682–1699.

[63] Fourati, S., Talla, A., Mahmoudian, M., Burkhart, J. G., Klén, R., Henao, R., Yu, T., Aydin, Z., Yeung, K. Y., Ahsen, M. E., Almugbel, R., Jahandideh, S., Liang, X., Nordling, T. E. M., Shiga, M., Stanescu, A., Vogel, R., Abdallah, E. B., Aghababazadeh, F. A., Amadoz, A., Bhalla, S., Bleakley, K., Bongen, E., Borzacchielo, D., Bucher, P., Carbonell-Caballero, J., Chaudhary, K., Chinesta, F., Chodavarapu, P., Chow, R. D., Cokelaer, T., Cubuk, C., Dhanda, S. K., Dopazo, J., Faux, T., Feng, Y., Flinta, C., Guziolowski, C., He, D., Hidalgo, M. R., Hou, J., Inoue, K., Jaakkola, M. K., Ji, J., Kumar, R., Kumar, S., Kursa, M. B., Li, Q., Lopuszynski, M., Lu, P., Magnin, M., Mao, W., Miannay, B., Nikolayeva, I., Obradovic, Z., Pak, C., Rahman, M. M., Razzaq, M., Ribeiro, T., Roux, O., Saghapour, E., Saini, H., Sarhadi, S., Sato, H., Schwikowski, B., Sharma, A., Sharma, R., Singla, D., Stojkovic, I., Suomi, T., Suprun, M., Tian, C., Tomalin, L. E., Xie, L., Yu, X., Pandey, G., Chiu, C., McClain, M. T., Woods, C. W., Ginsburg, G. S., Elo, L. L., Tsalik, E. L., Mangravite, L. M., Sieberts, S. K., and Consortium, T. R. V. D. C. (2018). A crowdsourced analysis to identify ab initio molecular signatures predictive of susceptibility to viral infection. *Nature Communications*, 9(1):4418.

[64] França, V. V., Vieira, D., and Capelle, K. (2012). Simple parameterization for the ground-state energy of the infinite hubbard chain incorporating mott physics, spin-dependent phenomena and spatial inhomogeneity. *New Journal of Physics*, 14(7):073021.

[65] Gaubatz, U., Rudecki, P., Becker, M., Schiemann, S., Külz, M., and Bergmann, K. (1988). Population switching between vibrational levels in molecular beams. *Chemical Physics Letters*, 149(5):463 – 468.

[66] Gear, C. W. (1971). *Numerical Initial Value Problems in Ordinary Differential Equations*. Prentice Hall PTR, Upper Saddle River, NJ, USA.

[67] Gell-Mann, M. and Brueckner, K. A. (1957). Correlation energy of an electron gas at high density. *Phys. Rev.*, 106:364–368.

[68] Gerber, R. B., Buch, V., and Ratner, M. A. (1982). Time-dependent self-consistent field approximation for intramolecular energy transfer. I. Formulation and application to dissociation of van der Waals molecules. *The Journal of Chemical Physics*, 77(6):3022–3030.

[69] Gómez Pueyo, A., Blanes, S., and Castro, A. (2020). Propagators for quantum-classical models: Commutator-free magnus methods. *Journal of Chemical Theory and Computation*, 16(3):1420–1430. PMID: 31999460.

[70] Gómez Pueyo, A., Marques, M. A. L., Rubio, A., and Castro, A. (2018). Propagators for the time-dependent kohn–sham equations: Multistep, runge–kutta, exponential runge–kutta, and commutator free magnus methods. *Journal of Chemical Theory and Computation*, 14(6):3040–3052. PMID: 29672048.

[71] Goldbeck, G. (2012). The economic impact of molecular modelling of chemicals and materials.

[72] Goldbeck, G. and Court, C. (2016). The economic impact of materials modelling.

[73] Goldbeck, G. and Simperler, A. (2019). Business models and sustainability for materials modelling software.

[74] Gómez Pueyo, A., Budagosky M., J. A., and Castro, A. (2016). Optimal control with nonadiabatic molecular dynamics: Application to the coulomb explosion of sodium clusters. *Phys. Rev. A*, 94:063421.

[75] Gómez Pueyo, A. and Castro, A. (2018). About the relation of electron–electron interaction potentials with exchange and correlation functionals. *The European Physical Journal B*, 91(6):105.

[76] Grochowski, P. and Lesyng, B. (2003). Extended hellmann–feynman forces, canonical representations, and exponential propagators in the mixed quantum-classical molecular dynamics. *The Journal of Chemical Physics*, 119(22):11541–11555.

[77] Gross, E. K. U., Dobson, J. F., and Petersilka, M. (1996). *Density functional theory of time-dependent phenomena*, pages 81–172. Springer Berlin Heidelberg, Berlin, Heidelberg.

[78] Gunnarsson, O. and Schönhammer, K. (1986). Density-functional treatment of an exactly solvable semiconductor model. *Phys. Rev. Lett.*, 56:1968–1971.

[79] Hairer, E., Lubich, C., and Wanner, G. (2006). *Geometric Numerical Integration*. Springer Verlag, Berlin Heidelberg.

[80] Hairer, E., Nørsett, S. P., and Wanner, G. (1993). *Solving Ordinary Differential Equations I*. Springer Verlag, Berlin Heidelberg.

[81] Hairer, E. and Wanner, G. (1996). *Solving Ordinary Differential Equations II*. Springer Verlag, Berlin Heidelberg.

[82] Halilov, S. V., Perlov, A. Y., Oppeneer, P. M., and Eschrig, H. (1997). Magnon spectrum and related finite-temperature magnetic properties: A first-principle approach. *Europhysics Letters (EPL)*, 39(1):91–96.

[83] Hastings, M. B. (2007). An area law for one-dimensional quantum systems. *Journal of Statistical Mechanics: Theory and Experiment*, 2007(08):P08024–P08024.

[84] Hirose, K., Ono, T., Fujimoto, Y., and Tsukamoto, S. (2005). *First-Principles Calculations in Real-Space Formalism*. World Scientific Pub Co Pte Lt.

[85] Hochbruck, M. and Lubich, C. (1997). On krylov subspace approximations to the matrix exponential operator. *SIAM J. Numer. Anal.*, 34(5):1911–1925.

[86] Hochbruck, M. and Lubich, C. (1999a). A bunch of time integrators for quantum/classical molecular dynamics. In Deuflhard, P., Hermans, J., Leimkuhler, B., Mark, A. E., Reich, S., and Skeel, R. D., editors, *Computational Molecular Dynamics: Challenges, Methods, Ideas*, pages 421–432, Berlin, Heidelberg. Springer Berlin Heidelberg.

[87] Hochbruck, M. and Lubich, C. (1999b). Exponential integrators for quantum-classical molecular dynamics. *BIT Numerical Mathematics*, 39.

[88] Hochbruck, M. and Ostermann, A. (2005). Exponential runge–kutta methods for parabolic problems. *Appl. Numer. Math.*, 53(2):323 – 339.

[89] Hochbruck, M. and Ostermann, A. (2006). Explicit exponential runge-kutta methods for semilinear parabolic problems. *SIAM J. Numer. Anal.*, 43(3):1069–1090.

[90] Hohenberg, P. and Kohn, W. (1964). Inhomogeneous electron gas. *Physical Review*, 136(3B):B864.

[91] Huang, G. M., Tarn, T. J., and Clark, J. W. (1983). On the controllability of quantum-mechanical systems. *Journal of Mathematical Physics*, 24(11):2608–2618.

[92] III, R. D. J. (2015). Nist computational chemistry comparison and benchmark database, nist standard reference database number 101.

[93] Ivády, V., Abrikosov, I. A., and Gali, A. (2018). First principles calculation of spin-related quantities for point defect qubit research. *npj Computational Materials*, 4(1):76.

[94] Jakubetz, W., Manz, J., and Schreier, H.-J. (1990). Theory of optimal laser pulses for selective transitions between molecular eigenstates. *Chemical Physics Letters*, 165(1):100 – 106.

[95] Jamorski, C., Casida, M. E., and Salahub, D. R. (1996). Dynamic polarizabilities and excitation spectra from a molecular implementation of time-dependent density-functional response theory: N2 as a case study. *The Journal of Chemical Physics*, 104(13):5134–5147.

[96] Jbili, N., Hamraoui, K., Glaser, S. J., Salomon, J., and Sugny, D. (2019). Optimal periodic control of spin systems: Application to the maximization of the signal-to-noise ratio per unit time. *Phys. Rev. A*, 99:053415.

[97] Jensen, D. S. and Wasserman, A. (2016). Numerical density-to-potential inversions in time-dependent density functional theory. *Phys. Chem. Chem. Phys.*, 18:21079–21091.

[98] Jiang, H. and Zhao, X. S. (2000). New propagators for quantum-classical molecular dynamics simulations. *The Journal of Chemical Physics*, 113(3):930–935.

[99] Johnson, B. G., Gill, P. M. W., and Pople, J. A. (1993). The performance of a family of density functional methods. *The Journal of Chemical Physics*, 98(7):5612–5626.

[100] Johnson, S. G. (version 2.6.1). The NLopt nonlinear-optimization package. http://ab-initio.mit.edu/nlopt.

[101] Judson, R. S. and Rabitz, H. (1992). Teaching lasers to control molecules. *Phys. Rev. Lett.*, 68:1500–1503.

[102] Kaufman, H. (1964). The mathematical theory of optimal processes, by l. s. pontryagin, v. g. boltyanskii, r. v. gamkrelidze, and e. f. mishchenko. authorized translation from the russian. translator: K. n. trirogoff, editor: L.. w. neustadt. interscience publishers (division of john wiley and sons, inc. , new york) 1962. viii 360 pages. *Canadian Mathematical Bulletin*, 7(3):500–500.

[103] Keller, U. (2003). Recent developments in compact ultrafast lasers. *Nature*, 424(6950):831–838.

[104] Kidd, D., Covington, C., and Varga, K. (2017). Exponential integrators in time-dependent density-functional calculations. *Phys. Rev. E*, 96:063307.

[105] Kohn, W. (1999). Nobel lecture: Electronic structure of matter—wave functions and density functionals. *Rev. Mod. Phys.*, 71:1253–1266.

[106] Kohn, W. and Sham, L. J. (1965). Self-consistent equations including exchange and correlation effects. *Physical Review*, 140(4A):A1133.

[107] Kong, J., Proynov, E., Yu, J., and Pachter, R. (2017). Describing a strongly correlated model system with density functional theory. *The Journal of Physical Chemistry Letters*, 8(13):3142–3146. PMID: 28622472.

[108] Kosloff, R., Rice, S., Gaspard, P., Tersigni, S., and Tannor, D. (1989). Wavepacket dancing: Achieving chemical selectivity by shaping light pulses. *Chemical Physics*, 139(1):201–220.

[109] Kraft, D. (1994). Algorithm 733: Tomp–fortran modules for optimal control calculations. *ACM Trans. Math. Softw.*, 20(3):262–281.

[110] Kramers, H. A. (1926). Wellenmechanik und halbzahlige Quantisierung. *Zeitschrift für Physik*, 39(10):828–840.

[111] Krausz, F. and Ivanov, M. (2009). Attosecond physics. *Reviews of Modern Physics*, 81(1):163–234.

[112] Krieger, K., Castro, A., and Gross, E. (2011). Optimization schemes for selective molecular cleavage with tailored ultrashort laser pulses. *Chemical Physics*, 391(1):50–61.

[113] Kunert, T. and Schmidt, R. (2001). Excitation and Fragmentation Mechanisms in Ion-Fullerene Collisions. *Phys. Rev. Lett.*, 86(23):5258–5261.

[114] Kurth, S., Stefanucci, G., Khosravi, E., Verdozzi, C., and Gross, E. K. U. (2010). Dynamical coulomb blockade and the derivative discontinuity of time-dependent density functional theory. *Phys. Rev. Lett.*, 104:236801.

[115] Kutta, W. (1901). Beitrag zur näherungsweisen Integration totaler Differentialgleichungen. *Zeit. Math. Phys.*, 46:435–53.

[116] Lebedeva, I. V., Lebedev, A. V., Popov, A. M., and Knizhnik, A. A. (2017). Comparison of performance of van der waals-corrected exchange-correlation functionals for interlayer interaction in graphene and hexagonal boron nitride. *Computational Materials Science*, 128:45 – 58.

[117] Levy, M. (1979). Universal variational functionals of electron densities, first-order density matrices, and natural spin-orbitals and solution of the v-representability problem. *Proceedings of the National Academy of Sciences*, 76(12):6062–6065.

[118] Levy, M. (1995). Excitation energies from density-functional orbital energies. *Phys. Rev. A*, 52:R4313–R4315.

[119] Lieb, E. H. (1983). Density functionals for coulomb systems. *International Journal of Quantum Chemistry*, 24(3):243–277.

[120] Lieb, E. H. and Simon, B. (1977). The thomas-fermi theory of atoms, molecules and solids. *Advances in Mathematics*, 23(1):22 – 116.

[121] Lieb, E. H. and Wu, F. (2003). The one-dimensional hubbard model: a reminiscence. *Physica A: Statistical Mechanics and its Applications*, 321(1):1 – 27. Statphys-Taiwan-2002: Lattice Models and Complex Systems.

[122] Lieb, E. H. and Wu, F. Y. (1968). Absence of mott transition in an exact solution of the short-range, one-band model in one dimension. *Phys. Rev. Lett.*, 20:1445–1448.

[123] Lima, N. A., Oliveira, L. N., and Capelle, K. (2002). Density-functional study of the mott gap in the hubbard model. *EPL (Europhysics Letters)*, 60(4):601.

[124] Lima, N. A., Silva, M. F., Oliveira, L. N., and Capelle, K. (2003). Density functionals not based on the electron gas: Local-density approximation for a luttinger liquid. *Phys. Rev. Lett.*, 90:146402.

[125] Liu, D. C. and Nocedal, J. (1989). On the limited memory BFGS method for large scale optimization. *Mathematical Programming*, 45(1-3):503–528.

[126] Lo, V. L. and Millane, R. P. (2009). Ab initio determination of virus electron density in x-ray crystallography. In *Frontiers in Optics 2009/Laser Science XXV/Fall 2009 OSA Optics & Photonics Technical Digest*, page STuB2. Optical Society of America.

[127] López-Sandoval, R. and Pastor, G. M. (2000). Density-matrix functional theory of the hubbard model: An exact numerical study. *Phys. Rev. B*, 61:1764–1772.

[128] López-Sandoval, R. and Pastor, G. M. (2004). Interaction-energy functional for lattice density functional theory: Applications to one-, two-, and three-dimensional hubbard models. *Phys. Rev. B*, 69:085101.

[129] Lubasch, M., Fuks, J. I., Appel, H., Rubio, A., Cirac, J. I., and Bañuls, M.-C. (2016). Systematic construction of density functionals based on matrix product state computations. *New Journal of Physics*, 18(8):083039.

[130] Ma, L., Suraud, E., and Reinhard, P.-G. (2001). Laser excitation and ionic motion in small clusters. *The European Physical Journal D*, 14(2):217–223.

[131] MA, S.-k. and BRUECKNER, K. A. (1968). Correlation energy of an electron gas with a slowly varying high density. *Phys. Rev.*, 165:18–31.

[132] Maday, Y. and Turinici, G. (2003). New formulations of monotonically convergent quantum control algorithms. *The Journal of Chemical Physics*, 118(18):8191.

[133] Magierski, P., Sekizawa, K., and Wlazłowski, G. (2017). Novel role of superfluidity in low-energy nuclear reactions. *Phys. Rev. Lett.*, 119:042501.

[134] Magnus, W. (1954). On the exponential solution of differential equations for a linear operator. *Commun. Pure Appl. Math.*, 7(4):649–673.

[135] Mai, S., Richter, M., Marquetand, P., and González, L. (2017). The dna nucleobase thymine in motion – intersystem crossing simulated with surface hopping. *Chemical Physics*, 482:9 – 15. Electrons and nuclei in motion - correlation and dynamics in molecules (on the occasion of the 70th birthday of Lorenz S. Cederbaum).

[136] Maitra, N. T. (2016). Perspective: Fundamental aspects of time-dependent density functional theory. *The Journal of Chemical Physics*, 144(22):220901.

[137] Maitra, N. T. (2017). Charge transfer in time-dependent density functional theory. *Journal of Physics: Condensed Matter*, 29(42):423001.

[138] Maitra, N. T., Burke, K., and Woodward, C. (2002). Memory in time-dependent density functional theory. *Phys. Rev. Lett.*, 89:023002.

[139] Marques, M. (2003). octopus: a first-principles tool for excited electron–ion dynamics. *Computer Physics Communications*, 151(1):60–78.

[140] Marques, M. A., Castro, A., Bertsch, G. F., and Rubio, A. (2003). octopus: a first-principles tool for excited electron–ion dynamics. *Comput. Phys. Commun.*, 151(1):60 – 78.

[141] Marques, M. A., Maitra, N. T., Nogueira, F. M., Gross, E., and Rubio, A., editors (2012a). *Fundamentals of Time-Dependent Density Functional Theory*. Springer Berlin Heidelberg.

[142] Marques, M. A., Oliveira, M. J., and Burnus, T. (2012b). Libxc: A library of exchange and correlation functionals for density functional theory. *Computer Physics Communications*, 183(10):2272 – 2281.

[143] Marques, M. A. L. and Gross, E. K. U. (2003). *A Primer in Density Functional Theory*, chapter Time-Dependent Density Functional Theory, pages 144–184. Springer Berlin Heidelberg, Berlin, Heidelberg.

[144] Maset, S. and Zennaro, M. (2009). Unconditional stability of explicit exponential runge-kutta methods for semi-linear ordinary differential equations. *Math. Comput.*, 78:957–967.

[145] ITensor Library (version 2.0.1). http://itensor.org.

[146] Medvedev, M. G., Bushmarinov, I. S., Sun, J., Perdew, J. P., and Lyssenko, K. A. (2017). Density functional theory is straying from the path toward the exact functional. *Science*, 355(6320):49–52.

[147] Mei, L. and Wu, X. (2017). Symplectic exponential runge–kutta methods for solving nonlinear hamiltonian systems. *J. Comput. Phys.*, 338:567 – 584.

[148] Mittleman, M. H. (1961). Proton-hydrogen scattering system. *Phys. Rev.*, 122:499–506.

[149] Miyamoto, Y. and Zhang, H. (2008). Calculating interaction between a highly charged high-speed ion and a solid surface. *Phys. Rev. B*, 77(4).

[150] Møller, C. and Plesset, M. S. (1934). Note on an approximation treatment for many-electron systems. *Phys. Rev.*, 46:618–622.

[151] Navrátil, P., Quaglioni, S., Hupin, G., Romero-Redondo, C., and Calci, A. (2016). Unified ab initio approaches to nuclear structure and reactions. *Physica Scripta*, 91(5):053002.

[152] Nettesheim, P., Bornemann, F. A., Schmidt, B., and Schütte, C. (1996). An explicit and symplectic integrator for quantum-classical molecular dynamics. *Chemical Physics Letters*, 256(6):581 – 588.

[153] Nettesheim, P. and Reich, S. (1999). Symplectic multiple-time-stepping integrators for quantum-classical molecular dynamics. pages 412–420.

[154] Nettesheim, P. and Schütte, C. (1999). Numerical integrators for quantum-classical molecular dynamics. In Deuflhard, P., Hermans, J., Leimkuhler, B., Mark, A. E., Reich, S., and Skeel, R. D., editors, *Computational Molecular Dynamics: Challenges, Methods, Ideas*, pages 396–411, Berlin, Heidelberg. Springer Berlin Heidelberg.

[155] Nocedal, J. (1980). Updating quasi-Newton matrices with limited storage. *Mathematics of Computation*, 35(151):773–773.

[156] Okunishi, K., Hieida, Y., and Akutsu, Y. (1999). Universal asymptotic eigenvalue distribution of density matrices and corner transfer matrices in the thermodynamic limit. *Phys. Rev. E*, 59:R6227–R6230.

[157] Olevano, V. (2018). TDDFT, excitations and spectroscopy. In Schaniel, D. and Woike, T., editors, *Structures on different time scales*, pages 101–142. De Gruyter.

[158] Östlund, S. and Rommer, S. (1995). Thermodynamic limit of density matrix renormalization. *Phys. Rev. Lett.*, 75:3537–3540.

[159] P. Dederichs, P. M. and Tunger, D. (2010). The size of our field of ab initio simulations. *Psi-k Monthly Update, 3*.

[160] Pal, G., Lefkidis, G., Schneider, H. C., and Hübner, W. (2010). Optical response of small closed-shell sodium clusters. *The Journal of Chemical Physics*, 133(15).

[161] Peirce, A. P., Dahleh, M. A., and Rabitz, H. (1988). Optimal control of quantum-mechanical systems: Existence numerical approximation, and applications. *Phys. Rev. A*, 37(12):4950–4964.

[162] Pemmaraju, C. D., Rungger, I., Chen, X., Rocha, A. R., and Sanvito, S. (2010). Ab initio study of electron transport in dry poly(g)-poly(c) *a*-dna strands. *Phys. Rev. B*, 82:125426.

[163] Perdew, J. P. (1986). Density-functional approximation for the correlation energy of the inhomogeneous electron gas. *Phys. Rev. B*, 33:8822–8824.

[164] Perdew, J. P. (2003). *Can Density Functional Theory Describe Strongly Correlated Electronic Systems?*, pages 237–252. Springer US, Boston, MA.

[165] Perdew, J. P., Burke, K., and Ernzerhof, M. (1996). Generalized gradient approximation made simple. *Phys. Rev. Lett.*, 77:3865–3868.

[166] Perdew, J. P., Chevary, J. A., Vosko, S. H., Jackson, K. A., Pederson, M. R., Singh, D. J., and Fiolhais, C. (1992). Atoms, molecules, solids, and surfaces: Applications of the generalized gradient approximation for exchange and correlation. *Phys. Rev. B*, 46:6671–6687.

[167] Perdew, J. P. and Levy, M. (1983). Physical content of the exact kohn-sham orbital energies: Band gaps and derivative discontinuities. *Phys. Rev. Lett.*, 51:1884–1887.

[168] Perdew, J. P. and Schmidt, K. (2001). Jacob's ladder of density functional approximations for the exchange-correlation energy. *AIP Conference Proceedings*, 577(1):1–20.

[169] Perdew, J. P. and Yue, W. (1986). Accurate and simple density functional for the electronic exchange energy: Generalized gradient approximation. *Phys. Rev. B*, 33:8800–8802.

[170] Peschel, I., Kaulke, M., and Legeza, Ö. (1999). Density-matrix spectra for integrable models. *Annalen der Physik*, 8(2):153–164.

[171] Plenio, M. B., Eisert, J., Dreißig, J., and Cramer, M. (2005). Entropy, entanglement, and area: Analytical results for harmonic lattice systems. *Phys. Rev. Lett.*, 94:060503.

[172] Poincaré (1999). *Les Méthodes Nouvelles de la Mécanique Céleste. Tome III*. Gouthier-Villars, Paris.

[173] Rapaport, D. C. (2004). *The Art of Molecular Dynamics Simulation*. Cambridge University Press, Bar-Ilan University, Israel.

[174] Reich, S. (1999). Multiple time scales in classical and quantum–classical molecular dynamics. *Journal of Computational Physics*, 151(1):49 – 73.

[175] Rice, S. A. and Zhao, M. (2000). *Optical Control of Molecular Dynamics*. Wiley, New York.

[176] Rommer, S. and Östlund, S. (1997). Class of ansatz wave functions for one-dimensional spin systems and their relation to the density matrix renormalization group. *Phys. Rev. B*, 55:2164–2181.

[177] Ruiz-Blanco, Y. B., Almeida, Y., Sotomayor-Torres, C. M., and García, Y. (2017). Unveiled electric profiles within hydrogen bonds suggest dna base pairs with similar bond strengths. *PLOS ONE*, 12(10):1–11.

[178] Runge, C. (1895). Ueber die numerische auflösung von differentialgleichungen. *Mathematische Annalen*, 46:167–178.

[179] Runge, E. and Gross, E. K. U. (1984). Density-functional theory for time-dependent systems. *Phys. Rev. Lett.*, 52:997–1000.

[180] Russakoff, A., Bubin, S., Xie, X., Erattupuzha, S., Kitzler, M., and Varga, K. (2015). Time-dependent density-functional study of the alignment-dependent ionization of acetylene and ethylene by strong laser pulses. *Phys. Rev. A*, 91(2).

[181] Saalmann, U. and Schmidt, R. (1996). Non-adiabatic quantum molecular dynamics: basic formalism and case study. *Zeitschrift fü Physik D Atoms Molecules and Clusters*, 38(2):153–163.

[182] Sanz-Serna, J. M. (1988). Runge-kutta schemes for hamiltonian systems. *BIT Numer. Math.*, 28(4):877–883.

[183] Sargent, R. (2000). Optimal control. *Journal of Computational and Applied Mathematics*, 124(1):361 – 371. Numerical Analysis 2000. Vol. IV: Optimization and Nonlinear Equations.

[184] Sawada, T., Hashimoto, T., Tokiwa, H., Suzuki, T., Nakano, H., Ishida, H., Kiso, M., and Suzuki, Y. (2008). Ab initio fragment molecular orbital studies of influenza virus hemagglutinin–sialosaccharide complexes toward chemical clarification about the virus host range determination. *Glycoconjugate Journal*, 25(9):805–815.

[185] Schaefer, I., Tal-Ezer, H., and Kosloff, R. (2017). Semi-global approach for propagation of the time-dependent schrödinger equation for time-dependent and nonlinear problems. *J. Comput. Phys.*, 343(Supplement C):368 – 413.

[186] Schindlmayr, A. and Godby, R. W. (1995). Density-functional theory and the v-representability problem for model strongly correlated electron systems. *Phys. Rev. B*, 51:10427–10435.

[187] Schollwöck, U. (2005). The density-matrix renormalization group. *Rev. Mod. Phys.*, 77:259–315.

[188] Schollwöck, U. (2010). The density-matrix renormalization group in the age of matrix product states. *Annals of Physics - ANN PHYS N Y*, 326.

[189] Schönhammer, K., Gunnarsson, O., and Noack, R. M. (1995). Density-functional theory on a lattice: Comparison with exact numerical results for a model with strongly correlated electrons. *Phys. Rev. B*, 52:2504–2510.

[190] Schuch, N. and Verstraete, F. (2009). Computational complexity of interacting electrons and fundamental limitations of density functional?theory. *Nature Physics*, 5:732 EP –.

[191] Schuch, N., Wolf, M. M., Verstraete, F., and Cirac, J. I. (2008). Entropy scaling and simulability by matrix product states. *Phys. Rev. Lett.*, 100:030504.

[192] Schwerdtfeger, P. (2011). The Pseudopotential Approximation in Electronic Structure Theory. *ChemPhysChem*, 12(17):3143–3155.

[193] Schwieters, C. D. and Rabitz, H. (1993). Optimal control of classical systems with explicit quantum-classical-difference reduction. *Phys. Rev. A*, 48:2549–2557.

[194] Seraide, R., Bernal, M. A., Brunetto, G., de Giovannini, U., and Rubio, A. (2017). Tddft-based study on the proton–dna collision. *The Journal of Physical Chemistry B*, 121(30):7276–7283. PMID: 28679206.

[195] Shapiro, M. and Brumer, P. (2012). *Quantum Control of Molecular Processes, Second Edition*. Wiley-VCH Verlag GmbH & Co. KGaA, New York.

[196] Shi, S., Woody, A., and Rabitz, H. (1988). Optimal control of selective vibrational excitation in harmonic linear chain molecules. *The Journal of Chemical Physics*, 88(11):6870–6883.

[197] Solov'yov, I. A., Solov'yov, A. V., and Greiner, W. (2002). Structure and properties of small sodium clusters. *Phys. Rev. A*, 65:053203.

[198] Somlói, J., Kazakov, V. A., and Tannor, D. J. (1993). Controlled dissociation of I2 via optical transitions between the X and B electronic states. *Chemical Physics*, 172(1):85–98.

[199] Stefanucci, G. and van Leeuwen, R. (2013). *Nonequilibrium Many-Body Theory of Quantum Systems*. Cambridge University Press, Cambridge.

[200] Sternheimer, R. (1951). On nuclear quadrupole moments. *Phys. Rev.*, 84:244–253.

[201] Suraud, E. and Reinhard, P. G. (2000). Impact of Ionic Motion on Ionization of Metal Clusters under Intense Laser Pulses. *Phys. Rev. Lett.*, 85(11):2296–2299.

[202] Sussmann, H. J. and Willems, J. C. (1997). 300 years of optimal control: From the brachystochrone to the maximum principle.

[203] Szalay, P. G., Müller, T., Gidofalvi, G., Lischka, H., and Shepard, R. (2012). Multiconfiguration self-consistent field and multireference configuration interaction methods and applications. *Chemical Reviews*, 112(1):108–181. PMID: 22204633.

[204] Tannor, D. J., Kazakov, V., and Orlov, V. (1992). Control of Photochemical Branching: Novel Procedures for Finding Optimal Pulses and Global Upper Bounds. In *Nato ASI Series*, pages 347–360. Springer Science + Business Media.

[205] Tannor, D. J. and Rice, S. A. (1985). Control of selectivity of chemical reaction via control of wave packet evolution. *The Journal of Chemical Physics*, 83(10):5013–5018.

[206] Theilhaber, J. (1992). Ab initio simulations of sodium using time-dependent density-functional theory. *Phys. Rev. B*, 46:12990–13003.

[207] Thomas, L. H. (1927). The calculation of atomic fields. *Mathematical Proceedings of the Cambridge Philosophical Society*, 23(5):542–548.

[208] Töws, W. and Pastor, G. M. (2011). Lattice density functional theory of the single-impurity anderson model: Development and applications. *Phys. Rev. B*, 83:235101.

[209] Ullrich, C. A. (2011). *Time-Dependent Density-Functional Theory: Concepts and Applications*. Oxford Scholarship, Oxford.

[210] Ullrich, C. A. and Tokatly, I. V. (2006). Nonadiabatic electron dynamics in time-dependent density-functional theory. *Phys. Rev. B*, 73:235102.

[211] Van Acoleyen, K., Mariën, M., and Verstraete, F. (2013). Entanglement rates and area laws. *Phys. Rev. Lett.*, 111:170501.

[212] van Leeuwen, R. (1999). Mapping from densities to potentials in time-dependent density-functional theory. *Phys. Rev. Lett.*, 82:3863–3866.

[213] Varvenne, C., Bruneval, F., Marinica, M.-C., and Clouet, E. (2013). Point defect modeling in materials: Coupling ab initio and elasticity approaches. *Phys. Rev. B*, 88:134102.

[214] Verdozzi, C. (2008). Time-dependent density-functional theory and strongly correlated systems: Insight from numerical studies. *Phys. Rev. Lett.*, 101:166401.

[215] Verlet, L. (1967). Computer "experiments" on classical fluids. i. thermodynamical properties of lennard-jones molecules. *Phys. Rev.*, 159:98–103.

[216] Wentzel, G. (1926). Eine Verallgemeinerung der Quantenbedingungen für die Zwecke der Wellenmechanik. *Zeitschrift für Physik*, 38(6):518–529.

[217] Werschnik, J. and Gross, E. K. U. (2007). Quantum optimal control theory. *J. Phys. B: At. Mol. Opt. Phys.*, 40(18):R175–R211.

[218] White, S. R. (1992). Density matrix formulation for quantum renormalization groups. *Phys. Rev. Lett.*, 69:2863–2866.

[219] Wilson, K. G. (1975). The renormalization group: Critical phenomena and the kondo problem. *Rev. Mod. Phys.*, 47:773–840.

[220] Wopperer, P., Dinh, P., Reinhard, P.-G., and Suraud, E. (2015). Electrons as probes of dynamics in molecules and clusters: A contribution from Time Dependent Density Functional Theory. *Physics Reports*, 562:1–68.

[221] Wouters, S. and Van Neck, D. (2014). The density matrix renormalization group for ab initio quantum chemistry. *The European Physical Journal D*, 68(9):272.

[222] Wu, Z. (2006). More accurate generalized gradient approximation for solids. *Phys. Rev. B*, 73.

[223] Xu, J. (2019). Distance-based protein folding powered by deep learning. *Proceedings of the National Academy of Sciences*, 116(34):16856–16865.

[224] Yabana, K. and Bertsch, G. F. (1996). Time-dependent local-density approximation in real time. *Phys. Rev. B*, 54:4484–4487.

[225] Yamada, S., Noda, M., Nobusada, K., and Yabana, K. (2018). Time-dependent density functional theory for interaction of ultrashort light pulse with thin materials. *Phys. Rev. B*, 98:245147.

[226] Yang, Z.-h., Pribram-Jones, A., Burke, K., and Ullrich, C. A. (2017). Direct extraction of excitation energies from ensemble density-functional theory. *Phys. Rev. Lett.*, 119:033003.

[227] Yost, D. C., Yao, Y., and Kanai, Y. (2017). Examining real-time time-dependent density functional theory nonequilibrium simulations for the calculation of electronic stopping power. *Phys. Rev. B*, 96:115134.

[228] Zangwill, A. (2015). A half century of density functional theory. *Physics today*, 68(7):34.

[229] Zewail, A. H. (1980). Laser selective chemistry—is it possible? *Physics Today*, 33:27.

[230] Zewail, A. H. (1994). *Femtochemistry: Ultrafast Dynamics of the Chemical Bond (Volumes I & II)*. World Scientific Publishing Co. Pte. Ltd.

[231] Zhang, I. Y. and Grüneis, A. (2019). Coupled cluster theory in materials science. *Frontiers in Materials*, 6:123.

[232] Zhu, W., Botina, J., and Rabitz, H. (1998). Rapidly convergent iteration methods for quantum optimal control of population. *The Journal of Chemical Physics*, 108(5):1953.

[233] Zhu, W. and Rabitz, H. (1998). A rapid monotonically convergent iteration algorithm for quantum optimal control over the expectation value of a positive definite operator. *The Journal of Chemical Physics*, 109(2):385.